ARTIFICIAL INTELLIGENCE-BASED HYBRID ANOMALY DETECTION AND CLINICAL DECISION SUPPORT TECHNIQUES FOR AUTOMATED DETECTION OF CARDIOVASCULAR DISEASES AND COVID-19

A DISSERTATION SUBMITTED TO

THE GRADUATE SCHOOL OF ENGINEERING AND SCIENCE

OF BILKENT UNIVERSITY

IN PARTIAL FULFILLMENT OF THE REQUIREMENTS FOR

THE DEGREE OF

DOCTOR OF PHILOSOPHY

IN

ELECTRICAL AND ELECTRONICS ENGINEERING

By

Merve Begüm Terzi

October 2023

Artificial Intelligence-Based Hybrid Anomaly Detection and Clinical Decision Support Techniques for Automated Detection of Cardiovascular Diseases and COVID-19
By Merve Begüm Terzi
October 2023

We certify that we have read this dissertation and that in our opinion it is fully adequate, in scope and in quality, as a dissertation for the degree of Doctor of Philosophy.

Orhan Arıkan (Advisor)

Osman Eroğul

Ömer Morgül

Aykut Yıldız

Serkan Sarıtaş

Approved for the Graduate School of Engineering and Science:

Orhan Arıkan
Director of the Graduate School

ABSTRACT

ARTIFICIAL INTELLIGENCE-BASED HYBRID ANOMALY DETECTION AND CLINICAL DECISION SUPPORT TECHNIQUES FOR AUTOMATED DETECTION OF CARDIOVASCULAR DISEASES AND COVID-19

Merve Begüm Terzi
Ph.D. in Electrical and Electronics Engineering
Advisor: Orhan Arıkan
October 2023

Coronary artery diseases are the leading cause of death worldwide, and early diagnosis is crucial for timely treatment. To address this, we present a novel automated artificial intelligence-based hybrid anomaly detection technique composed of various signal processing, feature extraction, supervised, and unsupervised machine learning methods. By jointly and simultaneously analyzing 12-lead electrocardiogram (ECG) and cardiac sympathetic nerve activity (CSNA) data, the automated artificial intelligence-based hybrid anomaly detection technique performs fast, early, and accurate diagnosis of coronary artery diseases.

To develop and evaluate the proposed automated artificial intelligence-based hybrid anomaly detection technique, we utilized the fully labeled STAFF III and PTBD databases, which contain 12-lead wideband raw recordings non-invasively acquired from 260 subjects. Using the wideband raw recordings in these databases, we developed a signal processing technique that simultaneously detects the 12-lead ECG and CSNA signals of all subjects. Subsequently, using the pre-processed 12-lead ECG and CSNA signals, we developed a time-domain feature extraction technique that extracts the statistical CSNA and ECG features critical for the reliable diagnosis of coronary artery diseases. Using the extracted discriminative features, we developed a supervised classification technique based on artificial neural networks that simultaneously detects anomalies in the 12-lead ECG and CSNA data. Furthermore, we developed an unsupervised clustering technique based on the Gaussian mixture model and Neyman-Pearson criterion that performs robust detection of the outliers corresponding to coronary artery diseases.

By using the automated artificial intelligence-based hybrid anomaly detection

technique, we have demonstrated a significant association between the increase in the amplitude of CSNA signal and anomalies in ECG signal during coronary artery diseases. The automated artificial intelligence-based hybrid anomaly detection technique performed highly reliable detection of coronary artery diseases with a sensitivity of 98.48%, specificity of 97.73%, accuracy of 98.11%, positive predictive value (PPV) of 97.74%, negative predictive value (NPV) of 98.47%, and F_1-score of 98.11%. Hence, the artificial intelligence-based hybrid anomaly detection technique has superior performance compared to the gold standard diagnostic test ECG in diagnosing coronary artery diseases. Additionally, it outperformed other techniques developed in this study that separately utilize either only CSNA data or only ECG data. Therefore, it significantly increases the detection performance of coronary artery diseases by taking advantage of the diversity in different data types and leveraging their strengths. Furthermore, its performance is comparatively better than that of most previously proposed machine and deep learning methods that exclusively used ECG data to diagnose or classify coronary artery diseases. It also has a very short implementation time, which is highly desirable for real-time detection of coronary artery diseases in clinical practice.

The proposed automated artificial intelligence-based hybrid anomaly detection technique may serve as an efficient decision-support system to increase physicians' success in achieving fast, early, and accurate diagnosis of coronary artery diseases. It may be highly beneficial and valuable, particularly for asymptomatic coronary artery disease patients, for whom the diagnostic information provided by ECG alone is not sufficient to reliably diagnose the disease. Hence, it may significantly improve patient outcomes, enable timely treatments, and reduce the mortality associated with cardiovascular diseases.

Secondly, we propose a new automated artificial intelligence-based hybrid clinical decision support technique that jointly analyzes reverse transcriptase-polymerase chain reaction (RT-PCR) curves, thorax computed tomography images, and laboratory data to perform fast and accurate diagnosis of Coronavirus disease 2019 (COVID-19).

For this purpose, we retrospectively created the fully labeled Ankara University Faculty of Medicine COVID-19 (AUFM-CoV) database, which contains a wide variety of medical data, including RT-PCR curves, thorax computed tomography images, and laboratory data. The AUFM-CoV is the most comprehensive

database that includes thorax computed tomography images of COVID-19 pneumonia (CVP), other viral and bacterial pneumonias (VBP), and parenchymal lung diseases (PLD), all of which present significant challenges for differential diagnosis.

We developed a new automated artificial intelligence-based hybrid clinical decision support technique, which is an ensemble learning technique consisting of two preprocessing methods, long short-term memory network-based deep learning method, convolutional neural network-based deep learning method, and artificial neural network-based machine learning method. By jointly analyzing RT-PCR curves, thorax computed tomography images, and laboratory data, the proposed automated artificial intelligence-based hybrid clinical decision support technique benefits from the diversity in different data types that are critical for the reliable detection of COVID-19 and leverages their strengths.

The multi-class classification performance results of the proposed convolutional neural network-based deep learning method on the AUFM-CoV database showed that it achieved highly reliable detection of COVID-19 with a sensitivity of 91.9%, specificity of 92.5%, precision of 80.4%, and F_1-score of 86%. Therefore, it outperformed thorax computed tomography in terms of the specificity of COVID-19 diagnosis.

Moreover, the convolutional neural network-based deep learning method has been shown to very successfully distinguish COVID-19 pneumonia (CVP) from other viral and bacterial pneumonias (VBP) and parenchymal lung diseases (PLD), which exhibit very similar radiological findings. Therefore, it has great potential to be successfully used in the differential diagnosis of pulmonary diseases containing ground-glass opacities. The binary classification performance results of the proposed convolutional neural network-based deep learning method showed that it achieved a sensitivity of 91.5%, specificity of 94.8%, precision of 85.6%, and F_1-score of 88.4% in diagnosing COVID-19. Hence, it has comparable sensitivity to thorax computed tomography in diagnosing COVID-19.

Additionally, the binary classification performance results of the proposed long short-term memory network-based deep learning method on the AUFM-CoV database showed that it performed highly reliable detection of COVID-19 with a sensitivity of 96.6%, specificity of 99.2%, precision of 98.1%, and F_1-score of 97.3%. Thus, it outperformed the gold standard RT-PCR test in terms of the sensitivity of COVID-19 diagnosis.

Furthermore, the multi-class classification performance results of the proposed automated artificial intelligence-based hybrid clinical decision support technique on the AUFM-CoV database showed that it diagnosed COVID-19 with a sensitivity of 66.3%, specificity of 94.9%, precision of 80%, and F_1-score of 73%. Hence, it has been shown to very successfully perform the differential diagnosis of COVID-19 pneumonia (CVP) and other pneumonias. The binary classification performance results of the automated artificial intelligence-based hybrid clinical decision support technique revealed that it diagnosed COVID-19 with a sensitivity of 90%, specificity of 92.8%, precision of 91.8%, and F_1-score of 90.9%. Therefore, it exhibits superior sensitivity and specificity compared to laboratory data in COVID-19 diagnosis.

The performance results of the proposed automated artificial intelligence-based hybrid clinical decision support technique on the AUFM-CoV database demonstrate its ability to provide highly reliable diagnosis of COVID-19 by jointly analyzing RT-PCR data, thorax computed tomography images, and laboratory data. Consequently, it may significantly increase the success of physicians in diagnosing COVID-19, assist them in rapidly isolating and treating COVID-19 patients, and reduce their workload in daily clinical practice.

Keywords: Big data, artificial intelligence, machine learning, deep learning, transfer learning, ensemble learning, computer-aided diagnosis, signal processing, image processing, feature extraction, classification, clustering, convolutional neural network, recurrent neural network, long short-term memory, anomaly detection, Gaussian mixture model, synthetic minority oversampling technique (SMOTE), Neyman-Pearson hypothesis testing, COVID-19, radiology, computed tomography.

ÖZET

YAPAY ZEKÂ-TABANLI HİBRİT ANOMALİ TESPİT VE KLİNİK KARAR DESTEK TEKNİKLERİ İLE KARDİYOVASKÜLER HASTALIKLARIN VE COVID-19'UN OTOMATİK TESPİTİ

Merve Begüm Terzi
Elektrik ve Elektronik Mühendisliği, Doktora
Tez Danışmanı: Orhan Arıkan
Ekim 2023

Koroner arter hastalıkları, dünya çapında ölümlerin başlıca nedenidir ve zamanında tedavi için erken teşhis çok önemlidir. Bu sorunu ele almak amacıyla, çeşitli sinyal işleme, öznitelik çıkarma, denetimli, ve denetimsiz makine öğrenmesi yöntemlerini birleştiren yeni bir otomatik yapay zekâ-tabanlı hibrit anomali tespit tekniği öneriyoruz. Otomatik yapay zekâ-tabanlı hibrit anomali tespit tekniği, 12-derivasyonlu elektrokardiyogram (EKG) ve kardiyak sempatik sinir aktivitesi (KSSA) verilerini birlikte ve eş zamanlı analiz ederek, koroner arter hastalıklarının hızlı, erken, ve doğru teşhisini gerçekleştirmektedir.

Önerilen otomatik yapay zekâ-tabanlı hibrit anomali tespit tekniğini geliştirmek ve değerlendirmek için, 260 denekten non-invaziv olarak elde edilen 12-derivasyonlu geniş bantlı ham kayıtları içeren tamamen-etiketlenmiş STAFF III ve PTBD veri tabanlarını kullandık. Bu veri tabanlarındaki geniş bantlı ham kayıtları kullanarak, tüm deneklerin 12-derivasyonlu EKG ve KSSA sinyallerini eş zamanlı olarak tespit eden bir sinyal işleme tekniği geliştirdik. Ön-işlenmiş 12-derivasyonlu EKG ve KSSA sinyallerini kullanarak, koroner arter hastalıklarının güvenilir teşhisi için kritik olan istatistiksel EKG ve KSSA özniteliklerini elde eden bir zaman-düzlemi öznitelik çıkarma tekniği geliştirdik. Elde edilen ayırt edici öznitelikleri kullanarak, 12-derivasyonlu EKG ve KSSA verilerindeki anomalileri eş zamanlı olarak tespit eden yapay sinir ağı-tabanlı bir denetimli sınıflandırma tekniği geliştirdik. Ayrıca, koroner arter hastalıklarını temsil eden aykırı değerlerin gürbüz tespitini gerçekleştiren, Gauss karışım modeline ve Neyman-Pearson kriterine dayalı bir denetimsiz kümeleme tekniği geliştirdik.

Otomatik yapay zekâ-tabanlı hibrit anomali tespit tekniğini kullanarak, koroner arter hastalığı sırasında KSSA sinyalinin genliğindeki artış ile EKG sinyalindeki anomaliler arasında önemli bir ilişki olduğunu gösterdik. Otomatik yapay zekâ-tabanlı hibrit anomali tespit tekniği, 98.48% duyarlılık, 97.73% özgüllük, 98.11% doğruluk, 97.74% kesinlik, 98.47% negatif tahmin değeri, ve 98.11% F_1-skoru ile koroner arter hastalıklarının oldukça güvenilir tespitini gerçekleştirmiştir. Bu nedenle, yapay zekâ-tabanlı hibrit anomali tespit tekniği, koroner arter hastalıklarını teşhis etmek için altın standart tanı testi olarak kullanılan EKG'ye kıyasla daha üstün başarım göstermiştir. Ayrıca, yapay zekâ-tabanlı hibrit anomali tespit tekniği, bu çalışmada geliştirilen ve sadece KSSA verilerini veya sadece EKG verilerini kullanan diğer tekniklerden daha üstün başarım göstermiştir. Bu nedenle, farklı veri türlerinin çeşitliliğinden faydalanarak ve güçlü yönlerini kullanarak, koroner arter hastalıklarının tespit başarımını önemli ölçüde arttırmıştır. Ayrıca, yapay zekâ-tabanlı hibrit anomali tespit tekniğinin başarımı, koroner arter hastalıklarını teşhis etmek veya sınıflandırmak için yalnızca EKG verilerini kullanmış olan literatürdeki birçok makine öğrenmesi ve derin öğrenme yöntemlerinin başarımından daha üstündür. Ek olarak, klinik ortamlarda gerçek-zamanlı koroner arter hastalığı tespiti için oldukça arzu edilen çok kısa bir uygulama süresine sahiptir.

Önerilen otomatik yapay zekâ-tabanlı hibrit anomali tespit tekniği, koroner arter hastalıklarının hızlı, erken, ve doğru teşhisi konusunda doktorların başarısını arttıran etkili bir karar destek sistemi olarak hizmet edebilir. Özellikle EKG tarafından sağlanan teşhis bilgilerinin, hastalığın güvenilir teşhisi için tek başına yeterli olmadığı asemptomatik koroner arter hastaları açısından oldukça faydalı ve değerli olabilir. Bu nedenle, hasta sonuçlarını önemli ölçüde iyileştirebilir, zamanında tedavilere olanak sağlayabilir ve kardiyovasküler hastalıkların mortalitesini azaltabilir.

İkinci olarak, Koronavirüs hastalığının (COVID-19) hızlı ve doğru teşhisini gerçekleştirmek için ters transkriptaz-polimeraz zincir reaksiyonu (RT-PCR) eğrilerini, toraks bilgisayarlı tomografi görüntülerini, ve laboratuvar verilerini birlikte analiz eden yeni bir otomatik yapay zekâ-tabanlı hibrit klinik karar destek tekniği öneriyoruz.

Bu amaçla, tamamen-etiketlenmiş Ankara Üniversitesi Tıp Fakültesi COVID-19 (AÜTF-CoV) veri tabanını geriye dönük olarak oluşturduk. AÜTF-CoV veri tabanı, RT-PCR eğrileri, toraks bilgisayarlı tomografi görüntüleri, ve laboratuvar

verileri de dahil olmak üzere çok çeşitli tıbbi veriler içermektedir. AÜTF-CoV veri tabanı, COVID-19 pnömonisi (CVP), diğer viral ve bakteriyel pnömoniler (VBP), ve parankimal akciğer hastalıkları (PAH) gibi ayırıcı tanısı çok zor olan toraks bilgisayarlı tomografi görüntülerini içeren en kapsamlı veri tabanıdır.

İki ön-işleme yöntemi, uzun kısa-süreli bellek ağı-tabanlı derin öğrenme yöntemi, evrişimsel sinir ağı-tabanlı derin öğrenme yöntemi ve yapay sinir ağı-tabanlı makine öğrenmesi yönteminden oluşan bir topluluk öğrenmesi tekniği olan yeni bir otomatik yapay zekâ-tabanlı hibrit klinik karar destek tekniği geliştirdik. Önerilen otomatik yapay zekâ-tabanlı hibrit klinik karar destek tekniği, RT-PCR eğrilerini, toraks bilgisayarlı tomografi görüntülerini, ve laboratuvar verilerini birlikte analiz ederek, COVID-19'un güvenilir tespiti için kritik olan farklı veri türlerinin çeşitliliğinden ve güçlü yönlerinden faydalanmaktadır.

Önerilen evrişimsel sinir ağı-tabanlı derin öğrenme yönteminin AÜTF-CoV veri tabanı üzerindeki çok-sınıflı sınıflandırma başarım sonuçları, yöntemin 91.9% duyarlılık, 92.5% özgüllük, 80.4% kesinlik, ve 86% F_1-skoru ile COVID-19'un oldukça güvenilir tespitini sağladığını göstermiştir. Bu nedenle, COVID-19 teşhisinin özgüllüğü bakımından toraks bilgisayarlı tomografiye kıyasla daha üstün başarım göstermiştir. Ayrıca, evrişimsel sinir ağı-tabanlı derin öğrenme yönteminin, radyolojik bulguları çok benzer olan COVID-19 pnömonisini (CVP), diğer viral ve bakteriyel pnömonileri (VBP), ve parenkimal akciğer hastalıklarını (PAH) çok yüksek başarım ile ayırt ettiği gösterilmiştir. Bu nedenle, cam opasitelerini içeren akciğer hastalıklarının ayırıcı tanısında yüksek başarım ile kullanılma potansiyeline sahiptir. Önerilen evrişimsel sinir ağı-tabanlı derin öğrenme yönteminin iki-sınıflı sınıflandırma başarım sonuçları, yöntemin COVID-19 teşhisinde 91.5% duyarlılık, 94.8% özgüllük, 85.6% kesinlik, ve 88.4% F_1-skoru elde ettiğini göstermiştir. Bu nedenle, COVID-19 teşhisinde toraks bilgisayarlı tomografi ile karşılaştırılabilir duyarlılığa sahiptir.

Ayrıca, önerilen uzun kısa-süreli bellek ağı-tabanlı derin öğrenme yönteminin AÜTF-CoV veri tabanı üzerindeki iki-sınıflı sınıflandırma başarım sonuçları, yöntemin 96.6% duyarlılık, 99.2% özgüllük, 98.1% kesinlik, ve 97.3% F_1-skoru ile COVID-19'un oldukça güvenilir tespitini sağladığını göstermiştir. Bu nedenle, COVID-19 teşhisinin duyarlılığı bakımından altın standart RT-PCR testine kıyasla daha üstün başarım göstermiştir.

Önerilen otomatik yapay zekâ-tabanlı hibrit klinik karar destek tekniğinin AÜTF-CoV veri tabanı üzerindeki çok-sınıflı sınıflandırma başarım sonuçları,

tekniğin 66.3% duyarlılık, 94.9% özgüllük, 80% kesinlik, ve 73% F_1-skoru ile COVID-19'u teşhis ettiğini göstermiştir. Bu durum, hibrit klinik karar destek tekniğinin, COVID-19 pnömonisini (CVP) ve diğer pnömonileri çok başarılı bir şekilde ayırt edebildiğini göstermektedir. Otomatik yapay zekâ-tabanlı hibrit klinik karar destek tekniğinin iki-sınıflı sınıflandırma başarım sonuçları, tekniğin 90% duyarlılık, 92.8% özgüllük, 91.8% kesinlik, ve 90.9% F_1-skoru ile COVID-19'un oldukça gürbüz tespitini sağladığını göstermiştir. Bu nedenle, hibrit klinik karar destek tekniği, COVID-19 teşhisinde laboratuvar verilerine kıyasla daha üstün duyarlılığa ve özgüllüğe sahiptir.

Önerilen otomatik yapay zekâ-tabanlı hibrit klinik karar destek tekniğinin AÜTF-CoV veri tabanı üzerindeki başarım sonuçları, tekniğin RT-PCR verilerini, toraks bilgisayarlı tomografi görüntülerini ve laboratuvar verilerini birlikte analiz ederek, oldukça güvenilir COVID-19 teşhisi sağladığını göstermektedir. Sonuç olarak, önerilen teknik, doktorların COVID-19'u teşhis etme başarısını önemli ölçüde artırabilir, COVID-19 hastalarını hızlı izole etme ve tedavi etme konusunda onlara yardımcı olabilir ve günlük klinik uygulamadaki iş yüklerini azaltabilir.

Anahtar sözcükler: Büyük veri, yapay zekâ, makine öğrenmesi, derin öğrenme, transfer öğrenme, topluluk öğrenmesi, bilgisayar destekli tanı, sinyal işleme, görüntü işleme, öznitelik çıkarımı, sınıflandırma, kümeleme, evrişimsel sinir ağı, tekrarlayan sinir ağı, uzun kısa-süreli bellek, anomali tespiti, Gauss karışım modeli, sentetik azınlık aşırı örnekleme tekniği (SMOTE), Neyman-Pearson hipotez testi, COVID-19, radyoloji, bilgisayarlı tomografi.

Acknowledgement

First and foremost, I would like to express my deepest gratitude to my advisor, Prof. Orhan Arıkan, for his invaluable supervision and continuous support in the development of my Ph.D. thesis. I express my heartfelt thanks to him for encouraging me to develop as a scientist and researcher.

I am grateful to the members of my Thesis Tracking Committee, the Associate Provost, Assoc. Prof. Emine Ülkü Sarıtaş Çukur; and Prof. Çiğdem Gündüz Demir, for their supervision and suggestions during the completion of my Ph.D. thesis.

I am also grateful to Prof. Osman Eroğul, Prof. Ömer Morgül, Asst. Prof. Aykut Yıldız, and Asst. Prof. Serkan Sarıtaş for accepting to review this thesis, serving as jury members, and dedicating their precious time to provide extremely valuable feedback on my Ph.D. thesis.

I greatly appreciate the support I have received from the Vice President of the Board of Trustees, Prof. Abdullah Atalar; the Rector, Prof. Kürşat Aydoğan; the Director of the Graduate School of Engineering and Science, Prof. Orhan Arıkan; the Provost, Prof. Orhan Aytür; and the Vice Rector for Student Affairs, Prof. Ezhan Karaşan; during the process of obtaining my Ph.D. degree. I would also like to thank all the faculty members who have supported, encouraged, and motivated me during my graduate studies. Additionally, I would like to thank İpek Sultan Sürücü, the administrative assistant at the Graduate School.

I am thankful for the unwavering support of Bilkent University Department of Electrical and Electronics Engineering throughout my Ph.D. studies. I would like to express my special thanks to the department chair, Prof. Tolga Mete Duman, and the administrative assistants Aydan Eren, Armağan Gürsoy, and Funda Bülbül for their assistance with academic and administrative issues.

I would like to thank the faculty members Prof. Tolga Mete Duman, Prof. Orhan Arıkan, Prof. Sinan Gezici, and Asst. Prof. Muhammed Ömer Sayın, as well as the members of Bilkent University IEEE Student Branch for their

support in organizing the Graduate Research Conference (GRC) from 2018 to 2023, during which I served as the GRC Vice Chair.

I would like to thank faculty member Prof. Nail Akar for his support in granting me the authority to coordinate the GE 304-Technology, Society, and Professional Development Seminar course from 2018 to 2023. Moreover, I would like to thank faculty member Dr. Mehmet Alper Kutay for his trust in me and his support in entrusting me with all responsibilities related to this course.

I appreciate the financial support I received from the Scientific and Technological Research Council of Turkey (TÜBİTAK) Directorate of Science Fellowships and Grant Programmes (BİDEB) through the 2211-C National Ph.D. Scholarship Program in the Priority Fields in Science and Technology during my Ph.D. studies.

Furthermore, I appreciate the financial support I received from the Scientific and Technological Research Council of Turkey (TÜBİTAK) Research Support Programs Presidency (ARDEB) through the Scientific and Technological Research Projects Support Program (1001) during my Ph.D. studies.

Additionally, I appreciate the financial support I received from the Health Institutes of Turkey (TÜSEB) through the Strategic Research and Development Projects Support Program during my Ph.D. studies (Grant Number: 2020-CV-01).

Some of the content presented in this thesis is published in Biomedical Engineering/Biomedizinische Technik (BMT) and is reproduced with permission from De Gruyter [1].

Last but not least, I am grateful to my mother (Şeyda Terzi), my father (Haluk Terzi), and my brother (Miray Terzi) for their unconditional love and endless support throughout my Ph.D. studies and my life in general. I also sincerely thank my cat Misha for being my most loyal friend and for loving me unconditionally. I feel very fortunate to be a part of this family.

Dedicated to my beloved family and
my loyal feline companion Misha,
with profound love and enduring gratitude....

Contents

List of Figures

List of Tables

Chapter 1

Introduction

According to the World Health Organization (WHO), cardiovascular diseases (cardiovascular diseases) are the leading cause of death worldwide, with an estimated death rate of approximately 17.9 million deaths each year, accounting for 31% of all deaths worldwide annually [2]. The majority of these deaths are caused by coronary artery diseases (coronary artery diseases), which include myocardial ischemia, silent (asymptomatic) myocardial ischemia, and myocardial infarction (heart attack).

In patients with coronary artery diseases, significant anomalies occur in the ST segment, QRS complex, and T wave of the electrocardiogram (ECG) signals during myocardial ischemia and myocardial infarction [1, 3, 4, 5, 6, 7, 8, 9, 10, 11, 12]. However, a considerable number of coronary artery disease patients worldwide suffer from silent (asymptomatic) myocardial ischemia, during which there are no anomalies in patients' ECG signals. Thus, an ECG signal that does not contain any anomalies does not rule out the possibility of coronary artery diseases. Due to its limitations in diagnosing asymptomatic coronary artery disease patients with silent (asymptomatic) myocardial ischemia, ECG alone cannot be used to diagnose silent (asymptomatic) myocardial ischemia based solely on its diagnostic information. Since asymptomatic coronary artery disease patients with silent (asymptomatic) myocardial ischemia do not experience any symptoms, they are

prone to misinterpretation by cardiologists, which leads to false-negative results, making silent (asymptomatic) myocardial ischemia more dangerous and fatal.

Moreover, previous artificial intelligence (AI) studies that exclusively used ECG data to diagnose or classify coronary artery diseases may have significant limitations for asymptomatic coronary artery disease patients with silent (asymptomatic) myocardial ischemia [13]. Thus, an automated AI technique that can accurately and quickly diagnose both asymptomatic coronary artery disease patients (silent (asymptomatic) myocardial ischemia) and symptomatic coronary artery disease patients (myocardial ischemia and myocardial infarction) is a major and essential clinical need that may significantly increase the detection performance of cardiovascular diseases, provide timely treatment, and reduce mortality rates.

Previous studies have shown that the sympathetic nervous system plays an important role in regulating the cardiovascular system [14, 15]. These studies have established a direct and strong relationship between the sympathetic nervous system and various cardiovascular diseases, which is due to the fact that the extensions of the sympathetic nervous system that regulate the heart are distributed throughout the heart. The traditional method for directly recording and monitoring high-frequency signals, including activities of the sympathetic nervous system, is the microneurography technique, which requires invasive procedures, such as inserting very fine microelectrodes into the nerve fibers to detect and measure their electrical signals. However, the invasive and complex nature of the microneurography technique, which requires highly specialized expertise from trained clinicians, greatly limits its utilization for research studies in clinical practice.

Recent studies have shown that it is possible to non-invasively record high-frequency signals, called cardiac sympathetic nerve activity (CSNA), from the skin surface of the chest using data acquisition equipment with a wide frequency bandwidth and high sampling rate [14, 16, 17, 18]. A few studies investigating the relationship between CSNA and cardiac arrhythmias using signal processing techniques demonstrated an increase in the amplitude of CSNA during cardiac

arrhythmias [17, 18, 19]. Additionally, they indicated that this increase in CSNA was accompanied by a simultaneous increase in heart rate in the ECG signal. Therefore, they suggested that early and reliable diagnosis of cardiac arrhythmias can be achieved by detecting the anomalies in CSNA. However, none of these previous studies used AI techniques to diagnose cardiac arrhythmias using only CSNA data or both CSNA and ECG data.

Since it has long been accepted that there is a direct and strong relationship between the sympathetic nervous system and various cardiovascular diseases [14, 15], we hypothesized that there can be anomalies in CSNA during coronary artery diseases. To the best of our knowledge, there are no studies in the literature to date that have investigated whether there is an association between CSNA and coronary artery diseases using AI techniques. This constituted a research gap in the literature that highlights the need for further investigation. Additionally, most of the existing AI studies have only used ECG data to detect various cardiovascular diseases. However, there are no studies to date that have proposed an AI technique that jointly and simultaneously uses CSNA and ECG data to diagnose coronary artery diseases or other cardiovascular diseases.

The main aim and motivation of this study were to develop an automated AI technique that accurately diagnoses both asymptomatic coronary artery disease patients (silent (asymptomatic) myocardial ischemia) and symptomatic coronary artery disease patients (myocardial ischemia and myocardial infarction) by jointly and simultaneously analyzing 12-lead CSNA and ECG data [1]. Hence, this technique aims to address the limitations of existing related studies that have only used ECG data and fill the research gaps in the literature. For this purpose, we propose a novel artificial intelligence-based hybrid anomaly detection technique consisting of various signal processing, feature extraction, supervised, and unsupervised machine learning methods that jointly and simultaneously analyzes 12-lead CSNA and ECG data to perform fast, early, and accurate diagnosis of coronary artery diseases (i.e., silent (asymptomatic) myocardial ischemia, myocardial ischemia, and myocardial infarction).

By using the proposed automated artificial intelligence-based hybrid anomaly

detection technique, our aim was to investigate whether anomalies exist in CSNA signals during coronary artery diseases [1]. Moreover, our objective was to determine whether the joint and simultaneous detection of the anomalies in the 12-lead CSNA and ECG data provides an increase in the performance of coronary artery disease diagnosis. Furthermore, we also targeted to compare the performance of the artificial intelligence-based hybrid anomaly detection technique with that of the gold standard diagnostic test ECG, as well as previously proposed AI methods that have only used ECG data to diagnose or classify coronary artery diseases.

1.1 Main Contributions of the Thesis

The main contributions and novelty in Chapter 2 are summarized as follows:

- We have developed the first automated artificial intelligence-based hybrid anomaly detection technique consisting of various signal processing, feature extraction, supervised, and unsupervised machine learning methods that jointly and simultaneously analyze 12-lead ECG and CSNA data to perform fast, early, and accurate diagnosis of coronary artery diseases.

- Our study is the first to demonstrate that there are anomalies in CSNA signals during coronary artery diseases. Additionally, we have shown a significant association between the increase in CSNA and the anomalies in ECG signals during coronary artery diseases.

- The proposed artificial intelligence-based hybrid anomaly detection technique outperforms other techniques developed in this study that separately use either only CSNA data or only ECG data. Therefore, it significantly increases the detection performance of coronary artery diseases by benefiting from the diversity in different data types and leveraging their strengths.

- The artificial intelligence-based hybrid anomaly detection technique can automatically process all 12-leads for enhanced diagnosis. Therefore, it takes advantage of the diversity in diagnostic information provided by all

12-leads and can accurately detect coronary artery disease cases that cannot be diagnosed using only one-lead.

- The automated artificial intelligence-based hybrid anomaly detection technique demonstrates superior performance compared to the gold standard diagnostic test ECG in the diagnosis of coronary artery diseases.
- The performance of the artificial intelligence-based hybrid anomaly detection technique is higher than that of most previously proposed machine or deep learning methods that have only used ECG data to diagnose or classify coronary artery diseases.
- The artificial intelligence-based hybrid anomaly detection technique has a very short implementation time, which is highly desirable for real-time detection of coronary artery diseases. This capability may support fast decision-making by physicians in clinical settings, which may have significant implications in emergency situations where rapid diagnosis is crucial for timely patient treatment.

1.2 Literature Review

We conducted a comprehensive review of the existing relevant literature to gain an in-depth understanding of the current machine learning techniques applied to ECG signals and images for the diagnosis and classification of cardiovascular diseases. In the literature, various machine learning and deep learning methods have been previously proposed for the diagnosis and classification of various cardiovascular diseases using only ECG data. The feature extraction methods can be categorized into three groups, which are time-domain techniques, frequency-domain techniques, and time-frequency domain techniques. Specifically, these techniques include Fourier transform [20, 21], wavelet transform [22, 23, 24, 25], Gabor transform [26, 27], discrete cosine transform [28, 29, 30], shearlet and contourlet transform [31, 32], Hilbert-Huang transform [33, 34], discrete orthogonal Stockwell transform [30, 35], empirical and variational mode

decompositions [36, 37], Wigner-Ville distribution technique [38], Fourier-Bessel series expansion [39, 40, 41], and independent and principal component analyses [19, 26, 42, 43, 44, 45].

The previously proposed machine learning methods for the diagnosis and classification of various cardiovascular diseases using only ECG data include logistic regression [46, 47], artificial neural network [7, 8, 9, 10, 11, 25, 46, 48], k-nearest neighbor [41, 49], hidden Markov model [50, 51], Gaussian mixture model [6, 8, 10, 11, 43, 48, 50, 52, 53], support vector machine [3, 5, 6, 42, 54, 55, 56, 57, 58, 59], random forest [60, 61], naive Bayes [43, 59], decision tree [59, 62, 63], fuzzy logic [64, 65], self-organizing map [64, 66], mixture of experts [67, 68], association rule learning [69, 70], and linear discriminant analysis [22, 71].

The study by Magrans et al. aimed to develop a non-linear support vector machine model with a radial basis function (RBF) kernel to detect coronary artery disease [72]. The study included patients undergoing elective percutaneous coronary intervention with 12-lead continuous and signal-averaged ECG recordings before and during percutaneous coronary intervention. Feature selection was performed using a univariate statistical test and an algorithm for sequentially selecting the most important statistically significant variables. The grid search method was employed to optimize support vector machine parameters and generate the final prediction model. Repeated 5-fold cross-validation was used to estimate the model's generalization performance. The model exhibited a sensitivity of 83.3%, specificity of 91.7%, precision of 90.9%, and negative predictive value (NPV) of 85.7%.

Sadhukhan et al. proposed using the harmonic phase distribution pattern of ECG data for myocardial infarction identification [73]. The morphological and temporal changes in the ECG waveform caused by the presence of myocardial infarction were reflected in the phase distribution pattern of the Fourier harmonics. The changes in the ECG waveform morphology were clearly manifested as changes in the relative phases of the harmonic components. Two discriminative features that reflected these variations were identified for 3-lead ECG. Binary

classification was performed using a threshold-based classification rule and logistic regression. The model achieved an accuracy of 95.6%, sensitivity of 96.5%, and specificity of 92.7%. The algorithm was then implemented and validated on a commercially available microcontroller-based Arduino board. The firmware used the pre-trained logistic regression classifier. The model did not outperform all earlier reported techniques, but it offers computational simplicity of the features, reduced feature dimensionality, and the use of simple linear classifiers. The drawback of this study is the use of only 3-lead ECG, which can limit the detection performance for certain types of myocardial infarction.

Tripathy et al. proposed an approach for the detection of myocardial infarction using multi-resolution analysis of 12-lead ECG signals [74]. Baseline wander noise in ECG data was filtered out using a high-pass filter. The filtered ECG data was segmented using a rectangular window. The segmented ECG frames were subjected to Fourier-Bessel series expansion-based empirical wavelet transform for the time-scale decomposition of the 12-lead ECG signals. For each ECG lead, nine subband signals were evaluated using Fourier-Bessel series expansion-based empirical wavelet transform to extract the statistical features. The deep layer least-squares support vector machine classification layer, which was formulated using the hidden layers of sparse auto-encoders and the least-squares support vector machine, was employed for the detection of myocardial infarction based on the feature vector of the 12-lead ECG. The entropy features were found to be more significant for the detection of myocardial infarction and exhibited higher performance using the proposed classifier compared to the kurtosis and skewness features, which failed to capture the pathological variations in the subband signals. The combination of Fourier-Bessel series expansion-based empirical wavelet transform based entropy features and deep layer least-squares support vector machine reached an accuracy of 99.7%, sensitivity of 99.8%, and specificity of 99.6%.

Dohare et al. proposed a method for detecting coronary artery disease using 12-lead ECG data and analyzed each lead with the help of a composite lead [54]. The min-max normalization method was used to rescale the attributes. The raw signal was preprocessed by a two stage median filter to remove baseline drift using a sliding window. The composite lead was used to detect ECG wave components

and clinical wave intervals. The complexes of the composite signal were enhanced using the sixth power of the signal. The mean value of the enhanced signal was used as the threshold to determine the high peak of the QRS complex in the composite signal and individual leads at a variable window size. The four clinical ECG features were determined globally from the average beats of the 12-lead ECGs. Peak-to-peak amplitude, area, mean, standard deviation, skewness, and kurtosis were determined for the ECG features. Binary classification for the detection of coronary artery disease was performed using a simple support vector machine classifier with an RBF kernel. After implementing principal component analysis as a feature dimension reduction method to reduce the number of features and computational complexity, the sensitivity remained the same (96.6%), while the specificity (96.6%), and accuracy (96.6%) were slightly reduced.

Ahmad et al. proposed two computationally efficient multimodal fusion frameworks for myocardial infarction detection, called Multimodal Image Fusion (MIF) and Multimodal Feature Fusion (MFF) [75]. At the input of these frameworks, they converted the raw ECG data into three types of two-dimensional (2D) images using three different statistical methods, which are Gramian Angular Field (GAF), Recurrence Plot (RP), and Markov Transition Field (MTF). In MIF, they performed image fusion by combining three grayscale input images (GAF, RP, MTF) to create a three-channel colored single image, which served as input to the convolutional neural network. They utilized the AlexNet convolutional neural network for feature extraction and a softmax classifier for classification tasks, respectively. The limitation of the MIF framework was that it required exactly three different statistical grayscale images to create a three-channel compound image. In MFF, they transformed ECG heartbeats into GAF, RP, and MTF images. They extracted features from the penultimate layer of the AlexNet convolutional neural network, which consisted of three convolutional layers, two pooling layers, and one fully connected layer. By employing a Gated Fusion Network (GFN), they fused these extracted features, which were ultimately used to train a support vector machine classifier. MFF demonstrated higher performance compared to MIF. However, the limitation of the MFF framework was that it required the use of three separate AlexNet convolutional neural networks

for training on the GAF, RP, and MTF images, which necessitated more time for both training and inference. The support vector machine classifier performed better than the softmax classifier. They achieved a classification accuracy of 98.4%, sensitivity of 94%, and precision of 98%. They concluded that the multimodal fusion of the modalities increased the machine learning task's performance compared to using the modalities individually. The disadvantage of this study is the use of only one-lead ECG, which can limit the detection performance for certain types of myocardial infarction.

Acharya et al. introduced a method for the automated detection and localization of myocardial infarction [76]. Firstly, ECG signals were pre-processed to eliminate noise and baseline wander using a wavelet basis function. Using the Pan–Tompkins algorithm, the pre-processed ECG signals were segmented and subjected to discrete wavelet transform up to four levels of decomposition. Thus, a total of eight discrete wavelet transform coefficients were obtained, and twelve nonlinear features were extracted from these coefficients. Feature ranking methods, such as Student's t-test and ANOVA, were used to rank the extracted features according to their significance. The selected significant features were used for binary and multi-class classification using a k-nearest neighbor classifier for the detection and localization of myocardial infarction, respectively. The ranked features were fed into the k-nearest neighbor classifier one by one to find the minimum number of features necessary for obtaining the highest classification performance. The classifier exhibited an average accuracy of 98.8%, sensitivity of 99.4%, and specificity of 96.2% for myocardial infarction detection. They claimed that the method can be used as an automated diagnostic tool for the detection of myocardial infarction using 12-lead ECG and the localization of myocardial infarction using one-lead ECG.

Sharma et al. presented a technique for the detection and localization of myocardial infarction using one-lead ECG [49]. Firstly, the ECG signals were segmented into short-duration ECG segments, which were then passed through a two-stage median filter to remove baseline wander. This was followed by a Savitzky-Golay filter to obtain smoothened ECG segments, which were decomposed into wavelet bands using stationary wavelet transform (SWT), so that

they could be analyzed at different frequencies. Energy, entropy, and slope-based features were extracted at specific wavelet bands from the decomposed ECG segments. The relevance of the features was measured based on the Fisher score. The top-ranked features were fed into the k-nearest neighbor classifier with Mahalanobis and Euclidean distance functions to perform binary classification for myocardial infarction detection. To address the issue of imbalanced data, the adaptive synthetic (ADASYN) sampling approach was employed due to disparities in the instance space. They utilized 10-fold cross-validation for both myocardial infarction detection and localization. The technique has demonstrated a sensitivity of 98.3%, specificity of 99.4%, precision of 99.4% and accuracy of 99% for myocardial infarction detection using the top-ranked features. The drawback of this study is the use of only one-lead ECG, which can limit the detection and localization performance for certain types of myocardial infarction.

Jothiramalingam et al. proposed a polynomial curve-fitting technique based on optimization strategies to diagnose coronary artery disease [77]. Firstly, the noises in ECG signals were removed using a discrete wavelet transform. The ECG signals were then partitioned using a Hamming window. The polynomial coefficients were obtained by choosing the best polynomial order using the genetic algorithm and particle swarm optimization algorithm. Using these polynomial coefficients, five features were computed, including area, variance, kurtosis, root mean, and form factor. These features were input into different classifiers for binary classification, such as multilayer perceptron, support vector machine, K-nearest neighbor, Levenberg–Marquardt Neural Network, and Scaled Conjugate Gradient Backpropagation Neural Network. The genetic algorithm and particle swarm optimization-based classifiers achieved good performances compared to classifiers that were not based on genetic algorithm and particle swarm optimization. The highest classification performance was achieved using the k-nearest neighbor classifier, with a sensitivity of 77.4%, specificity of 81.8%, and accuracy of 82.8%.

Sraitih et al. investigated an automatic coronary artery disease detection system using ECG data and presented an approach to evaluate its robustness in

classifying coronary artery disease under different types of noise [78]. The preprocessing stage consisted of normalizing 12-lead ECG signals using the min–max normalization method. They used a low-pass Butterworth filter to remove the noises from the ECG data. They employed three well-known supervised machine learning models, which are support vector machine, k-nearest neighbor, and random forest. They tested their performances in classifying normal and coronary artery disease classes. These models were trained on the preprocessed data, and no feature extraction was performed. They conducted a grid search on each model by supplying a mixture of parameter grids to obtain the appropriate combinations of hyper-parameters that provide the most accurate predictions. The performances of all the models in detecting coronary artery disease were low, especially in detecting the normal class samples. Random forest obtained the best performance in predicting coronary artery disease with an accuracy of 75%, precision of 74%, and sensitivity of 73%. While dealing with the noisy test set, the support vector machine classifier outperformed the other models with an accuracy of 68%, precision of 66%, and sensitivity of 66%.

Agrawal et al. investigated the application of machine learning techniques on the vector magnitude data of heart signals generated via vectorcardiography to distinguish coronary artery disease patients from healthy subjects [79]. To eliminate low-frequency noise in cardiac signals, the patients' vectorcardiography data were filtered using a bandpass filter via Biopac Acqknowledge software's built-in functions. The vector magnitude was derived from patients' orthogonal vectorcardiography leads using the 3D Pythagorean theorem. Each patient's QT and RR intervals were marked on the vector magnitude using Biopac Acqknowledge software's computer-assisted manual marking methods. The statistical features were extracted from the QT and RR intervals and used as inputs for machine learning techniques, such as artificial neural network, support vector machine with RBF kernel, and decision tree, to perform binary classification. Stratified 10-fold cross-validation was employed for all models. Results indicated that vector magnitude-derived QT variability has more predictive value than RR variability in classifying coronary artery disease patients, and showed a higher contribution toward increased accuracy in predicting the class. However, adding

the RR variability to obtain combined variables further improved the overall performance. The decision tree generated relatively higher performance for coronary artery disease classification with an accuracy of 98.3% and specificity of 96.5%, while using fewer predictor variables than other models. IBM SPSS Modeler and KNIME were employed as the software platforms.

Liu et al. proposed an ECG feature for coronary artery disease detection by fitting a given ECG signal with a 20th-order polynomial function, which they defined as PolyECG-S [80]. First, a discrete wavelet transform was employed to remove high-frequency noise and baseline shifting from the ECG signals. Next, all the R peaks in the ECG signals were detected using the wavelet transform, and all the ECG signals were split into ECG cycles. These cycles were then normalized on both the time and voltage axes to enable comparison between different ECG signals. The polynomial function was fitted to the ECG signals, and each ECG cycle was represented as a vector of the coefficients of this polynomial function. The Akaike information criterion (AIC) was used to determine the optimal polynomial fitting function order with the minimum AIC value. The optimal similarity between the PolyECG-S curve and ECG signals was observed when the polynomial fitting function order was set to 20. The fitted coefficients were defined as the ECG representing features. The best feature subsets were selected using feature selection algorithms, such as genetic algorithm and particle swarm optimization. There were seventeen features chosen by genetic algorithm and seven features chosen by particle swarm optimization. The two feature subsets chosen by genetic algorithm and particle swarm optimization were tested for their discrimination performance with four classification models, which are J48 decision tree, random tree, support vector machine, and naive Bayes. The feature selection and binary classification models were implemented using the Weka software, and the software's default parameters were utilized. The top-performing coronary artery disease detection model was the J48 decision tree with the feature subset chosen by genetic algorithm, which showed an accuracy of 89.5%, sensitivity of 94.2%, and specificity of 74%. The disadvantage of this study is that, although different individuals may have different optimal polynomial fitting functions for their ECG signals, the polynomial fitting function's order was set

to be the same for all individuals.

Chang et al. presented a diagnosis system for classifying coronary artery disease by converting 4-lead ECG data into a density model [81]. During ECG signal segmentation, the location of the R peak was used to divide the ECG complex into separate heartbeats. A hybrid system that combined hidden Markov model and Gaussian mixture model was employed to classify 4-lead ECG data. Four hidden Markov models were used to learn the 4-lead ECG complex and calculate the probability of state changes in each lead. These probabilities were further converted into log-likelihood values, which were treated as different statistical feature vectors that were then given as input to Gaussian mixture model and support vector machine. The 16-State hidden Markov models were trained using coronary artery disease data, so that coronary artery disease and normal data can have differences in likelihood values. The four-dimensional (4D) feature vector extracted by the four hidden Markov models was clustered by Gaussian mixture model with different numbers of distributions. The density model of data distribution was fitted by the maximum likelihood estimation (MLE) using the expectation–maximization (EM) algorithm via the NETLAB tool. The support vector machine classifier with the RBF kernel function was also utilized for binary classification, since the data were linearly inseparable. The combination of hidden Markov models as a feature extraction tool and Gaussian mixture model as a classification tool performed significantly better for coronary artery disease detection when dealing with overlapped data distributions, as the feature space in this study. The sensitivity, specificity, and accuracy were 85.7%, 79.8%, and 82.5%, respectively. They claimed that this was because the 4D feature inputs posed significant challenges for classification. The drawback of this study is that the length of each heartbeat was fixed at 400 points.

Green et al. employed artificial neural network ensembles on ECG data to detect acute coronary syndrome, which is a type of coronary artery disease [46]. The ECG data were acquired from acute coronary syndrome patients presenting to an emergency department with chest pain. Feature reduction was accomplished using principal component analysis, and 16 principal component analysis variables were used for training the models. The cross-entropy error function was used

and minimized using the gradient descent method. Two methods were used for constructing the ensemble models, which were the bagging method and S-fold cross-splitting. The bagging ensemble contained multilayer perceptrons trained on bootstrap samples of the original training set. Model selection was performed using a grid search, and the best model was found to be an artificial neural network cross-splitting ensemble trained solely on the ECG data. As a result, they found an advantage in using artificial neural network ensembles compared to both multilayer perceptrons and logistic regression. The addition of clinical data did not improve the performance of the artificial neural network ensemble. At the sensitivity of 95%, the specificity was 41%, corresponding to a negative predictive value (NPV) of 97%. They claimed that the ensemble model, combined with the judgment of trained emergency department personnel, could be useful for the early discharge of chest pain patients. The limitation of the study is the relatively small study population.

Al-Zaiti et al. used artificial neural network, logistic regression, and gradient boosting machine for the prediction of myocardial ischemia in patients with chest pain using only the 12-lead ECG [82]. First, they preprocessed all ECGs using manufacturer-specific commercial software and manually inspected tracings for noise and artifacts. After ectopic beats were removed, and median beats were computed, they extracted the temporal–spatial ECG features from each prehospital ECG using previously validated commercial algorithms. Feature selection and annotation based on existing clinical knowledge improved the classification performance of linear prediction models like logistic regression. This is reasonable, given that data reduction and labeling could reduce the dimensionality and complexity of the data. Nonlinear models like artificial neural network and gradient boosting machine were more powerful tools for handling the high-dimensional and highly correlated nature of ECG features. They trained and tested the performance of these three classifiers on two independent prospective patient cohorts using the same temporal-spatial features. They employed the classifiers with the best low bias–low variance trade-off to create a simple machine learning fusion classifier, which showed a sensitivity of 77%, specificity of 76%, precision of 43%, and negative predictive value (NPV) of 94%. Supplementing the algorithm with

patient history data did not improve classification performance. They claimed that the model can be used as a clinical decision support tool, when combined with the judgment of trained emergency department personnel, to help improve clinical outcomes in patients with chest pain.

Daraei et al. presented a prediction model for myocardial infarction using classification data mining methods that considered the imbalanced nature of the problem [83]. Firstly, the min-max normalization method was applied to scale the features' values. A hybrid feature selection method, which includes a genetic algorithm and Weight by Relief, was then applied to select the best subset of features. The top-weighted features selected by the Weight by Relief method were given to the genetic algorithm to choose the best final features. Feature selection improved the performance of both cost-sensitive and cost-insensitive models. The metacost classifier was applied to create a cost-sensitive J48 (C4.5) decision tree by assigning different cost ratios for misclassified cases. Implementing the cost-sensitive J48 decision tree on the imbalanced dataset provided better results compared to not using a cost-sensitive model. Moreover, making the J48 decision tree cost-sensitive improved performance over traditional classifiers. Using the hybrid feature selection method along with the cost-sensitive classification method yielded an accuracy of 82.6%, sensitivity of 86.6%, and F-measure of 80%, respectively. Rapidminer was used to implement the proposed model. The limitation of the study is the unavailability of the Q-wave features and rhythm data in the dataset.

Sun et al. presented a method for the detection of myocardial ischemia in patients with subtle ECG waveform changes using ensemble learning to integrate ECG dynamic features obtained via deterministic learning [84]. Wavelet transform-based analysis was performed to remove the noise in the 12-lead ECG signals, which were then linearly converted to 3-lead vectorcardiography signals using the Kors matrix to minimize computational complexity. The dynamic modeling of vectorcardiography by deterministic learning was implemented to generate a cardiodynamicsgram. Three low-dimensional and discriminative dynamic features, namely the spectrum fitting exponent, Lyapunov exponent, and Lempel-Ziv complexity, were extracted from the cardiodynamicsgram. Random

feature selection was used to obtain different feature subsets. A random sampling method was employed to generate various data subsets for each feature subset to train multiple individual classifiers, including support vector machine with an RBF kernel, support vector machine with a linear kernel, and a boosting tree. Subsequently, the bagging-based heterogeneous ensemble learning algorithm was applied to these features to generate different base classifiers. The bagging algorithm was used to fuse outputs of different individual base classifiers using a weighted voting method to generate a final classifier for myocardial ischemia detection. The heterogeneous ensemble learning algorithm exhibited an accuracy of 89.1%, sensitivity of 91.7%, and specificity of 82.7% using repeated 5-fold cross-validation. They claimed that the proposed ensemble model, which fused support vector machine and the boosting tree, outperformed conventional base classifiers and homogeneous ensemble models. However, their proposed ensemble model did not achieve better results on the external test set, which was obtained from a different medical center.

Bashir et al. proposed a weighted vote-based ensemble model for predicting cardiovascular diseases [59]. Firstly, different preprocessing techniques were employed to clean the data. They claimed that the proposed ensemble model overcomes the limitations of conventional data-mining techniques by combining various types of heterogeneous classifiers, including support vector machines, naive Bayes, decision tree, and instance-based learners. They used a weighted vote-based ensemble technique to combine all the individually trained classifiers. They employed the 10-fold cross-validation method to alleviate the insufficiency of samples. The ensemble model exhibited an accuracy of 87.3%, sensitivity of 93.7%, specificity of 92.8%, and F-measure of 82.1%. It achieved better performance compared to other individual classification techniques. RapidMiner was utilized for model building, training, and testing.

Ramasamy et al. presented a rhythm-based approach to screen patients with cardiac arrhythmias at the primary level [41]. During pre-processing, various noises associated with the ECG signals were removed. The R peaks in the ECG signals were located, and the signals were segmented based on the R peak locations to detect a single heartbeat. The Fourier-Bessel series expansion features

of the segmented ECG signals were extracted by computing the Fourier-Bessel coefficients using the Fourier-Bessel series expansion method on the segmented ECG beats. The feature vector dimensions were reduced using principal component analysis to acquire low-dimensional Fourier-Bessel series expansion features, reducing the computational complexity. These features were used as input to the Jaya-optimized ensemble random subspace k-nearest neighbor (JO-ERSKNN) classifier to classify five types of CAR beats. Jaya optimization was applied to gradually tune the hyper-parameters of the ensemble random subspace k-nearest neighbor classifier. The model demonstrated an accuracy of 99.4%, sensitivity of 95.4%, and specificity of 99.4% for the classification of cardiac arrhythmias. They claimed that the model can be made compatible with various wearable devices.

Exarchos et al. presented an automated methodology based on association rules for the detection of myocardial ischemia in long-duration ECG recordings [69]. During preprocessing, the noise was removed from the ECG signals. The ECG features were extracted from the ST segment and T wave of ECG beats. The features were then discretized by transforming the continuous-valued features into categorical using the modified classification tree algorithm. This tree was created from the training set during the discretization stage and was applied to classify the cases in the test set. They used an association rule extraction algorithm and a rule-based classification model to perform binary classification. The classification tree discretizer, combined with the predictive association rules algorithm, yielded higher classification performance and required less time for rule generation. The model showed a sensitivity and specificity of 87% and 93%, respectively. They claimed that the model has the ability to provide interpretation for the decisions made, due to the employment of association rules for classification. The disadvantage of the study is that the association rules method can also find spurious relationships among the data.

Moreover, most of the previously proposed deep learning methods for the diagnosis and classification of various cardiovascular diseases are based on one-dimensional (1D) convolutional neural network architectures, commonly trained using transfer learning or fine-tuning methods and utilizing exclusively ECG data [85, 86]. Furthermore, the other existing deep learning methods that used only

ECG data include recurrent neural networks [85, 87, 88], combined convolutional neural network-recurrent neural network [89, 90], transformer networks [91, 92], capsule networks [93, 94], deep neural networks [95, 96], deep belief networks [97, 98], autoencoders [99, 100], and restricted Boltzmann machines [85, 101]. However, none of these existing machine and deep learning studies have jointly utilized CSNA and ECG data to benefit from the diversity in different data types and leverage their strengths for the accurate and reliable diagnosis of cardiovascular diseases.

Brisk et al. conducted a retrospective and observational study designed to assess the feasibility of detecting induced coronary artery disease in human subjects earlier than experienced cardiologists using a deep convolutional neural network trained with transfer learning [102]. Firstly, ECG signals were split into short-length ECG segments. They used a 34-layer convolutional neural network with residual connections, culminating in a fully connected layer with a single, sigmoid-activated output node. The model was evaluated using 10-fold cross-validation, and the loss was calculated using binary cross-entropy. The model achieved a sensitivity of 84.2%, specificity of 94.7%, accuracy of 80.3%, and F1-score of 81.4%. They claimed that the dataset was too small for the model to achieve meaningful performance, despite the use of transfer learning. The study highlighted the risk of deep learning models leveraging data leaks to produce spurious and falsely high results. The drawback of this study is that the model was initiated using weights from the CAR detection task, based on the assumption that the ECG features learned during CAR detection would improve generalization for coronary artery disease detection, which may not be accurate for all types of coronary artery diseases.

Reasat et al. presented a shallow convolutional neural network architecture for the detection of myocardial infarction using 3-lead ECG signals [103]. Firstly, each signal was downsampled from 1 kHz to 250 Hz. A two-stage median filter was then used to remove baseline wander. Next, a Savitzky-Golay smoothing filter was used to remove other noises. The de-noised signal was further downsampled to 64 Hz to decrease computational burden and reduce training time. The signals were then partitioned into short-length ECG segments. The convolutional neural

network benefited from the use of varying filter sizes in the same convolutional layer, which allowed it to learn features from signal regions of varying lengths. Feature maps extracted by the inception blocks were concatenated and passed on to a global average pooling layer. Lastly, there was a two-unit dense layer with a softmax activation layer, providing categorical probability. The weights of the dense layer were L2 regularized to prevent over-fitting. The back-propagation training algorithm and the Adam optimizer was used to update the weights. A subject-oriented approach was employed, in which the convolutional neural network was tested on one patient and trained on the rest of the patients. The model achieved an accuracy of 84.5%, sensitivity of 85.3%, and specificity of 84.1% when compared to the benchmark. The model was implemented using the Keras neural network library.

Makimoto et al. presented a convolutional neural network equipped with a 6-layer architecture to diagnose myocardial infarction using ECG images obtained from a reduced and optimized number of ECG leads [104]. During the network training, they incorporated data augmentation to increase the learning efficacy. They generated activation maps of the final convolutional layer using Grad-CAM to visualize the convolutional neural network's focus points on the ECGs during its myocardial infarction recognition. They observed that the convolutional neural network strongly focused on the ST segment and T wave elevation in the ECG to diagnose myocardial infarction, similar to how cardiologists do. The model was then tested together with 10 physicians using the data in the test set and their performances in recognizing myocardial infarction were compared. The performance of the convolutional neural network model was higher compared to that of the physicians. The method revealed an accuracy of 75%, sensitivity of 65%, specificity of 86%, precision of 82%, negative predictive value (NPV) of 71%, and F1-score of 72%. Hence, they suggested that a simple 6-layer convolutional neural network architecture derived from a small ECG database may achieve comparable capability to cardiologists in recognizing myocardial infarction using ECG images. Additionally, ECG image compression up to a quarter of the resolution did not significantly decrease the myocardial infarction detection capability of the convolutional neural network.

Hammad et al. presented a method based on an end-to-end deep convolutional neural network model to perform binary classification for automated detection of myocardial infarction using ECG data [105]. The proposed convolutional neural network model included three blocks of 1D convolutional layers, batch normalization, dropout operations, two dense layers, rectified linear unit (ReLU), and softmax activation functions. To reduce the impact of imbalanced ECG data, they focused on the loss of the minority classes and optimized the model using the focal loss function. They used the Adam optimization algorithm and implemented a stratified 5-fold cross-validation. The proposed method using the focal loss performed better and converged earlier than the one without using the focal loss. It showed an overall accuracy of 89.7%, precision of 88.5%, sensitivity of 81.1%, and an F1-score of 83%.

Darmawahyuni et al. suggested sequence modeling based on a long short-term memory network for the binary classification of sequential ECG data to automatically detect myocardial infarction using ECG signals [106]. The performance of the proposed method was compared to that of the standard recurrent neural network and gated recurrent unit network. The best sequence model classifier was found to be long short-term memory with a 90%:10% training and test set split. They claimed that a simple long short-term memory network presented better performance results in the training and test sets compared to the standard recurrent neural network and gated recurrent unit network architectures with identical hyper-parameters. Specifically, long short-term memory had a sensitivity of 98.4%, specificity of 97.9%, precision of 95.6%, and F1-score of 96.3%, respectively. They stated that long short-term memory was able to learn and select which data needs to be stored or discarded, resulting in its better performance compared to the standard recurrent neural network and gated recurrent unit network.

Feng et al. used a combined 16-layer convolutional neural network-long short-term memory model for binary classification of myocardial infarction using one-lead ECG data [107]. During pre-processing, they used the wavelet transform method to filter the original ECG noise and the Daubechies wavelet basis function to decompose the ECG signals into 10 levels. They applied the Pan–Tompkins

algorithm to detect the R-peaks in ECG recordings, which were subsequently used for heartbeat segmentation to a fixed length. Given the imbalanced nature of the ECG data, they performed random over-sampling to avoid over-fitting during training and improve the model's generalizability. The convolutional neural network-long short-term memory model was trained to automatically learn the spatial and temporal characteristics of ECG signals. It was observed that the model achieved the highest accuracy when the data of five adjacent heartbeats were selected as the input, and the Adam optimizer was utilized. They obtained an accuracy of 95.4%, sensitivity of 98.2%, specificity of 86.5%, and F1-score of 96.8%.

Rath et al. used four deep learning models, including an autoencoder, restricted Boltzmann machine, self-organizing map, and a radial basis function network, to detect coronary artery disease using ECG signals [108]. Additionally, they developed an ensemble model by combining the two best-performing deep learning models, which were the autoencoder and self-organizing map models, based on the principle of majority voting. The order of performance rankings for coronary artery disease detection, from the highest to the lowest, belonged to the self-organizing map-autoencoder, autoencoder, self-organizing map, radial basis function network, and restricted Boltzmann machine, respectively. Hence, the self-organizing map-autoencoder ensemble model outperformed all individual deep learning models with an accuracy of 98.4% and an F1-score of 97.1%. They asserted that this could be attributed to the ensemble model's ability to overcome the statistical, computational, and representational problems associated with the datasets.

Prabhakararao et al. introduced an end-to-end multi-lead diagnostic attention-based recurrent neural network (MLDA-RNN) for the automated classification of the three myocardial infarction severity stages and healthy control subjects [88]. They employed recurrent neural networks to encode the temporal variations in the 12-lead ECG signals. These encoded vectors from the recurrent neural network encoding blocks were then input into the intra-lead attention module to summarize the within-lead discriminative vectors and obtain lead-attentive representations. Subsequently, the inter-lead attention module aggregated these

representative vectors from the intra-lead attention module based on their clinical relevance to obtain a high-level feature representation for reliable diagnosis. The vector obtained from the inter-lead attention module was fed to the fully connected layer with a softmax activation function to classify the severity stages of myocardial infarction. They also incorporated batch normalization layers after the inter-lead attention module to improve the convergence speed. They used a dropout layer before the output layer to improve the model generalization. They trained the model using back-propagation through time and implemented early stopping method to avoid over-fitting. They employed the grid search method to optimize the hyper-parameters of the recurrent neural network and attention modules. The model exhibited an overall accuracy of 97.7%, sensitivity of 97.6%, and specificity of 99.4% without compromising on class-wise detection rates. They claimed that MLDA-RNN showed promising results in terms of model interpretability, as the learned attention weights often correlated with clinicians' way of diagnosing myocardial infarction severity stages.

Hernandez et al. proposed an automated method for the detection of myocardial infarction from continuous ECG monitoring using a set of ECG and vectorcardiography features [109]. First, they applied a median filter to remove high-frequency noise. Next, they implemented a moving window over the filtered signal and calculated the distribution parameter values in each window. They selected the optimal distribution parameters by performing a statistical analysis to control the model's complexity, prevent over-fitting, and facilitate the model's learning process. From this, they obtained another time-series for each distribution parameter. They derived seven ECG features from vectorcardiography, which were found to be optimal for detecting myocardial infarction using the reduced 3-lead ECG signals. Out of the seven ECG features, five were vectorcardiography features derived from the QRS and T wave complexes, while the other two were ST elevation features. They analyzed the distribution properties of each ECG feature to facilitate the identification of underlying patterns in the data. They used these features to train and validate the recurrent neural network composed of two unidirectional long short-term memory networks with a fully connected layer and ReLU activation function. They observed a clear separation in ECG

feature median values between the baseline and myocardial infarction conditions for the two distribution parameters, indicating that these may be suitable parameters for characterizing myocardial infarction. The proposed method had an accuracy of 97.4% and sensitivity of 94.7%. The drawback of this study is the use of a reduced number of ECG leads, which can limit the detection performance of certain types of myocardial infarction.

Miao et al. presented an enhanced deep neural network model for the diagnosis and prognosis of coronary artery disease [110]. The proposed deep neural network model includes two hidden layers and an output layer with a sigmoid activation function. It was built based on a deep multilayer perceptron architecture equipped with linear and non-linear transfer functions, regularization, dropout, and a binary classification layer. During the training of the deep neural network, dropout rates in both hidden layers were randomly applied, resulting in random connections within the deep neural network architecture to reduce over-fitting. The model achieved an accuracy of 83.6%, sensitivity of 93.5%, specificity of 72.8%, precision of 79.1%, and F1-score of 85.7%. The limitation of this study is that they did not use cross-validation to ensure robustness.

Bigler et al. introduced a convolutional neural network trained with transfer learning to perform binary classification for myocardial ischemia diagnosis using one-lead ECG images [111]. They conducted a retrospective observational study to test a hypothesis-generating approach using an open-access convolutional neural network model with different depth and network architecture that was pre-trained using the images from the ImageNet dataset. Before training the convolutional neural network on this study's database, all training images were randomly shuffled and processed by adding noise to prevent over-fitting. The underlying morphology responsible for the network prediction for myocardial ischemia detection focused mainly on the distinctive features in the ST-segment and T-wave of the ECG. During transfer learning, the last three layers of the convolutional neural network responsible for the network prediction were replaced for the new task. Remaining layers responsible for pattern recognition and feature extraction were not changed. A dropout layer was added to prevent the convolutional neural network from over-fitting. The convolutional neural network

showed a sensitivity of 83%, specificity of 98%, accuracy of 91.5%, and F1-score of 89.9%, which revealed higher performance than manually obtained quantitative intracoronary ECG ST-segment shift for myocardial ischemia detection.

Altan et al. suggested a decision-support system to aid cardiologists in coronary artery disease diagnosis [34]. Firstly, short-term ECG segments were randomly obtained from 24-hour ECG signals using the moving window analysis technique to increase the number of samples from each subject. In the first stage of the Hilbert-Huang transform, frequency-modulated signals, known as intrinsic mode functions, were obtained by applying empirical mode decomposition (EMD) to the short-term ECG segments. In the second stage, the Hilbert transform was applied to each intrinsic mode function to calculate the instantaneous frequency spectral features. Binary classification using the statistical features of intrinsic mode functions was performed using a deep belief network classifier. The classifier consisted of one input layer, two hidden layers, and one output layer with two outputs for binary classification. The deep belief network classifier initially evaluates weights and biases between visible and hidden layers through unsupervised pre-training of stacked restricted Boltzmann machines. In the subsequent supervised learning phase, weights and biases were updated using fine-tuning to optimize the parameters for improving classification performance. The activation functions of the hidden and output layers in the supervised learning phase were the hyperbolic tangent and sigmoid functions, respectively. The deep belief network classifier achieved an accuracy of 98%, specificity of 98.8%, and sensitivity of 96% using the 10-fold cross-validation method.

Xiao et al. explored the application of convolutional neural networks to detect significant changes in the ST segments of whole-day Holter ECG signals for coronary artery disease diagnosis [112]. They generated image-based samples by capturing 10-second snapshots of one-lead ECG waveforms and then transforming them into grayscale images using a grid overlay to remove redundant color information that does not contribute to the classification task. These images were saved as 8-bit JPEG files and resized using bilinear interpolation to adhere to the input requirements of the Google Inception V3 model, which had been pre-trained using transfer learning from images in the ImageNet dataset. The image features

that distinguish between ST from non-ST conditions were extracted by the convolutional layers in the convolutional neural network model for the classification of each 10-second image sample. They retained all the model parameters in the Google Inception V3 model, except for the final layer, which was retrained using the training images from the present study. The model exhibited a sensitivity of 82.6%, specificity of 80.3%, and F1-score of 87.3%. It achieved performance comparable to that of expert cardiologists in the detection of ST changes. The limitation of the study is that the algorithm was built upon one-lead ECG data.

Butun et al. proposed a computer-aided diagnosis system featuring a 1D capsule network (1D-CapsNet) for the automated detection of coronary artery disease from short-length ECG segments [93]. Initially, they applied discrete wavelet transform to raw ECG signals to eliminate noise. Subsequently, they employed Z-score normalization to make the ECG signals suitable for input into the proposed network. They modified the original capsule network model for 1D signal applications by redefining layer parameters and adding sub-layers to detect coronary artery disease. They employed two ECG capsules that represented the normal and coronary artery disease classes. The decoder section of the capsule networks compressed the ECG signals and served as a regulator to protect important features in the capsule layers during training. The model yielded an accuracy of 98.6%, sensitivity of 97.9%, specificity of 98.7%, and precision of 93.3% for short-length ECG segments using a 5-fold cross-validation method. They asserted that the model can serve as a diagnostic tool to assist cardiologists during medical examinations by providing a second opinion on the patient's condition.

Acharya et al. employed a 1D-convolutional neural network structure for diagnosing of coronary artery disease using short-length ECG segments [113]. First, they applied discrete wavelet transform to the ECG segments to eliminate noise. Subsequently, they used z-score normalization to normalize the ECG segments. They developed an 11-layered convolutional neural network structure, which included four convolutional layers, four max-pooling layers, and three fully connected layers, to perform binary classification. The 1D-convolutional neural network was able to differentiate between normal and abnormal ECGs with an accuracy of 95.1%, sensitivity of 91.1%, specificity of 95.8%, and precision

of 80.8%. They claimed that the proposed convolutional neural network structure was robust to shifting and scaling invariance, and they suggested that the proposed system is suitable for real-time monitoring.

Dutta et al. presented a simple 2-layer convolutional neural network resistant to class imbalance. It performed binary classification on significantly class-imbalanced ECG data for coronary artery disease diagnosis [114]. Data preprocessing was performed using the least absolute shrinkage and selection operator (LASSO) based feature weight assessment. LASSO regression was repeatedly performed using multiple instances of randomly subsampled datasets to assess the consistency of attribute contributions. A majority-voting algorithm was applied to extract important features and identify the contribution of significant attributes in data variation, resulting in dimensionality reduction by excluding unimportant variables. Subsequently, the important features were fed into a 1D-convolutional neural network and homogenized using a fully connected layer. They employed a training schedule resembling simulated annealing to minimize the generalization error between train and test losses. Nonlinear transformation was performed using ReLU, and dropout was applied to reduce over-fitting. The shallow convolutional neural network architecture demonstrated a classification accuracy of 77% in correctly classifying the presence of coronary artery disease in the test set. The recall values for other machine learning methods, such as support vector machines and random forests, were comparable to those of the convolutional neural network model. However, the accuracy of convolutional neural network (79.5%) was superior to the individual accuracies of support vector machines or random forest classifiers, and the convolutional neural network exhibited better accuracy in predicting negative cases. They asserted that the convolutional neural network exhibited a considerable degree of resilience toward data imbalance.

Sharma et al. presented a rhythm-based methodology for the point-of-care diagnosis of cardiac arrhythmias at a primary level [40]. During pre-processing, frequency normalization was performed to match the sampling frequency of the datasets from different sources to the input of the proposed algorithm. Therefore, the three databases were downsampled to 300 Hz to maintain homogeneity

with the training data and the algorithm. A Butterworth band-pass filter was employed to eliminate baseline drift and high frequency noise from one-lead ECG signals. A dataset-dependent notch filter with an appropriate frequency of either 50 Hz or 60 Hz was used to remove power-line interference. The QRS detection algorithm was applied to the filtered ECG signals, and RR-interval sequences of one-lead and short-length ECG segments were computed. Fourier-Bessel sequences were calculated using the Fourier-Bessel series expansion to transform RR-interval sequences into more meaningful sequences that can better characterize the cardiac rhythms into normal and abnormal classes. The computed Fourier-Bessel coefficients of different lengths for different subjects were upsampled to a fixed number to make Fourier-Bessel sequences homogeneous in terms of length. The derived Fourier-Bessel sequences-based intelligent series were used as input to the unidirectional long short-term memory model, which was used to directly extract significant information required for binary classification. They obtained an accuracy of 78.4%, sensitivity of 65.1%, specificity of 86.8%, and F1-score of 76.5% in classifying normal and CAR classes using 10-fold cross-validation. They claimed that the addition of the Fourier-Bessel series expansion-layer improved CAR detection performance, and that the proposed intelligent series can reveal the differences between normal and CAR ECG signals.

The emergence of the novel coronavirus disease 2019 (COVID-19) was attributed to a new, highly contagious Beta-Coronavirus known as Severe Acute Respiratory Syndrome Coronavirus-2 (SARS-CoV-2). This outbreak was officially declared a pandemic by the World Health Organization (WHO) in March 2020 [50, 115]. This unprecedented global health crisis has had far-reaching consequences worldwide. The clinical presentation of COVID-19 ranged from asymptomatic cases to highly severe pneumonia, multi-organ failure, and death. Moreover, a significant proportion of patients infected with various SARS-CoV-2 variants, which have different infectivity and pathogenicity levels, exhibited no symptoms. Nonetheless, asymptomatic carriers of the virus pose a substantial risk, as they can unknowingly transmit SARS-CoV-2 to healthy individuals unless isolated. Therefore, the rapid, early, and accurate detection of COVID-19 is of paramount importance for timely isolation and treatment, curbing the spread

of infection, and ultimately reducing the mortality associated with COVID-19.

Reverse transcription polymerase chain reaction (RT-PCR) is the gold standard diagnostic test for detecting COVID-19 [116]. Nevertheless, it has several limitations that necessitate the exploration of complementary diagnostic approaches. Previous studies reported that the RT-PCR test, while exhibiting high specificity, has low sensitivity and high false-negative rates, ranging from 45% to 60% [116, 117]. This reduced sensitivity can be attributed to several contributory factors, including the time interval between symptom onset and RT-PCR testing, the low viral ribonucleic acid (RNA) load in specimens, variations in specimen collection techniques, improper nucleic acid extraction from specimens, the technical proficiency of laboratory personnel, improper storage or transportation of viral RNA samples, the analytical performance characteristics of RT-PCR kits, and the rapid mutation capability of the SARS-CoV-2 virus. Consequently, a negative RT-PCR test result does not unequivocally exclude the possibility of SARS-CoV-2 infection and should not be construed as definitive proof of the absence of SARS-CoV-2 infection. Thus, it should not be employed as the sole criterion for patient diagnosis and isolation. Furthermore, it is worth noting that the duration between RT-PCR sampling and the receipt of test results can extend to several hours in some countries, and multiple repetitions of the RT-PCR test may be required to prevent false-negative results in individuals with suspected infection. In light of these challenges, the rapid, early, and accurate diagnosis, followed by prompt isolation and treatment of COVID-19 patients, remains a major challenge for physicians.

Thorax computed tomography plays a pivotal role in the diagnosis of moderate to severe COVID-19 due to its relatively higher sensitivity, ranging from 60% to 94% [118]. This heightened sensitivity is particularly valuable in cases where patients exhibit clinical symptoms consistent with COVID-19, but yield negative results in RT-PCR tests for SARS-CoV-2. However, thorax computed tomography exhibits a relatively lower specificity, reported between 25% and 53% [118]. This reduced specificity arises from the fact that radiological findings of SARS-CoV-2 infection often manifest similar patterns that overlap with those seen in

other viral infections and lung diseases, including but not limited to SARS, Middle East Respiratory Syndrome (MERS), influenza, avian influenza (bird flu), and swine influenza. In other words, thorax computed tomography possesses limitations stemming from its low performance in distinguishing COVID-19 pneumonia from various other lung diseases. Furthermore, thorax computed tomography has very limited clinical utility in the early stages of SARS-CoV-2 infection and for diagnosing asymptomatic patients with no anomalies in the lungs. Therefore, existing guidelines set forth by the American College of Radiology indicate that radiological data are necessary and essential, but not solely sufficient for the reliable diagnosis or classification of COVID-19.

Within the context of this thesis, our preference was to employ three-dimensional (3D) thorax computed tomography images rather than two-dimensional (2D) chest X-ray images. This choice is due to the fact that thorax computed tomography exhibits higher sensitivity compared to chest X-ray in the detection of subtle lung anomalies associated with COVID-19. Furthermore, thorax computed tomography provides detailed cross-sectional images of the lungs, offering a more comprehensive quantification of lung involvement. This can considerably aid in monitoring disease progression and assessing the severity of COVID-19. Notably, COVID-19 frequently manifests with ground-glass opacities (GGOs) in the lungs, which can be better visualized on thorax computed tomography images in contrast to chest X-ray. Thorax computed tomography is capable of detecting lung anomalies even in the early stages of the disease, which may not be visible on chest X-ray.

Laboratory data (complete blood counts) provide valuable information for the diagnosis of COVID-19. However, their utility is constrained by certain limitations, foremost among them being their inability to distinguish COVID-19 from other lung diseases. In other words, laboratory data, such as neutrophil count, lymphocyte count, and the neutrophil-lymphocyte ratio, lack specificity for the diagnosis of COVID-19. Numerous other viral and bacterial infections can produce similar anomalies in laboratory data, resembling those observed in COVID-19 patients. Consequently, this similarity can lead to false-positive outcomes. Therefore, laboratory data alone cannot definitively diagnose COVID-19

and are not sufficient for the reliable diagnosis or classification of COVID-19.

In this thesis, our primary objective was to address the limitations and drawbacks associated with individual diagnostic tests and to fill the research gaps in the literature. For this purpose, we constructed a new, fully labeled COVID-19 database called the Ankara University Faculty of Medicine COVID-19 (AUFM-CoV) database. It contains RT-PCR curves, thorax computed tomography images, and laboratory data of patients with COVID-19 pneumonia, other viral and bacterial pneumonia, parenchymal lung diseases, and healthy subjects. We intentionally designed this database to include a more comprehensive and diverse variety of medical data compared to publicly available COVID-19 databases. Additionally, thorax computed tomography images in the AUFM-COV database include other pneumonias and lung diseases with GGOs, which are very difficult to distinguish from COVID-19 pneumonia. Therefore, it represents a highly valuable resource that enables the development and benchmarking of robust supervised and unsupervised artificial intelligence techniques for COVID-19 diagnosis, classification, and prognosis.

Machine and deep learning techniques have revolutionized the analysis and interpretation of biomedical signals and images. These techniques have demonstrated remarkable potential in significantly enhancing the performance and effectiveness of disease diagnosis and classification. The existing artificial intelligence-based techniques proposed for COVID-19 detection and classification mostly focus on the utilization of a single type of medical data [119, 120]. To the best of our knowledge, no studies in the existing literature have presented a hybrid artificial intelligence technique that jointly utilizes RT-PCR curves, thorax computed tomography images, and laboratory data for the robust and reliable detection of COVID-19.

More precisely, the majority of existing deep learning studies have proposed various convolutional neural network models that utilize only digital radiological images [119, 120]. However, the current guidelines from the American College of Radiology indicate that radiological images are necessary, but not solely sufficient for the reliable diagnosis of COVID-19 [121]. Additionally, this concentration on

a singular data modality constituted a significant research gap in the literature, highlighting the need for further investigation. One of the primary motivations driving our study was to address the limitations of previous related studies that have only used radiological images and to fill the research gaps in the existing scientific literature.

Furthermore, it is worth noting that, as of the current state of the literature, no studies have yet introduced an ensemble learning technique that combines various deep learning and machine learning methods to perform robust detection of COVID-19. Additionally, there are no studies to date that have utilized this hybrid artificial intelligence technique for the differential diagnosis of COVID-19, other pneumonias, lung diseases, and healthy lungs. These research gaps within the literature underscore the need for further investigation.

For these reasons, the primary research focus of this thesis has been dedicated to developing a new, automated artificial intelligence-based Hybrid Clinical Decision Support Technique that jointly analyzes RT-PCR curves, thorax computed tomography images, and laboratory data. Unlike existing studies, our aim has been to benefit from the diversity in heterogeneous medical data sources and leverage their strengths, while mitigating their limitations.

This thesis addresses research gaps in the literature by proposing the first automated artificial intelligence-based hybrid clinical decision support technique, which leverages the power of ensemble learning by making use of the predictive capabilities of various artificial intelligence algorithms to increase the overall performance and generalizability of COVID-19 diagnosis. Specifically, the automated artificial intelligence-based hybrid clinical decision support technique integrates two preprocessing methods, long short-term memory and convolutional neural network-based deep learning methods, along with an artificial neural network-based machine learning method for fast, early, and accurate COVID-19 diagnosis.

Additionally, most of the previous artificial intelligence studies have primarily focused on binary classification tasks, mainly distinguishing between COVID-19 pneumonia and healthy lungs [119, 120]. In contrast, only a limited number

of studies have investigated the differential diagnosis of COVID-19 pneumonia, other pneumonias, other lung diseases, and healthy lungs by performing multi-class classification. Conversely, our artificial intelligence-based hybrid clinical decision support technique has demonstrated remarkable proficiency in accurately diagnosing COVID-19 and distinguishing COVID-19 pneumonia from other pneumonias, other lung diseases, and healthy lungs by performing four-class classification. It is essential to highlight that this four-class classification task presents a formidable challenge when contrasted with binary classification scenarios.

Furthermore, the automated artificial intelligence-based hybrid clinical decision support technique performs multi-class classification and very successfully differentiates COVID-19 from other pneumonias, lung diseases, and healthy lungs. This task is particularly challenging due to the remarkably similar radiological findings observed among patients with COVID-19 pneumonia, other pneumonias, and lung diseases within the AUFM-CoV database. We believe that this study presents a significant contribution to the existing literature due to its pioneering approach in introducing a new hybrid artificial intelligence technique, which incorporates an ensemble learning method to enhance the performance and reliability of COVID-19 detection. Consequently, the automated artificial intelligence-based hybrid clinical decision support technique holds promise in assisting physicians to render more accurate and well-informed decisions in clinical practice. This, in turn, has the potential to increase physicians' success rates and alleviate their workloads.

Furthermore, one of our principal objectives was to compare the performance of our long short-term memory-based deep learning method with the gold standard diagnostic test RT-PCR, as well as to benchmark it against existing artificial intelligence studies in the literature that utilized only RT-PCR data for COVID-19 diagnosis. Our findings conclusively demonstrate that our long short-term memory-based deep learning model exhibits superior sensitivity in diagnosing COVID-19 when compared to the gold standard RT-PCR test. Moreover, we have shown that our model achieves higher specificity, higher precision, and higher F_1 score compared to two previous artificial intelligence studies that exclusively employed RT-PCR data for COVID-19 diagnosis.

Additionally, one of our goals was to compare the performance of our convolutional neural network-based deep learning method with thorax computed tomography, as well as existing artificial intelligence studies in the literature that utilized only radiological images (thorax computed tomography or chest X-ray) for COVID-19 diagnosis through multi-class classification. Our findings conclusively demonstrate that our convolutional neural network-based deep learning model exhibits superior specificity in diagnosing COVID-19 when compared to thorax computed tomography. Moreover, we have shown that our model achieves higher sensitivity, comparable specificity, comparable precision, and comparable F_1 score when compared to previous artificial intelligence studies that exclusively employed radiological images for COVID-19 diagnosis through four-class classification.

Lastly, one of our purposes was to compare the performance of our automated artificial intelligence-based hybrid clinical decision support technique with diagnostic test laboratory data for COVID-19 diagnosis. Our findings conclusively illustrate that our automated artificial intelligence-based hybrid clinical decision support technique achieves superior sensitivity and specificity in diagnosing COVID-19 when compared to the diagnostic test laboratory data. Due to the absence of prior studies in the existing literature that proposed a hybrid artificial intelligence technique that jointly utilizes RT-PCR curves, thorax computed tomography images, and laboratory data to diagnose or classify COVID-19, it is not possible to compare the performance results of our artificial intelligence-based Hybrid Clinical Decision Support Technique with those of other previous studies.

1.3 Main Contributions of the Thesis

The main contributions and novelty in Chapter 3 are summarized as follows:

- We constructed a new, fully-labeled COVID-19 database that contains RT-PCR curves, thorax computed tomography images, and laboratory data of patients with COVID-19 pneumonia, other viral and bacterial pneumonia, parenchymal lung diseases, and healthy subjects. Among the publicly

available COVID-19 databases, our database contains the widest variety of medical data.

- We have proposed a new automated artificial intelligence-based hybrid clinical decision support technique. It is an ensemble learning technique that consists of preprocessing methods, long short-term memory and convolutional neural network-based deep learning methods, and artificial neural network-based machine learning method that performs fast and accurate diagnosis of COVID-19. The proposed artificial intelligence-based hybrid clinical decision support technique jointly analyzes RT-PCR curves, thorax computed tomography images, and laboratory data to benefit from the diversity in different data types and leverage their strengths.

- The proposed long short-term memory-based deep learning method outperforms the gold standard RT-PCR test in terms of sensitivity of COVID-19 diagnosis. Moreover, it demonstrates higher specificity, higher precision, and higher F_1 score compared to the two previous artificial intelligence studies that utilized RT-PCR data for COVID-19 diagnosis.

- The proposed convolutional neural network-based deep learning method demonstrates superior specificity compared to thorax computed tomography in COVID-19 diagnosis. Additionally, it exhibits higher sensitivity than previous artificial intelligence studies that utilized radiological images for COVID-19 diagnosis through multi-class classification.

- The proposed automated artificial intelligence-based hybrid clinical decision support technique shows higher sensitivity and specificity compared to laboratory data in diagnosing COVID-19. Moreover, it has been shown to very successfully differentiate COVID-19 pneumonia from other pneumonias, and healthy lungs.

1.4 Literature Review

We conducted a comprehensive review of the existing relevant literature to gain an in-depth understanding of the current machine and deep learning techniques proposed for the diagnosis or classification of COVID-19. In recent years, due to the burden of the COVID-19 pandemic on healthcare systems around the world, various machine and deep learning techniques have been proposed for COVID-19 diagnosis [50, 115, 122], classification [50, 115, 122], prognosis [19, 123, 124], triage [125, 126, 127, 128], predicting severity and mortality risk [129, 130, 131, 132, 133, 134, 135, 136, 137], contact tracing [138], drug and vaccine development [139, 140], and forecasting patient numbers and the spread of the pandemic [141].

In the context of COVID-19 detection and classification, existing artificial intelligence-based techniques mainly focus on utilizing a single type of medical data, thereby limiting their ability to leverage the diversity and strengths of multi-modal data integration. Specifically, most of the existing deep learning studies have proposed various convolutional neural network architectures, commonly trained using transfer learning or fine-tuning methods, and have relied solely on radiological images, such as 3D thorax computed tomography images, 2D chest X-ray images, or lung ultrasonography (LUS) images.

Apostolopoulos et al. modeled an architecture for the spontaneous identification of COVID-19 individuals by employing deep transfer learning with five different pre-trained convolutional neural networks (Inception, Extreme Inception (Xception), InceptionResNetV2, Visual Geometry Group19 (VGG19), MobileNetV2) [142]. The database included chest X-ray images comprising COVID-19, bacterial pneumonia, viral pneumonia, and healthy lungs. The model using MobileNetV2 attained the highest binary classification performance with 96.7% accuracy, 98.6% sensitivity, 96.4% specificity.

Haghanifar et al. proposed a framework for identifying COVID-19 using transfer learning, where they utilized the CheXNet model to develop COVID-CXNet

[143]. The database comprised chest X-ray images of COVID-19 pneumonia, non-COVID-19 pneumonia, and the normal class. CheXNet was constructed based on the densely connected convolutional network (DenseNet) architecture and was trained on frontal chest X-ray images. The proposed COVID-CXNet, equipped with 431 layers and 7 million parameters, was subsequently fine-tuned using the chest X-ray database. This system includes a lung separation unit to increase the model's localization of lung irregularities. For hierarchical multi-class classification, COVID-CXNet achieved an accuracy of 87.2% and an F1-score of 92%. COVID-CXNet utilized Grad-CAM for visualizing the results.

Ucar et al. projected a network structure for COVID-19 diagnosis using Deep Bayes-SqueezeNet, which was built on the pre-trained SqueezeNet model [144]. The SqueezeNet was fine-tuned for the COVID-19 diagnosis task with Bayesian optimization additive. Data augmentation was employed due to the limited number of chest X-ray images for COVID-19. The database contained chest X-ray images for COVID-19 pneumonia, other pneumonia, and normal classes. The experimental results revealed that Deep Bayes-SqueezeNet achieved an accuracy of 98.2%, specificity of 99.1%, and F1-measure of 98.2%. They claimed that fine-tuning hyper-parameters and augmenting the dataset increased the performance of COVID-19 diagnosis compared to existing network designs.

Sharma et al. developed an explainable diagnosis system for the detection and quantification of the infection region in COVID-19 [145]. They utilized the Covid-MANet network, which is an automated end-to-end multi-task attention network designed for COVID-19 infection screening across five classes and three stages. In the first stage, the model localizes attention to the relevant lungs region for disease recognition. The second stage distinguishes COVID-19 cases from bacterial pneumonia, viral pneumonia, normal cases, and tuberculosis cases. In the third stage, the model quantifies the extent of infection and the severity of COVID-19 in the lungs. Furthermore, they proposed the multi-scale attention model MA-DenseNet201 for the classification of COVID-19 cases. The MA-DenseNet201 classification model outperformed eight other convolutional neural network models in terms of interpretability when combined with the lung localization network. The proposed network highlights infections through segmentation

and localization of model-focused regions to support explainable decisions. The MADenseNet201 model with a segmentation-based cropping approach achieved a maximum interpretability of 96% and sensitivity of 97.7%. Finally, based on class-specific sensitivity analysis, the Covid-MANet ensemble network consisting of MA-DenseNet201, Residual Network (ResNet-50), and MobileNet achieved an accuracy of 95% and sensitivity of 98.1%.

Kedia et al. proposed the CoVNet-19 model, which is an ensemble deep convolutional neural network model that can unveil important diagnostic characteristics for detecting COVID-19 in patients using chest X-ray images [146]. CoVNet-19 combines two pre-trained deep convolutional neural network models, which are Visual Geometry Group19 (VGG19) and densely connected convolutional network (DenseNet-121). The extracted features are given as input to the support vector machine classifier's stacked ensemble structure, which was trained to achieve binary classification (COVID-19 vs. NON-COVID-19) and three-class classification (COVID-19, normal, and pneumonia). Data augmentation was applied to COVID-19 images to increase the sample size. Experimental results revealed an accuracy of 98.3%, precision of 98.3%, and recall of 98.3% for three-class classification.

Ismael et al. proposed deep learning-based approaches, namely deep feature extraction, fine-tuning of pre-trained convolutional neural networks, and end-to-end training of a convolutional neural network, to detect COVID-19 using chest X-ray images [147]. They utilized five variants of pre-trained convolutional neural networks, which are Visual Geometry Group16 (VGG16), Visual Geometry Group19 (VGG19), Residual Network (ResNet-101), Residual Network (ResNet-18), and Residual Network (ResNet-50), for deep feature extraction and the fine-tuning procedure. For binary classification (COVID-19 and normal (healthy)), they employed support vector machines with different kernel functions, including quadratic, cubic, linear, and Gaussian. The deep features extracted using the residual network (ResNet-50) model were classified using a support vector machine with a linear kernel function, which was the model combination that yielded the highest performance. They achieved an accuracy of 94.7%, sensitivity of 91%, specificity of 98.8%, and F1-score of 94.7%.

Jain et al. proposed a deep learning-based method to detect COVID-19 using chest X-ray images [148]. The database contained chest X-ray images of three classes, including healthy, COVID-19, and pneumonia. After cleaning up the images and applying data augmentation, they used deep learning-based convolutional neural network models and compared their performances. Specifically, they utilized three pre-trained variants, which are InceptionV3, Extreme Inception (Xception), and ResNeXt. The Extreme Inception (Xception) model achieved the highest accuracy of 97.9% in detecting COVID-19 using chest X-ray images.

Elkorany et al. developed a tailored COVID-19 detection model called COVIDetectionNet using chest X-ray images [149]. The database contains chest X-ray images labeled into three classes, which are COVID-19, normal, viral, and bacterial pneumonia. COVIDetectionNet was based on the ShuffleNet and SqueezeNet architectures to extract deep-learned features and multi-class support vector machines for classification. The model exhibited a recall of 94.4%, specificity of 98.1%, precision of 94.4%, and F1-score of 94.4%.

Ko et al. aimed to develop a simple 2D deep learning framework to diagnose COVID-19 pneumonia based on a single chest computed tomography image and differentiate it from non–COVID-19 pneumonia and non-pneumonia diseases [150]. Transfer learning was used to create the proposed FCONet (Fast-Track COVID-19 Classification Network). FCONet was developed using transfer learning with pre-trained deep learning models as a backbone, which are Visual Geometry Group16 (VGG16), Residual Network (ResNet-50), InceptionV3, or Extreme Inception (Xception). They performed data augmentation on chest computed tomography images, which were categorized into four groups that are COVID-19 pneumonia, other pneumonia, normal lung, and lung-cancer. Among the four pre-trained models of FCONet, residual network (ResNet-50) demonstrated the highest performance with a sensitivity of 99.5%, specificity of 100%, and accuracy of 96.8%, outperforming the other three pre-trained models in the test set.

Rohila et al. proposed automated diagnosis of COVID-19 from chest computed tomography images of the patients using a deep learning technique [151]. The database was partitioned based on the severity of COVID-19 contamination. The

proposed model, ReCOV-101, utilizes full chest computed tomography images to detect various degrees of COVID-19 infection. To enhance detection accuracy, computed tomography images were initially preprocessed through segmentation and interpolation. They employed pre-trained deep convolutional neural network models, such as residual network (ResNet-50), residual network (ResNet-101), densely connected convolutional network (DenseNet-169), and densely connected convolutional network (DenseNet-201). A deep convolutional neural network with residual network (ResNet-101) as a pillar for ReCOV-101 overcomes the challenges of vanishing gradients by utilizing skip connections. It avoids training from shallow layers and connects directly to the output layer. Regularization is applied to skip the layer that impacts performance. The proposed model achieved an accuracy of 94.9% using residual network (ResNet-101).

Ouchicha et al. proposed CVDNet, a deep convolutional neural network model, for classifying COVID-19 infections from normal and other pneumonia cases using chest X-ray images [152]. The database contained chest X-ray images labeled into three classes, which are COVID-19, viral-pneumonia, and normal. The CVDNet architecture is based on the residual neural network and is constructed using two parallel levels with different kernel sizes to capture local and global features of the inputs. The CVDNet model achieved accuracies of 97.2% for the COVID-19 class, 96.7% for the normal class, and 96.5% for the viral pneumonia class.

Wang et al. suggested a deep convolutional neural network structure to detect COVID-19 [153]. They used the projection-expansion-projection-extension design in the construction of COVID-Net. They employed a human–machine collaborative system design in the initial step. In COVID-Net, the implemented approach blends a human-driven fundamental system architecture prototype with a machine-driven screening tool in the second step. The database contained chest X-ray images categorized into COVID-19, normal, and non-COVID-19 pneumonia classes. The COVID-Net model achieved sensitivities of 73.9%, 93.1%, 81.9%, 100% for four-class classification (normal, bacterial, non-COVID-19 viral, and COVID-19 classes), respectively. It exhibited precisions of 95.1%, 87.1%, 67%, 80% for four-class classification, respectively.

Song et al. created a deep learning-based chest computed tomography diagnostic system called "Deep Pneumonia" to identify patients with COVID-19 [154]. The database included three labels, which are COVID-19 pneumonia, bacterial pneumonia, and healthy subjects. The DRENet structure was constructed using residual network (ResNet-50), with the Feature Pyramid Network responsible for extracting the top K data features from every image. The proposed DRENet could accurately discriminate COVID-19 patients from bacterial pneumonia patients with an accuracy of 86%, sensitivity of 96%, precision of 79%, and F1-score of 87%. They claimed that the model could extract primary lesion features, especially ground-glass opacity (GGO), which are visually helpful for assisting doctors in making diagnoses.

Turkoglu proposed a method for the detection of COVID-19 through chest computed tomography images using a Multiple Kernels-Extreme Learning Machine-based Deep Neural Network [155]. They applied data augmentation techniques on computed tomography images to perform binary classification. The deep features were extracted from computed tomography images using a convolutional neural network. For this purpose, a pre-trained convolutional neural network-based densely connected convolutional network (DenseNet-201) architecture, which is based on the transfer learning approach, was used. An extreme learning machine classifier, based on different activation methods, was employed to assess the architecture's performance. Lastly, the final class label was determined using the majority voting method to predict the results obtained from each architecture based on ReLU-extreme learning machine, PReLU-extreme learning machine, and TanhReLU-extreme learning machine. The highest accuracy was achieved by ReLU activation in the multiple kernels-extreme learning machine framework.

Wu et al. proposed a weakly supervised deep active learning framework called COVID-AL for diagnosing COVID-19 using computed tomography images and patient-level labels [156]. The database included computed tomography images labeled into three classes, which are COVID-19 pneumonia, pneumonia, and the normal class. COVID-AL consists of a 2D U-Net for lung region segmentation and a novel hybrid active learning strategy with a tailor-designed 3D residual

network for COVID-19 diagnosis. In four downsampling steps, the encoder of the network segmentation retrieves image features through two convolutional and pooling layers. The decoder of the segmentation network avoids connecting to add features in the same phase. The COVID-AL model achieves an accuracy of 86.6% and precision of 96.2%. With only 30% of the labeled data, it achieves high accuracy using the entire dataset.

Tiwari et al. proposed an architecture based on deep learning by integrating a capsule network with different variants of convolutional neural networks [157]. Specifically, densely connected convolutional network (DenseNet), Residual Network (ResNet), Visual Geometry Group Network (VGGNet), and MobileNet were utilized with CapsNet to detect COVID-19 cases using lung computed tomography images. It has been found that all four models provide adequate accuracy. The highest classification accuracy of 99% was attained by MobileCapsNet. They claimed that an Android-based app can be deployed using the MobileCapsNet model to detect COVID-19, as it is a lightweight model and best suited for handheld devices like mobile phones.

Hussain et al. constructed a convolutional neural network model called CoroDet using chest X-ray and computed tomography images for COVID-19 detection [158]. The model achieved 99.1% accuracy, 99.2% precision, 98.1% recall, and 98.5% F1-score for binary classification (i.e., COVID-19 pneumonia and normal). It also exhibited 94.2% accuracy, 95.3% precision, 97.4% recall, and 98.6% F1-score for three-class classification (i.e., COVID-19 pneumonia, non-COVID pneumonia, and normal). They claimed that CoroDet may assist clinicians in making appropriate decisions for COVID-19 detection and may mitigate the problem of a scarcity of testing kits.

Perumal et al. introduced a deep learning approach for classifying COVID-19 from chest X-ray and computed tomography images [159]. The database contained three classes, which are COVID-19 pneumonia, other viral and bacterial pneumonias, pulmonary diseases, and normal classes. Weiner filters were used to enhance image quality by eliminating noise. Texture feature extraction was accomplished using Haralick features, which focus only on the area of interest to

detect COVID-19 through statistical analyses. The proposed convolutional neural network model used transfer learning and three pre-trained networks, which are Visual Geometry Group16 (VGG16), Residual Network (ResNet50), and InceptionV3. The Visual Geometry Group16 (VGG16) model offered the highest accuracy of 93.8% for COVID-19 detection.

Chandra et al. presented an automatic COVID screening system that uses radiomic texture descriptors extracted from chest X-ray images to identify normal, suspected, and non-COVID-19 infected patients [160]. The authors distinguished between non-COVID-19, pneumonia, normal and aberrant classes. For classification purposes, they employed artificial neural networks, decision trees, k-nearest neighbors, naive Bayes, majority voting algorithm, and support vector machines with different kernel functions, including RBF, polynomial, and linear kernels. The majority voting algorithm yielded the best performance. Hence, the proposed system utilizes a two-phase classification approach (normal vs. abnormal and non-COVID-19 vs. pneumonia) using a majority vote-based classifier ensemble of five benchmark supervised classification algorithms. It achieved an accuracy of 91.3% and an area under the ROC curve (AUC) of 83.1%. They stated that the Friedman post-hoc multiple comparisons and z-test statistics reveal that the results of the automatic COVID screening system are statistically significant.

Pahar et al. proposed a machine learning-based COVID-19 cough classifier, which can discriminate COVID-19-positive coughs from both COVID-19-negative and healthy coughs recorded on a smartphone [161]. Dataset skew was addressed by applying the synthetic minority oversampling technique (SMOTE). The normalization method was employed for data preparation. Features were extracted using mel-frequency cepstral coefficients, log frame energies, zero-crossing rate, and kurtosis. Conventional machine learning techniques, such as support vector machine, logistic regression, k-nearest neighbour, multilayer perceptron, convolutional neural network, long short-term memory network, and residual network (ResNet-50), were utilized for classification. A leave-p-out cross-validation scheme was used to train and evaluate these machine learning classifiers. The best performance was exhibited by the residual network (ResNet-50) classifier, which was best able to discriminate between COVID-19-positive and the healthy

coughs with an area under the ROC curve (AUC) of 98%. A long short-term memory classifier was best able to discriminate between COVID-19-positive and COVID-19-negative coughs, with an area under the ROC curve (AUC) of 94% after selecting the best 13 features through a sequential forward selection. They also indicated that COVID-19-positive coughs are 15%–20% shorter than non-COVID coughs.

Zheng et al. proposed a framework called "unsupervised meta-learning with self-knowledge distillation" for distinguishing between COVID-19 pneumonia and other pneumonia patients [162]. They utilized a database consisting of COVID-19 pneumonia, SARS, MERS, influenza, and bacterial pneumonia. The data augmentation approach was employed to generate images. This framework comprised of two modules: one based on network-based learning and the other on relational models, which capture and memorize the relationships among different images. Utilizing the densely connected convolutional network (DenseNet-121) architecture, they extracted network-based learning characteristics. The relational model was represented by an 8-pooling layer network architecture. The network was divided into several parts, with knowledge from the deeper layers is compressed into the shallow ones. The final results were obtained from the proposed model by teaching it to compare image features. This model achieved higher performance compared to supervised models, including DenseNet-121, DenseNet-161, ResNet-34, and Visual Geometry Group19 (VGG19).

Miao et al. created an unsupervised meta-learning model for screening COVID-19 patients [163]. This model does not require a pre-trained model, which resolves the limitation of model construction. Furthermore, the proposed unsupervised meta-learning framework addresses the issues of sample imbalance and sample quality. The unsupervised meta learning model consists of both a deep learning model and gradient-based optimization. Convolution, max-pooling, and batch normalization are some of the layers in the deep learning model. The accuracy of the proposed unsupervised meta-learning model is 3% to 10% higher than that of the existing convolutional neural network models.

Xu et al. investigated a location-attention technique-based screening method

to differentiate COVID-19 from influenza-A viral pneumonia and healthy subjects using pulmonary computed tomography images [164]. The collection comprises computed tomography images that were labeled into three classes, which are COVID-19, influenza-A viral pneumonia, and healthy. First, candidate infection regions were segmented from the pulmonary computed tomography image set using a 3D deep learning model. These separated images were then categorized into COVID-19, influenza-A viral pneumonia, and irrelevant to infection groups, along with the corresponding confidence scores, using a location-attention classification model. Finally, the infection type and overall confidence score for each computed tomography case were calculated using the Noisy-OR Bayesian function. The overall accuracy rate was 86.7% for all the computed tomography cases combined.

Rajaraman et al. developed a COVID-19 classification and localization methodology using chest X-ray images [165]. The model comprises various steps, including a segmentation block, repeated specific transfer learning models, and class-selective relevance mapping-based region of interest (ROI) localization. A custom U-net architecture was designed for segmentation purposes. Visual Geometry Group16 (VGG16), Visual Geometry Group19 (VGG19), Inception-V3, Extreme Inception (Xception), densely connected convolutional network (DenseNet-121), NasNet-Mobile, MobileNet-V2, and Residual Network (ResNet-18) were utilized for knowledge transfer purposes. Class-selective relevance mapping-based region of interest (ROI) localization was applied to interpret the predictions of individual convolutional neural networks and compare them against the ground truth. They found that ensemble approaches significantly improved classification and localization performance.

Additionally, a few previous studies have developed machine learning techniques that utilize patients' clinical data (fever and cough), laboratory data (complete blood counts), or exposure history for COVID-19 detection [166, 167].

Cabitza et al. used laboratory data, specifically complete blood counts, which are both cost-effective and capable of delivering rapid results for the identification of COVID-19 [166]. They employed five different machine learning models, which

included logistic regression, naive Bayes, k-nearest neighbor, random forest, and support vector machine, to perform classification. The area under the receiver operating characteristic curve (AUC) for these models ranged from 75% to 78%, while the specificity ranged from 92% to 96%. Notably, the k-nearest neighbor classifier exhibited the highest accuracy. They concluded that machine learning models can be effectively applied to laboratory data as both an adjunct and an alternative method to the RT-PCR test for identifying COVID-19 patients.

Arpaci et al. developed a method based on clinical-characteristics for predicting COVID-19 [167]. They employed 14 clinical features and utilized 6 traditional machine learning classifiers, including a Bayesian classifier, meta-classifier (classification via regression), rule learner (PART), decision tree (J48), lazy classifier (IBk), and logistic regression. The results showed that the CR meta-classifier was the most accurate classifier for predicting positive and negative COVID-19 cases, achieving an accuracy of 84.2%. Weka (v.3.8.4) data mining tool was used for data analysis and testing the predictive models.

Chapter 2

Machine Learning based Hybrid Anomaly Detection Technique for Automatic Diagnosis of Cardiovascular Diseases using Cardiac Sympathetic Nerve Activity and Electrocardiogram

This study proposes the first automated artificial intelligence-based hybrid anomaly detection technique consisting of various signal processing, feature extraction, supervised, and unsupervised machine learning methods that jointly and simultaneously analyze 12-lead CSNA and ECG data to perform fast, early, and accurate detection of coronary artery diseases. The block diagram illustrating the overall structure and methodology of the study is shown in Figure 2.1. In-depth explanations of the various components and processing steps of the proposed artificial intelligence-based hybrid anomaly detection technique can be found within the subheadings of the Materials and Methods section.

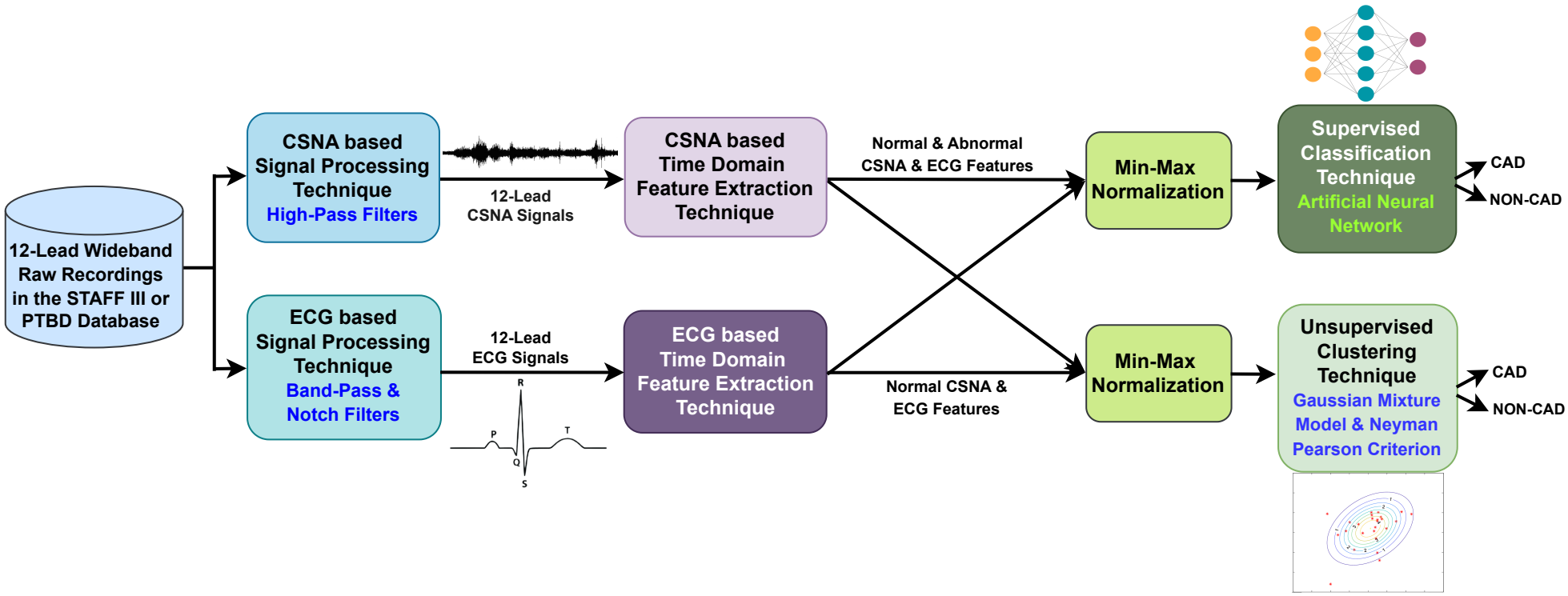

Figure 2.1: The block diagram that demonstrates various components of the proposed automated artificial intelligence-based hybrid anomaly detection technique, which are signal processing, feature extraction, supervised classification, and unsupervised clustering methods. The supervised and unsupervised machine learning methods were independently trained with 12-lead ECG and CSNA data, during which they learned to successfully distinguish between patients with and without coronary artery disease.

2.0.1 Data Acquisition and Preparation

2.0.1.1 The Staff III Database

One of the databases used for the development and performance evaluation of the proposed automated artificial intelligence-based hybrid anomaly detection technique is the fully labeled STAFF III database on PhysioNet, which is a publicly available repository of medical research data [168, 169]. The STAFF III database was constructed by acquiring wideband recordings from 104 patients with coronary artery disease who underwent percutaneous coronary intervention at Charleston Area Medical Center (U.S.). The demographics and clinical characteristics of the patients included in the study are presented in Table 2.1.

TABLE 2.1: The DEMOGRAPHICS and CLINICAL CHARACTERISTICS of the PATIENTS

Age	55.6 ± 17
Male	65 (62.5 %)
Diabetes	27 (26 %)
Hypertension	43 (41.3 %)
Smoking	33 (31.7 %)

The numerical variables are presented as the mean ± standard deviation.
The categorical variables are presented as the number of patients
and percentage with respect to the total population.

The database was constructed by Duke University as a part of a clinical research study to investigate high-frequency anomalies in ECG signals that occur during artificially induced myocardial ischemia caused by complete coronary artery occlusion due to percutaneous coronary intervention [168, 169]. Percutaneous coronary intervention is a minimally invasive surgical procedure that can cause significant anomalies in the ST segment and T wave of the ECG signal.

Two different types of 12-lead wideband recordings that were acquired before and during percutaneous coronary intervention from all patients in the STAFF III database were included in this study, as detailed in Table 2.2. Hence, a total of 1248 pre-inflation (normal) and 1248 inflation (abnormal) recordings were utilized to develop and evaluate the proposed artificial intelligence-based hybrid anomaly detection technique. To date, this database is the largest that simulates high-frequency anomalies in wideband recordings acquired during artificially induced myocardial ischemia under a percutaneous coronary intervention-controlled environment. Therefore, it serves as an excellent testbed for developing and evaluating various artificial intelligence techniques that can diagnose and classify coronary artery disease.

Before percutaneous coronary intervention, the 12-lead pre-inflation (normal) recordings were acquired prior to catheter insertion into the coronary artery at the preoperative room. During percutaneous coronary intervention, the 12-lead inflation (abnormal) recordings that started before coronary balloon inflation and ended after coronary balloon deflation were continuously acquired at the cardiac catheterization laboratory (operation room).

TABLE 2.2: TWO DIFFERENT TYPES of RECORDINGS and NUMBERS of the PATIENTS and RECORDINGS for EACH TYPE

Diagnostic Classes	**Numbers of the Patients**	**Numbers of the Recordings**	**Numbers of the Leads**	**Total Numbers of the Recordings**
Pre-inflation (Normal)	104	104	12	1248
Inflation (Abnormal)	104	104	12	1248
Total	104*	208	12	2496

*The pre-inflation and inflation recordings belong to the same patients. Therefore, the total number of patients is the same as the number of patients with the pre-inflation or inflation recordings.

The database contains a total of 152 stenoses in the major coronary arteries, distributed as 58 stenoses in the left anterior descendant artery (LAD), 59 stenoses in the right coronary artery (RCA), 32 stenoses in the left circumflex artery (LCX), and 3 stenoses in the left main artery (LM) (Table 2.3). A total of 35 patients had previous myocardial infarction as determined by ECG criteria defined by the American Heart Association [2]. Additionally, the database includes important annotations provided by experienced cardiologists, including the occluded coronary artery in which percutaneous coronary intervention was performed, the time instants related to coronary balloon inflation and coronary balloon deflation during percutaneous coronary intervention, the patient's history of previous myocardial infarction, and the location of previous myocardial infarction.

TABLE 2.3: CLINICAL CHARACTERISTICS of the PATIENTS

Left anterior descendant artery (LAD)	58 (55.8 %)
Right coronary artery (RCA)	59 (56.7 %)
Left circumflex artery (LCX)	32 (30.8 %)
Left main artery (LM)	3 (2.9 %)
Balloon inflation time (second)	263 ± 54
History of previous myocardial infarction	35 (33.7 %)

The numerical variables are presented as the mean ± standard deviation.

The categorical variables are presented as the number of patients and percentage with respect to the total population.

The data were acquired using custom-made ECG data acquisition equipment (Siemens–Elema AB, Sweden) with a wider frequency bandwidth (500 Hz) and higher sampling rate compared to conventional ECG devices. The recordings were digitized with a sampling rate of 1000 Hz, 16-bit sampling resolution, and 0.6 μV amplitude resolution. The patients who suffered from cardiac arrhythmia or myocardial infarction during data acquisition were excluded from the database.

2.0.1.2 The Physikalisch-Technische Bundesanstalt Diagnostic Database

Another database used for the development and performance evaluation of the proposed automated artificial intelligence-based hybrid anomaly detection technique is the fully labeled Physikalisch-Technische Bundesanstalt (PTB) Diagnostic (PTBD) database on the PhysioNet repository [169, 170, 171]. It was constructed by Benjamin Franklin University (Berlin, Germany) to investigate high-frequency anomalies in ECG signals of the patients with various cardiovascular diseases. Among several different diagnostic classes of cardiovascular diseases present in the PTBD database that are shown in Table 2.4, the only diagnostic class which is a type of coronary artery disease is the myocardial infarction class.

TABLE 2.4: DIAGNOSTIC CLASSES of the SUBJECTS in the PTBD DATABASE

Diagnostic Classes	**Number of the Subjects**
Healthy Controls	52
Myocardial Infarction	148
Cardiomyopathy/Heart Failure	18
Bundle Branch Block	15
Dysrhythmia	14
Myocardial Hypertrophy	7
Valvular Heart Disease	6
Myocarditis	4
Miscellaneous	4

Since one of the aims of this study was to perform accurate and reliable detection of coronary artery disease, we considered the myocardial infarction patients in the PTBD database as the abnormal class and the healthy controls as the normal class to perform binary classification. Hence, the 12-lead wideband recordings acquired from 52 healthy controls and 104 myocardial infarction patients, which account for a total of 156 subjects, were included in this study to develop and evaluate the proposed artificial intelligence-based hybrid anomaly detection technique (Table 2.5).

TABLE 2.5: TWO DIFFERENT TYPES of RECORDINGS and NUMBERS of the SUBJECTS and RECORDINGS for EACH TYPE

Diagnostic Classes	**Numbers of the Subjects**	**Numbers of the Recordings**	**Numbers of the Leads**	**Total Numbers of the Recordings**
Healthy Controls (Normal)	52	104*	12	1248
Myocardial Infarction (Abnormal)	104	104	12	1248
Total	156	208	12	2496

*The number of the recordings after the implementation of the synthetic minority oversampling technique (SMOTE) to generate new synthetic samples in the minority class (healthy controls).

In order to overcome the class imbalance between the two classes (myocardial infarction and healthy controls) in the PTBD database and prevent bias towards the majority class (myocardial infarction), we adjusted the numbers of recordings belonging to each of the two classes to be equal. In order to equate the numbers of recordings in the minority and majority classes, we employed the synthetic minority oversampling technique (SMOTE) was employed to generate new synthetic samples in the minority class (healthy controls) by interpolating between existing minority class samples and their nearest neighbors. SMOTE created new synthetic samples that resemble the existing minority class samples, while introducing some variations to expand the feature space. Thus, by producing synthetic samples that are representative of the minority class in the training set, the number of samples in the minority class was equalized with that of the majority class.

This way, it was ensured that the class distributions were balanced using a data resampling method and both classes had an equal number of recordings (Table 2.5). This approach guaranteed that the artificial intelligence-based hybrid anomaly detection technique assigned equal importance to both classes, improved the technique's ability to learn from the minority class, and increased the technique's generalizability. We implemented SMOTE exclusively on the training set, hence it was not applied to the validation or test sets, which ensured a fair performance evaluation of the proposed technique. Consequently, a total of 1248 normal recordings of 52 healthy controls, and 1248 abnormal recordings of 104 myocardial infarction patients were used for the development and evaluation of the proposed artificial intelligence-based hybrid anomaly detection technique (Table 2.5). The training of the automated artificial intelligence-based hybrid anomaly detection technique was performed on the oversampled and balanced training set.

All data were acquired by experienced physicians using data acquisition equipment (PTB prototype recorder, Germany) with a wide frequency bandwidth (500 Hz) and high sampling rate. The recordings were digitized with a sampling rate of 1000 Hz, 16-bit sampling resolution, and 0.5 μV amplitude resolution. They were annotated by experienced physicians to indicate the demographic and clinical information about the patient's age, gender, diagnosis, medical history, coronary artery pathology, ventriculography, and echocardiography. Hence, the database offers an excellent testbed for developing and evaluating various AI techniques that can diagnose and classify coronary artery disease.

2.0.1.3 Enhanced Signal Processing Technique for CSNA and ECG Data Analysis

The electrical signals obtained from the skin surface of the chest wall contain signals from a wide variety of nerve activities and myocardium [1, 7, 9, 11, 14, 16, 17, 18, 19]. Because of the intensive connections between the sympathetic, motor, and sensory nerves in the body, the nerves originating from different sources can activate simultaneously. Thus, the electrical signals acquired from the chest

wall ($y_i(t)$) contain raw ECG ($e_i(t)$), cardiac sympathetic nerve activity (CSNA) ($c_i(t)$), motor and sensory nerve activities (MSNA) ($s_i(t)$), and muscle activity (EMG) ($m_i(t)$) (Equation 2.1).

$$y_i(t) = e_i(t) + c_i(t) + s_i(t) + m_i(t), \quad i = 1, .., N. \tag{2.1}$$

In electrical signals acquired from the chest wall, CSNA will be delayed and will decrease in amplitude as it propagates away from its source. This delay and decrease in amplitude can be mathematically modeled by the delay parameter τ_i and the amplitude parameter α_i (Equation 2.2).

$$c_i(t) = \alpha_i \, c(t - \tau_i), \qquad 0 < \alpha_i < 1 \tag{2.2}$$

Most of the diagnostic information in ECG resides below 150 Hz, therefore, the American Heart Association recommends a frequency bandwidth of 0.5 Hz to 150 Hz for the diagnostic monitoring of ECG [2]. Moreover, the electromyogram (EMG) is approximately band-limited to 100 Hz, with small amounts of muscle activity occasionally reaching 400 Hz [2, 14]. Therefore, the implementation of a high-pass filter with a cut-off frequency of f_C=150 Hz to the wideband raw recordings acquired from the chest wall will effectively eliminate ECG and EMG to a large extent.

The hypothesis of this study, which is based on the previous studies in the literature [14, 16, 17, 18], indicates that CSNA is uncorrelated with MSNA, and thus, it is possible to decouple CSNA from MSNA. Therefore, the signal activity obtained as a result of high-pass filtering the electrical signals acquired from the chest wall will mostly originate from CSNA. In cases where the parameters α_i and τ_i are known, CSNA can be estimated as shown in Equation 2.3.

$$\hat{c}(t) = \frac{\sum_{i=1}^{N} \alpha_i \; y_i(t + \tau_i)}{\sum_{i=1}^{N} \alpha_i^2} \tag{2.3}$$

Two signal processing techniques, which include various digital filtering methods that remove unwanted frequency components from the wideband raw recordings while preserving the diagnostic information within the recordings, were developed to detect the 12-lead CSNA and ECG signals of all subjects in the STAFF III and PTBD databases (Figure 2.1).

Firstly, the band-pass and Notch filters were developed and implemented on the wideband raw recordings in the STAFF III and PTBD databases to detect the 12-lead ECG signals of all subjects. The lowest frequency component of the ECG signal is generally defined by the slowest possible heart rate, which is 40 beats per minute (bpm) [2, 14]. Hence, assuming a periodic signal, the lowest frequency component of the ECG signal can be at least 0.67 Hz. Therefore, to enhance the quality of ECG signals by eliminating low-frequency noises, such as baseline wander and respiratory signals, the lower cut-off frequency of the band-pass filter was designed to be f_{L_1}= 0.5 Hz.

Moreover, the high-frequency noises in ECG signals, such as muscle activity (EMG) and motion artifacts, were eliminated by designing the band-pass filter to have a higher cut-off frequency of f_{H_1}=150 Hz, which is compatible with the recommendations of the American Heart Association for the diagnostic monitoring of ECG [2].

Furthermore, the 60 Hz power-line interference in the STAFF III database was eliminated by developing Notch filters with lower and higher cut-off frequencies of f_{L_2}= 59 Hz and f_{H_2}= 61 Hz, respectively [1, 2, 3, 4, 5, 6, 7, 8, 9, 10, 11, 12, 19, 48, 87]. Similarly, the 50 Hz power-line interference in the PTBD database was eliminated by developing Notch filters with lower and higher cut-off frequencies of f_{L_3}= 49 Hz and f_{H_3}= 51 Hz, respectively.

A QRS complex detection technique that can adapt to the instantaneous changes in ECG signals by setting an adaptive threshold for each patient, which is higher than the P and T waves and lower than the QRS complex in amplitude, was developed [1, 2, 3, 4, 5, 6, 7, 8, 9, 10, 11, 12, 19, 48, 87]. By detecting the signal values where the ECG signal amplitude is higher than the predefined

threshold, the robust localization of the QRS complexes in the time domain was performed. By using the detected QRS complexes as the reference points, the ECG signals of all subjects were segmented into individual periods, each corresponding to a single heartbeat. Lastly, the isoelectric line, which represents the reference potential level of the measured heart activity for each recorded heartbeat, was determined and removed from each ECG period to accurately detect ischemic ECG anomalies.

Secondly, high-pass filters with a cut-off frequency of f_C=150 Hz were developed and implemented on the wideband raw recordings in the STAFF III and PTBD databases to detect the 12-lead CSNA signals of all subjects [1, 7, 9, 11, 19]. Moreover, the performances of various high-pass filters with different cut-off frequencies up to 500 Hz were investigated to detect CSNA. The efforts made to optimize the filters' cut-off frequency for displaying CSNA revealed that a high-pass filter with a cut-off frequency of f_C=150 Hz provides higher amplitude CSNA and better signal-to-noise ratio (SNR), while effectively suppressing ECG signals. Further increases in the cut-off frequency of the filter eliminated EMG signals to a large extent. However, it also resulted in lower amplitude CSNA and worse signal-to-noise ratio (SNR). Therefore, for higher cut-off frequencies of the filter, the specificity of CSNA recording increased. However, a majority of CSNA was filtered out, which reduced the sensitivity of CSNA recording.

Furthermore, the power ratios of the inflation (abnormal) CSNA (PR_i) were investigated across different frequency bands for all patients in the STAFF III and PTBD databases by designing band-pass filters that have six consecutive overlapping frequency ranges, as shown in Table 2.6 .

TABLE 2.6: CONSECUTIVE OVERLAPPING FREQUENCY BANDS and RANGES

Frequency Bands	**Frequency Ranges**
i=1	150 Hz−250 Hz
i=2	200 Hz−300 Hz
i=3	250 Hz−350 Hz
i=4	300 Hz−400 Hz
i=5	350 Hz−450 Hz
i=6	400 Hz−500 Hz

The power ratio of the inflation (abnormal) CSNA (PR_i) was obtained by calculating the ratio of the average inflation CSNA power during percutaneous coronary intervention (P_{burst}) to the average inflation CSNA power before percutaneous coronary intervention ($P_{baseline}$), as shown in Equation 2.4, where $c_i(t)$ denotes the inflation (abnormal) CSNA.

$$PR_i = \frac{P_{burst}}{P_{baseline}} = \frac{\frac{1}{\Delta t_1}\int_{t_2}^{t_3} |c_i(t)|^2 dt}{\frac{1}{\Delta t_0}\int_{t_0}^{t_1} |c_i(t)|^2 dt} \ , \qquad \Delta t_1 = t_3 - t_2 \ , \quad \Delta t_0 = t_1 - t_0 \tag{2.4}$$

The experiment results demonstrated that the power ratio of the inflation (abnormal) CSNA (PR_i) was consistently higher for frequency ranges between 150 Hz and 400 Hz (frequency bands between $1 \leq i \leq 4$) for all patients in the STAFF III and PTBD databases.

2.0.2 Enhanced Feature Extraction Technique

By using the pre-processed 12-lead CSNA and ECG signals in the STAFF III and PTBD databases, a time-domain feature extraction technique that extracts the statistical CSNA and ECG features that are critical for the reliable diagnosis of coronary artery disease was developed [1, 3, 4, 5, 6, 7, 8, 9, 10, 11, 12, 19, 48].

2.0.2.1 Enhanced Feature Extraction Technique for CSNA Signals

2.0.2.1.1 Number of CSNA Peaks: Peaks of the CSNA signals ($p[n]$) were detected by defining an adaptive threshold (ξ) that is specific to the CSNA signal ($c[n]$) of each patient. By identifying signal values at which the amplitude of CSNA was greater than the predefined threshold (ξ) through a sliding time window (N), the time domain localization of CSNA peaks was performed (Equation 2.5). The number of CSNA peaks ($u[n]$) was obtained by calculating the summation of CSNA peaks through the sliding time window (N) (Equation 2.6).

$$p[n] = \begin{cases} 1, & c[n+k] \geq \xi \ , \quad k = 0, .., N-1. \\ 0, & c[n+k] < \xi \end{cases} \tag{2.5}$$

$$u[n] = \sum_{m=0}^{N-1} p[n+m] \tag{2.6}$$

2.0.2.1.2 Average CSNA: The average voltage of CSNA per sample ($a[n]$) was estimated by integrating CSNA ($c[n]$) over the sliding time window (N) and dividing the total voltage by the overall number of samples (N) in the same window (Equation 2.7).

$$a[n] = \frac{1}{N} \sum_{m=0}^{N-1} |c[n+m]| \tag{2.7}$$

2.0.2.1.3 Maximum CSNA: It was obtained by calculating the maximum signal amplitude of CSNA ($c[n]$) through the sliding time window (N) (Equation 2.8).

$$m[n] = \max_{0 \leq m \leq N-1} (c[n+m]) \tag{2.8}$$

2.0.2.2 Enhanced Feature Extraction Technique for ECG Signals

2.0.2.2.1 ST Segment Level: It was obtained by calculating the summation of all signal amplitudes through the ST segment ($q[n]$) and dividing the total voltage by the overall number of samples (L) in the same interval (Equation 2.9).

$$s[n] = \frac{1}{L}\sum_{k=0}^{L-1} q[n+k] \tag{2.9}$$

2.0.2.2.2 ST Segment Slope ($\hat{\beta}_1$): It was estimated as the slope of the best fitting line ($\hat{q}[n]$) in Equation 2.11 in terms of least squares to the samples of the ST segment ($q[n]$). This estimation was performed by finding the least squares estimates β_0 and β_1 that minimize the sum of squared residuals in Equation 2.10 .

$$f[\beta_0,\ \beta_1] = \sum_{k=0}^{L-1}(q[n+k] - (\beta_1 w[n+k] + \beta_0))^2 \tag{2.10}$$

$$\hat{q}[n] = \hat{\beta}_1 w[n] + \hat{\beta}_0 \tag{2.11}$$

2.0.2.2.3 T Wave Area: It was approximated by implementing the trapezoidal rule through the samples of the T wave ($v[n]$) (Equation 2.12).

$$t[n] = \sum_{k=1}^{M} \frac{(v[n_{k-1}] + v[n_k])}{2}\,\Delta n_k \ , \qquad \Delta n_k = \frac{n_k - n_{k-1}}{M} \tag{2.12}$$

2.0.2.2.4 T Wave Amplitude: It was obtained by locating the maximum or minimum amplitude of the T wave ($v[n]$) in the time domain (Equation 2.13).

$$w[n] = \begin{cases} \min\limits_{n_0 \le n \le n_M}(v[n]), & v[n] \le 0 \\ \max\limits_{n_0 \le n \le n_M}(v[n]), & v[n] > 0 \end{cases} \tag{2.13}$$

2.0.3 Supervised Classification Technique using Artificial Neural Networks

In the literature, artificial neural network is the most preferred machine learning method for the diagnosis or classification of various cardiovascular diseases by detecting anomalies in ECG data [7, 8, 9, 10, 11, 20, 26, 46, 48]. This preference can be attributed to the various advantages of artificial neural network, including its strong ability to learn and model non-linear complex relationships between the input and output, its robustness to noise, its ability to handle missing or insufficient data, its generalization capability, its remarkable scalability, its ability to perform parallel processing, and its high speed. Additionally, various types of artificial neural networks can be customized to create tailored solutions that address specific tasks required by physicians, which significantly contributes to their superior performance in the detection of cardiovascular diseases.

Therefore, in this study, a supervised learning method based on artificial neural network that performs simultaneous and robust detection of anomalies in the 12-lead CSNA and ECG data was developed to realize fast, early, and accurate diagnosis of coronary artery disease. Firstly, the 12-lead normal and abnormal CSNA and ECG features were normalized using the min-max normalization method to scale the features of different classes in the same range and to ensure that the developed artificial neural network classifier assigns equal importance to data belonging to the two classes (i.e., normal and abnormal). Hence, by bringing all input variables within a standardized range, our aim was to avoid any bias that may arise due to differences in the scales of the features and to guarantee that the artificial neural network classifier can accurately learn from the data, thereby assuring fairness in the classification process.

In order to evaluate the performance of the developed artificial neural network classifier on previously unseen data, the whole data in the STAFF III and PTBD databases were independently and randomly split into non-intersecting training and test sets using the 10-fold cross-validation method, as shown in Tables 3.3 and 3.6 . Therefore, the entire data in each database were randomly partitioned into 10 equal-sized subsets, where one of these subsets formed the test set that was

exclusively used to assess the generalization performance of the artificial neural network classifier. The remaining subsets were aggregated to form the training set that was used to train the artificial neural network classifier and optimize its (hyper)parameters. The test set remained unexposed during the training of the artificial neural network to ensure an unbiased estimate of the classifier's performance on previously unseen data.

Additionally, the training sets in the STAFF III and PTBD databases were further independently and randomly divided into the training (75%) and validation (25%) subsets, as shown in Tables 3.3 and 3.6 , using the holdout cross-validation method to prevent the artificial neural network classifier from over-fitting to the training sets and ensure better generalization. To guarantee robustness, this process was repeated 10 times for each cross-validation fold, resulting in 10 independent and non-intersecting training, validation, and test subsets that were randomly constituted. Each pattern was used in the test set exactly once in each cross-validation fold to maintain fairness.

By taking the average of the statistical performance results calculated across 10 different cross-validation folds, a single estimation that represents the binary classification performance of the optimum artificial neural network classifier for each of the training, validation, and test subsets was independently produced for the STAFF III and PTBD databases. The absence of class imbalance between the two classes in the training and validation sets of both databases prevented bias and over-fitting during training, and allowed the artificial neural network classifier to generalize very well on previously unseen data.

TABLE 2.7: The NUMBERS of the RECORDINGS in the TRAINING, VALIDATION and TEST SETS for the STAFF III DATABASE

Diagnostic Classes	Training Set	Validation Set	Test Set	Total
Pre-inflation (Normal)	840	276	132	1248
Inflation (Abnormal)	840	276	132	1248
Total	1680	552	264	2496

The numerical variables are presented as the total number of recordings including all 12-leads.

TABLE 2.8: The NUMBERS of the RECORDINGS in the TRAINING, VALIDATION and TEST SETS for the PTBD DATABASE

Diagnostic Classes	Training Set	Validation Set	Test Set	Total
Healthy Controls (Normal)	840	276	132	1248
Myocardial Infarction (Abnormal)	840	276	132	1248
Total	1680	552	264	2496

The numerical variables are presented as the total number of recordings including all 12-leads.

The feed-forward artificial neural network classifier architecture consists of three layers, which are an input layer with seven neurons, a hidden layer, and an output layer with two neurons. The number of neurons in the input layer is equal to the total number of CSNA and ECG features. In order to empirically determine the optimum number of hidden layers, various multilayer perceptron with single and multiple hidden layers were developed. The experimental results showed that multilayer perceptron with a single hidden layer exhibited better performance and shorter training time. Moreover, the optimum number of neurons and the ideal activation function in the hidden layer were determined using the grid search method. For this purpose, various multilayer perceptrons with varying numbers of hidden neurons and different activation functions were developed, including linear, sigmoid (logistic), binary step, hyperbolic tangent, and Gaussian. The experimental results indicated that multilayer perceptrons with 24 and 26 hidden neurons provided the best classification performances on the STAFF III and PTBD databases, respectively. Furthermore, the activation function in the hidden and output layers that provided the highest classification performances on both databases was the sigmoid (logistic), which was also the most commonly preferred activation function in the literature for binary classification tasks due to its good generalizability [10, 11, 20, 26, 46, 48] Consequently, the output of the optimum artificial neural network classifier demonstrates a patient's probability of belonging to one of the two classes (coronary artery disease and non-coronary artery disease).

The training of the artificial neural network classifier consisted of the feed-forward and back-propagation training parts, which is one of the most commonly used training algorithms for supervised learning [7, 8, 9, 10, 11, 20, 26, 46, 48]. The weights of the artificial neural network classifier were initially assigned arbitrarily using small random and normally distributed numbers. In the course of training, the artificial neural network classifier was exposed to the training set for a predefined number of feed-forward and back-propagation iterations to perform the learning task. During the feed-forward phase, the output of the artificial neural network classifier was calculated for each sample. During the back-propagation phase, the artificial neural network classifier utilized the error

in the output to correct its future calculations, aiming to converge towards the desired output. Hence, during back-propagation training, the weights were gradually adjusted to optimize the overall computation carried out by the artificial neural network classifier and minimize the difference between the actual and predicted outputs of the classifier. This difference is commonly referred to as the cost function (E) expressed in Equation 2.14, where M represents the number of samples in the training set, $\mathbf{o}_i$ denotes the output vector of the artificial neural network classifier, and $\mathbf{d}_i$ corresponds to the target vector for each training pair i.

$$E = \frac{1}{M} \sum_{i=1}^{M} \|\mathbf{d}_i - \mathbf{o}_i\|^2 \tag{2.14}$$

The back-propagation algorithm is a gradient-descent method used to minimize the mean squared error E, where $\mathbf{w}$ in Equation 2.16 represents the weight vector between the layers, and η in Equation 2.15 denotes the learning rate of the artificial neural network classifier, which was optimized as 10^{-3}.

$$\Delta \mathbf{w}_i = -\eta \frac{\partial E}{\partial \mathbf{w}_i} , \qquad 0 < \eta < 1 \tag{2.15}$$

$$\mathbf{w}_{(i+1)} = \mathbf{w}_i - \eta \frac{\partial E}{\partial \mathbf{w}_i} \tag{2.16}$$

The training length of the artificial neural network classifier was periodically evaluated using the early stopping regularization method to optimize its performance and prevent over-fitting to the training set due to over-training. Hence, after every predefined number of feed-forward and back-propagation iterations, the current weights were saved, and the performance of the artificial neural network classifier was assessed on the validation set, which represents an estimate of its generalizability on previously unseen data. The training of the artificial neural network classifier was terminated when the mean squared error (MSE) on the validation set was minimized. Thus, by stopping the training early, the risk of over-optimizing the parameters of the artificial neural network classifier for the training set was avoided.

Therefore, the optimum configuration of the artificial neural network classifier with the ideal combination of (hyper)parameters, including input-output weights and biases, that provides the best classification performance on the independent validation set was determined using the early stopping regularization method. Finally, the binary classification performance and generalizability of the optimum artificial neural network classifier on previously unseen data were evaluated by testing the classifier on the independent test set. The experiments were conducted using a computer equipped with an Intel^R Core^{TM} i7 processor, 16 GB RAM, CPU at 3.60 GHz, and NVIDIA GeForce RTX 2070 GPU. The software that processes and analyzes the data was prepared using MATLAB (R2021) (MathWorks, USA).

2.0.4 Unsupervised Clustering Technique using Gaussian Mixture Models and Neyman-Pearson Criterion

In order to develop a method that can be used in cases where the abnormal CSNA and ECG data are missing, we propose an unsupervised learning method based on Gaussian mixture model and the Neyman-Pearson criterion that performs simultaneous and robust detection of anomalies in the 12-lead normal CSNA and ECG data to realize fast, early, and accurate diagnosis of coronary artery disease.

In the literature, Gaussian mixture model has been widely employed as an unsupervised machine learning method for the diagnosis and classification of various cardiovascular diseases [6, 8, 10, 11, 43, 48, 52, 53, 81]. This can be attributed to the numerous advantages of Gaussian mixture model, including its efficiency in clustering and model fitting, its ability to model and estimate a wide range of probability distributions, its capability to effectively handle missing or insufficient data, and its robustness to outliers in the data. Moreover, Gaussian mixture model is a generative method that is capable of generating new synthetic data samples that resemble the original dataset, which can be beneficial for data augmentation tasks. It can also be utilized to identify outliers in the data by assigning low probabilities to data points that do not fit the estimated

mixture model, making it very useful in anomaly detection tasks. Furthermore, it provides interpretable parameters of the Gaussian components, which can offer insights into the underlying distribution of the data.

In this study, the optimization of the Gauss parameters ($\boldsymbol{\Upsilon}$) was performed using the Expectation-Maximization (EM) algorithm to maximize the probability density function (PDF) of the mixture, which is mathematically formulated as a weighted sum of K Gaussian density components, as shown in Equation 2.18 . Here, $\mathbf{x}$ represents the D-dimensional feature vector, π_k denotes the mixture coefficients (weights of the Gaussian components), μ_k corresponds to the mean vector, and $\boldsymbol{\Sigma}_k$ represents the covariance matrix. The density of each component was mathematically described by the multivariate Gaussian distribution, which is a widely employed statistical model for characterizing data distributions (Equation 2.17) [6, 8, 10, 11, 43, 48, 52, 53, 81].

$$\mathcal{N}(\mathbf{x}|\mu_k, \boldsymbol{\Sigma}_k) = \frac{1}{(2\pi)^{\frac{D}{2}} \ |\boldsymbol{\Sigma}_k|^{\frac{1}{2}}} \ exp\Big\{ -\frac{1}{2}(\mathbf{x}-\mu_k)^T \ \boldsymbol{\Sigma}_k^{-1}(\mathbf{x}-\mu_k)\Big\} \tag{2.17}$$

$$g(\mathbf{x}|\boldsymbol{\Upsilon}) = \sum_{k=1}^{K} \pi_k \, \mathcal{N}(\mathbf{x}|\mu_k, \boldsymbol{\Sigma}_k) \tag{2.18}$$

The probability density function (PDF) of the Gaussian mixture was parameterized using the Gauss parameters ($\boldsymbol{\Upsilon}$) in Equation 2.19 , which consist of the mixture coefficients, the mean vector, and the covariance matrix of each component.

$$\boldsymbol{\Upsilon} = (\pi_k, \ \mu_k, \ \boldsymbol{\Sigma}_k), \qquad k = 1, .., K. \tag{2.19}$$

The mixture coefficients satisfied the conditions outlined in Equation 2.20 to assure that the total probability distribution was normalized. This guaranteed that the sum of the mixture coefficients equals one, thereby ensuring that the resulting probability distribution represents a valid probability density function (PDF).

$$\sum_{k=1}^{K} \pi_k = 1, \qquad 0 \leq \pi_k \leq 1 \tag{2.20}$$

The 12-lead normal CSNA and ECG features were normalized using the min-max normalization method to scale the features of different data types in the same range and to ensure that the developed unsupervised clustering technique assigns equal importance to different data types (i.e., CSNA and ECG data). Hence, by bringing all input variables within a standardized range, our aim was to avoid any bias that may arise due to differences in the scales of the features and to guarantee that the unsupervised clustering technique can accurately learn from the data, thereby assuring fairness in the clustering process.

The whole data in the STAFF III and PTBD databases were independently and randomly divided into non-intersecting training and test sets using the 10-fold cross-validation method to evaluate the performance of the unsupervised clustering technique on previously unseen data, as shown in Tables 3.9 and 2.10 . Each pattern was used in the test set exactly once in each cross-validation fold to maintain fairness. The test set remained unexposed during the training of the Gaussian mixture model to ensure an unbiased estimate of the technique's performance on previously unseen data.

Moreover, the training sets in the STAFF III and PTBD databases were further independently and randomly divided into the training (75%) and validation (25%) subsets, as shown in Tables 3.9 and 2.10 , using the holdout cross-validation method to prevent the Gaussian mixture model from over-fitting to the training sets and ensure better generalization. To assure robust performance evaluation, the statistical performance results calculated across 10 different cross-validation folds were averaged to obtain a single estimation that represents the clustering performance of the optimum Gaussian mixture model for each of the training, validation, and test subsets in the STAFF III and PTBD databases independently.

TABLE 2.9: The NUMBERS of the RECORDINGS in the TRAINING, VALIDATION and TEST SETS for the STAFF III DATABASE

Diagnostic Class	Training Set	Validation Set	Test Set	Total
Pre-inflation (Normal)	840	276	132	1248

The numerical variables are presented as the total number of recordings including all 12-leads.

TABLE 2.10: The NUMBERS of the RECORDINGS in the TRAINING, VALIDATION and TEST SETS for the PTBD DATABASE

Diagnostic Class	Training Set	Validation Set	Test Set	Total
Healthy Controls (Normal)	840	276	132	1248

The numerical variables are presented as the total number of recordings including all 12-leads.

The optimum parameters of the Gaussian components ($\boldsymbol{\Upsilon}$) were estimated using the Expectation-Maximization (EM) algorithm, which is an efficient iterative method for finding the maximum likelihood estimation (MLE) of the parameters in statistical models [6, 8, 10, 11, 43, 48, 52, 53, 81]. Subsequently, the joint probability density function (PDF) of the normal CSNA and ECG features was robustly estimated by fitting the optimum Gaussian mixture model with the ideal (hyper)parameters, which was optimized to improve the performance of the joint probability density function (PDF) estimation.

Furthermore, a Neyman-Pearson type approach was developed to perform the robust detection of outliers associated with coronary artery disease [8, 23, 172]. The Neyman-Pearson decision strategy is based on the concept of statistical hypothesis testing, which includes two competing hypotheses that are the null hypothesis (H_0) and the alternative hypothesis (H_1). It provides an optimal solution to hypothesis testing when making decisions based on limited data while effectively controlling the false positive and negative rates. The objective is to determine which hypothesis is more likely based on the observed data.

The 12-lead normal CSNA and ECG features were partitioned into N equal-length segments denoted as $X=\{\boldsymbol{x}_1, ..., \boldsymbol{x}_N\}$. Each segment was assumed to be independent and identically distributed (i.i.d.), meaning that each segment has the same probability distribution, and all segments are statistically mutually independent. The Neyman-Pearson decision strategy was implemented by calculating the average log-likelihood value of the segments ($P(X|H_0)$), as shown in Equation 2.22 , where N represents the total number of segments. Subsequently, these average log-likelihood values were compared with different discrimination thresholds ($\boldsymbol{\Gamma}$), as shown in the decision rule in Equation 2.23 , where H_1 represents the outliers that correspond to coronary artery disease. The decision rule in Equation 2.23 states that if the average log-likelihood value exceeded the discrimination threshold, the null hypothesis (H_0) was rejected in favor of the alternative hypothesis (H_1).

$$H_0 \colon X \in C_0 \ , \qquad H_1 \colon X \notin C_0 \tag{2.21}$$

$$P(X|H_0) = \frac{1}{N}\, log\ g(X|\boldsymbol{\Upsilon}) = \frac{1}{N}\sum_{i=1}^{N} log\ g(\boldsymbol{x}_i|\boldsymbol{\Upsilon}) \tag{2.22}$$

$$\Theta(X) = \begin{cases} H_0, & P(X|H_0) \leq \boldsymbol{\Gamma} \\ H_1, & P(X|H_0) > \boldsymbol{\Gamma} \end{cases} \tag{2.23}$$

2.1 Experimental Results and Comparative Analysis

In this section, we explain and interpret the results of the experiments conducted to evaluate the performance and generalizability of the proposed automated artificial intelligence-based hybrid anomaly detection technique on the STAFF III and PTBD databases. For this purpose, we computed the confusion matrices to calculate all of the statistical performance evaluation metrics, such as sensitivity (TPR) (Eq. 2.24), specificity (TNR) (Eq. 2.25), positive predictive value (PPV) (Eq. 2.26), negative predictive value (NPV) (Eq. 2.27), F_1-score (F1) (Eq. 2.28), and accuracy (ACC) (Eq. 2.29). Here, TP, FN, FP, and TN indicate the numbers of the true positives, false negatives, false positives, and true negatives, respectively.

$$TPR\,(\%) = \frac{TP}{TP+FN} * 100 \tag{2.24}$$

$$TNR\,(\%) = \frac{TN}{TN+FP} * 100 \tag{2.25}$$

$$PPV\,(\%) = \frac{TP}{TP+FP} * 100 \tag{2.26}$$

$$NPV\,(\%) = \frac{TN}{TN+FN} * 100 \tag{2.27}$$

$$\text{F1}\,(\%) = 2\,\frac{PPV \text{x}\, TPR}{PPV + TPR} * 100 \tag{2.28}$$

$$ACC\,(\%) = \frac{TP+TN}{TP+TN+FP+FN} * 100 \tag{2.29}$$

2.1.1 The Performance Results of the Automated Artificial Intelligence based Hybrid Anomaly Detection Technique on the Staff III Database

As a result of the implementation of the developed enhanced signal processing technique on the 12-lead wideband raw recordings in the STAFF III database, the 12-lead ECG and CSNA signals of all patients were simultaneously detected. Figures 2.2 and 2.3 demonstrate a single lead pre-inflation (normal), inflation (abnormal), and post-inflation CSNA and ECG signals of a patient in the STAFF III database, respectively.

The pre-inflation (normal) CSNA and ECG signals of each patient were considered as a reference to accurately detect anomalies in the inflation (abnormal) CSNA and ECG signals for the reliable diagnosis of myocardial ischemia, which is a type of coronary artery disease [72, 84, 173]. The experimental results on the STAFF III database revealed that there is an increase in the amplitude of the inflation (abnormal) CSNA signals during artificially induced myocardial ischemia caused by coronary artery occlusion during percutaneous coronary intervention, which indicates that there is a significant association between CSNA and myocardial ischemia, as illustrated in Figure 2.2. This association offers novel perspectives into the relationship between electrical and physiological changes within the cardiac system during myocardial ischemia, thereby fostering a profound comprehension of the underlying pathological mechanisms.

Moreover, the findings of the study demonstrated that the increase in the amplitude of the inflation (abnormal) CSNA signals during artificially induced myocardial ischemia was accompanied by simultaneous elevation or depression in the ST segment, and polarity or amplitude changes in the T wave of ECG signals, as presented in Figure 2.3. Therefore, the results suggested that there is a correlation between the increase in the amplitude of CSNA signals and the anomalies in ECG signals during myocardial ischemia.

Furthermore, the comparison between the inflation (abnormal) and post-inflation signals revealed that the increase in the amplitude of CSNA signals

and the anomalies in the ECG signals almost disappeared within several seconds after percutaneous coronary intervention was terminated (Figures 2.2 and 2.3).

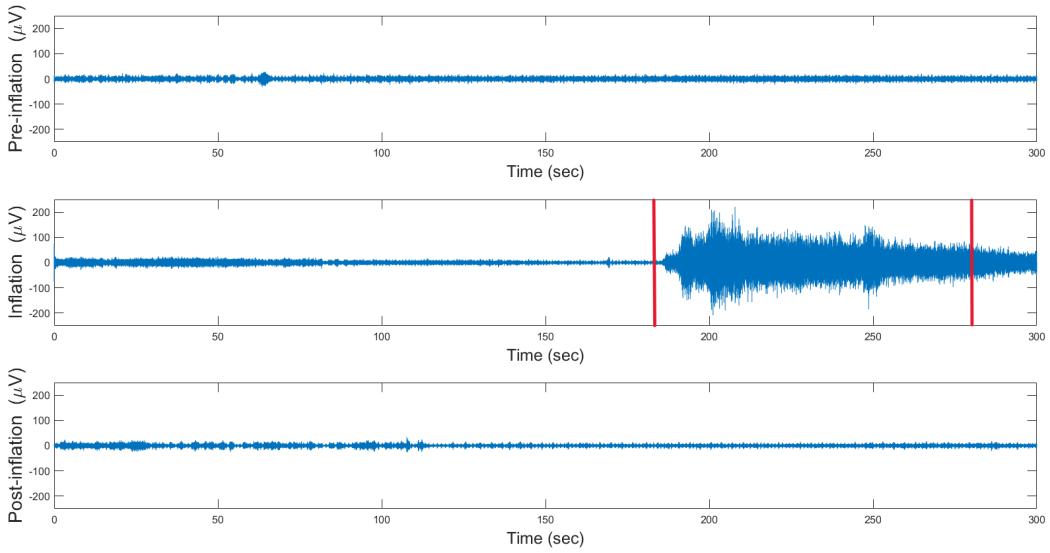

Figure 2.2: A single lead pre-inflation (normal), inflation (abnormal), and post-inflation CSNA signals of a patient in the STAFF III database that were acquired before, during, and after percutaneous coronary intervention, respectively. The cardiologists annotated the coronary balloon inflation and coronary balloon deflation times, which are illustrated with red lines at the 182nd second and 280th second, respectively. The inflation (abnormal) CSNA increases shortly after the onset of percutaneous coronary intervention and decreases after the termination of percutaneous coronary intervention. Moreover, there is very little difference in the baseline amplitudes of the pre-inflation and post-inflation CSNA signals. This may be due to the fact that these two signals were acquired in different environments with different noise levels, where the former and latter were acquired in the preoperative room and postoperative recovery room of the Medical Center, respectively.

Exceptionally, a few patients in the STAFF III database did not demonstrate any anomalies in their inflation (abnormal) CSNA and ECG signals acquired during coronary artery occlusion due to percutaneous coronary intervention, as depicted in Figure 2.4 . This may be attributed to the relatively shorter duration

of percutaneous coronary intervention or the comparatively small size of the coronary artery in which percutaneous coronary intervention was performed, which may not have been sufficient to induce myocardial ischemia in some patients.

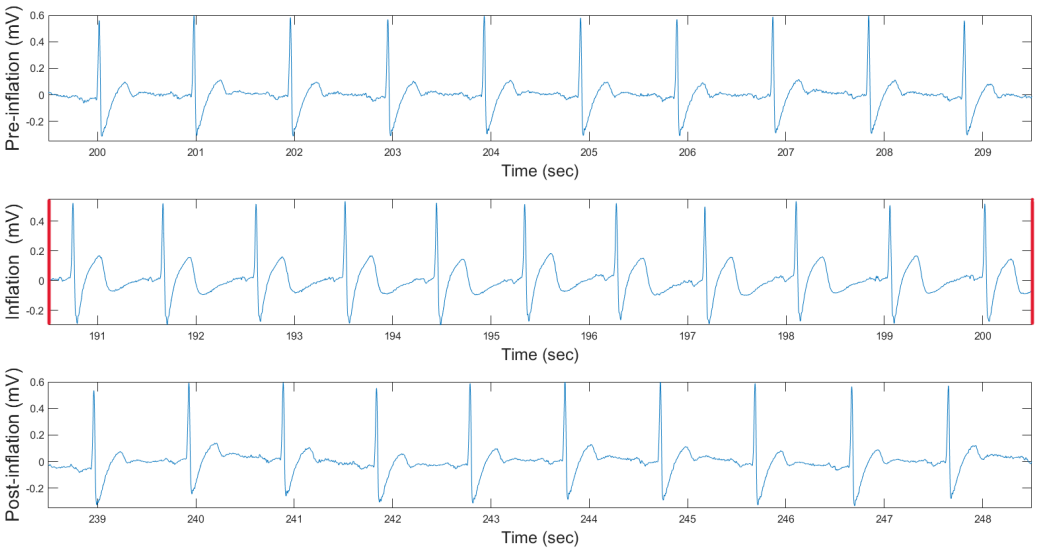

Figure 2.3: A single lead pre-inflation (normal), inflation (abnormal), and post-inflation ECG signals of the same patient in the STAFF III database that were acquired before, during, and after percutaneous coronary intervention, respectively. There is an elevation in the ST segment and an increase in the amplitude of the T wave of the inflation (abnormal) ECG signal, which are very common symptoms of myocardial ischemia. Hence, the anomalies in the ECG signal that occurred during artificially induced myocardial ischemia were accompanied by the simultaneous increase in the amplitude of CSNA signal.

For the development of the proposed supervised classification technique, we utilized the 12-lead pre-inflation (normal) and inflation (abnormal) CSNA and ECG data. Moreover, we used only the 12-lead pre-inflation (normal) CSNA and ECG data for the development of the proposed unsupervised clustering technique. The main motivation for developing the unsupervised clustering technique with the Neyman-Pearson criterion that can work using only the pre-inflation (normal) data was to construct a method that can successfully diagnose myocardial ischemia even in cases where the inflation (abnormal) data are missing.

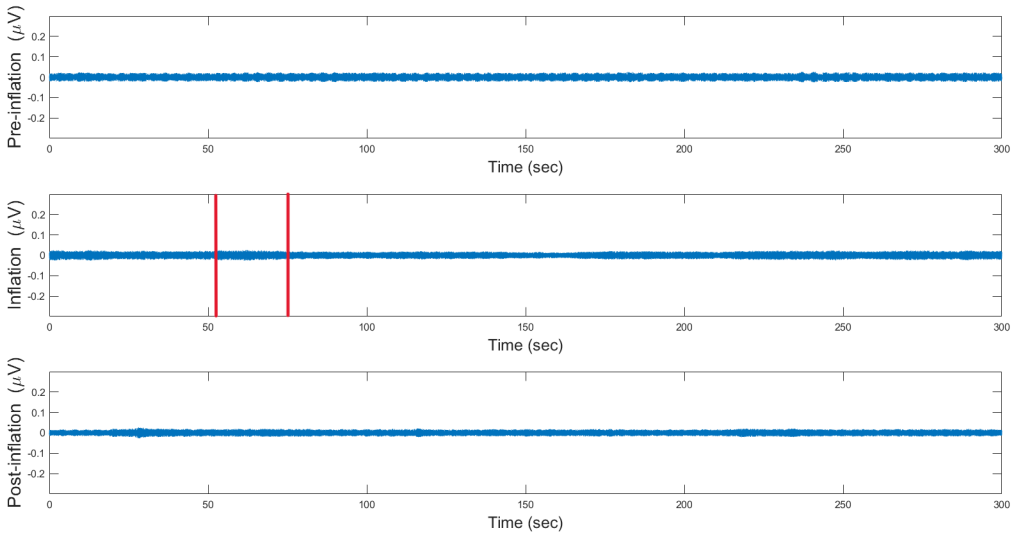

Figure 2.4: A single lead pre-inflation (normal), inflation (abnormal), and post-inflation CSNA signals of a different patient in the STAFF III database that were acquired before, during, and after percutaneous coronary intervention, respectively. The cardiologists annotated the coronary balloon inflation and coronary balloon deflation times, which are illustrated with red lines at the 53rd second and 74th second, respectively.

Table 2.11 presents the confusion matrix of the hybrid Gaussian mixture model-based clustering technique on the test set of the STAFF III database, which reveals its strong ability to distinguish between patients with and without myocardial ischemia (i.e., coronary artery disease). Out of a total of 132 coronary artery disease (abnormal) recordings in the test set, the proposed technique correctly classified 121 recordings, while misclassifying only 11 recordings as non-coronary artery disease (normal). Furthermore, out of a total of 132 non-coronary artery disease (normal) recordings in the test set, the proposed technique accurately classified 118 recordings, while misclassifying only 14 recordings as coronary artery disease (abnormal).

TABLE 2.11: The CONFUSION MATRIX of the HYBRID GAUSSIAN MIXTURE MODEL based CLUSTERING TECHNIQUE on the TEST SET of the STAFF III DATABASE for CORONARY ARTERY DISEASE DIAGNOSIS

TECHNIQUE	**CONFUSION MATRIX**			
			True Label	
			CAD	**NON-CAD**
GMM_{HYB}	**Predicted Label**	**CAD**	True Positive (TP) = **121**	False Positive (FP)= **14**
		NON-CAD	False Negative (FN) = **11**	True Negative (TN) = **118**

CAD: Coronary Artery Disease, NON-CAD: Not Coronary Artery Disease.

Table 2.12 shows the confusion matrix of the hybrid artificial neural network based classification technique on the test set of the STAFF III database, which reveals its strong ability in distinguishing between patients with and without coronary artery disease. Out of a total of 132 coronary artery disease (abnormal) recordings in the test set, the proposed technique correctly classified 127 recordings, while misclassifying only 5 recordings as non-coronary artery disease (normal). Additionally, out of a total of 132 non-coronary artery disease (normal) recordings in the test set, the proposed technique accurately classified 123 recordings, while misclassifying only 9 recordings as coronary artery disease (abnormal).

Table 2.13 demonstrates the statistical performance results of the optimum Gaussian mixture model-based clustering technique and the optimum artificial neural network based classification technique on the test set of the STAFF III database. The performance results of the developed techniques that separately utilized either only 12-lead CSNA data or only 12-lead ECG data are indicated by the notations GMM_{CSNA}, ANN_{CSNA} or GMM_{ECG}, ANN_{ECG}, respectively. Similarly, the performance results of the hybrid techniques that jointly and simultaneously utilized the 12-lead CSNA and ECG data are represented by the notations GMM_{HYB} and ANN_{HYB}.

TABLE 2.12: The CONFUSION MATRIX of the HYBRID ARTIFICIAL NEURAL NETWORK-based CLASSIFICATION TECHNIQUE on the TEST SET of the STAFF III DATABASE for CORONARY ARTERY DISEASE DIAGNOSIS

TECHNIQUE	**CONFUSION MATRIX**			
			True Label	
ANN_{HYB}			**CAD**	**NON-CAD**
	Predicted Label	**CAD**	True Positive (TP) = **127**	False Positive (FP)= **9**
		NON-CAD	False Negative (FN) = **5**	True Negative (TN) = **123**

CAD: Coronary Artery Disease, NON-CAD: Not Coronary Artery Disease.

The experimental results on the STAFF III database revealed that the proposed artificial neural network based classification technique has a relatively higher performance for the diagnosis of myocardial ischemia compared to the Gaussian mixture model-based clustering technique for both separate and joint use of 12-lead CSNA and ECG data. This can be explained by the fact that the artificial neural network based classification technique utilizes both the pre-inflation (normal) and inflation (abnormal) data, while the Gaussian mixture model-based clustering technique exclusively utilizes the pre-inflation (normal) data to detect the anomalies in CSNA and/or ECG data.

Moreover, the comparison between the performance results of all developed techniques indicated that the hybrid artificial neural network based classification technique (ANN_{HYB}), which jointly and simultaneously used CSNA and ECG data, achieved significantly higher performance compared to the other techniques that separately used either only CSNA data or only ECG data. Therefore, by taking advantage of the diversity in different data types, the proposed hybrid artificial neural network based classification technique (ANN_{HYB}) significantly increased the detection performance of myocardial ischemia. Hence, it can be highly beneficial and useful by providing improved diagnosis, especially for asymptomatic coronary artery disease patients with silent (asymptomatic) myocardial ischemia, for whom the diagnostic information provided by ECG alone is not sufficient to reliably diagnose the disease.

TABLE 2.13: The STATISTICAL PERFORMANCE RESULTS (%) of the OPTIMUM GAUSSIAN MIXTURE MODEL based CLUSTERING TECHNIQUE and OPTIMUM ARTIFICIAL NEURAL NETWORK-based CLASSIFICATION TECHNIQUE on the TEST SET of the STAFF III DATABASE for CORONARY ARTERY DISEASE DIAGNOSIS

Performance Measures	**12-Lead CSNA Features**		**12-Lead ECG Features**		**12-Lead CSNA and and ECG Features**	
	$\mathbf{GMM_{CSNA}}$	$\mathbf{ANN_{CSNA}}$	$\mathbf{GMM_{ECG}}$	$\mathbf{ANN_{ECG}}$	$\mathbf{GMM_{HYB}}$	$\mathbf{ANN_{HYB}}$
ACC	71.97	77.27	80.30	85.61	**90.53**	**94.70**
TPR	71.21	76.52	81.06	86.36	**91.67**	**96.21**
TNR	72.73	78.03	79.55	84.85	**89.39**	**93.18**
PPV	72.31	77.69	79.85	85.07	**89.63**	**93.38**
NPV	71.64	76.87	80.77	86.15	**91.47**	**96.09**
F1	71.76	77.10	80.45	85.71	**90.64**	**94.78**

The best results are written with bold characters.

Furthermore, the previous studies reported that the sensitivity (TPR) and specificity (TNR) of the gold standard diagnostic test ECG in the diagnosis of myocardial ischemia were approximately 76% and 88%, respectively [173].

In this study, the results obtained on the STAFF III database showed that the proposed hybrid artificial neural network based classification technique (ANN_{HYB}), which jointly and simultaneously uses CSNA and ECG data, exhibits superior sensitivity (TPR) and specificity (TNR) compared to the gold standard diagnostic test ECG in the diagnosis of myocardial ischemia (Table 2.13). For these reasons, the hybrid artificial neural network based classification technique (ANN_{HYB}) was selected to be used as the classification method in the proposed automated artificial intelligence-based hybrid anomaly detection technique.

Additionally, among the unsupervised machine learning methods developed using only the pre-inflation (normal) data, the hybrid Gaussian mixture model-based clustering technique (GMM_{HYB}), which jointly and simultaneously uses CSNA and ECG data, achieved the best performance. Therefore, it was selected to be used as the clustering method in the proposed automated artificial intelligence-based hybrid anomaly detection technique.

2.1.2 The Performance Results of the Automated Artificial Intelligence based Hybrid Anomaly Detection Technique on the PTBD Database

As a result of the implementation of the developed enhanced signal processing technique on the 12-lead wideband raw recordings in the PTBD database, the 12-lead ECG and CSNA signals of all healthy controls and myocardial infarction patients were simultaneously detected. Figures 2.5 and 2.6 demonstrate a single lead normal and abnormal CSNA and ECG signals of a healthy control and myocardial infarction patient in the PTBD database, respectively. The experimental results on the PTBD database revealed that there is an increase in the amplitude of the abnormal CSNA signals during myocardial infarction, which indicates that there is a significant association between CSNA and myocardial infarction, as illustrated in Figure 2.5. This association provides novel insights into the relationship between electrical and physiological changes within the cardiac system during myocardial infarction, thereby facilitating a deeper understanding of the

underlying pathological mechanisms.

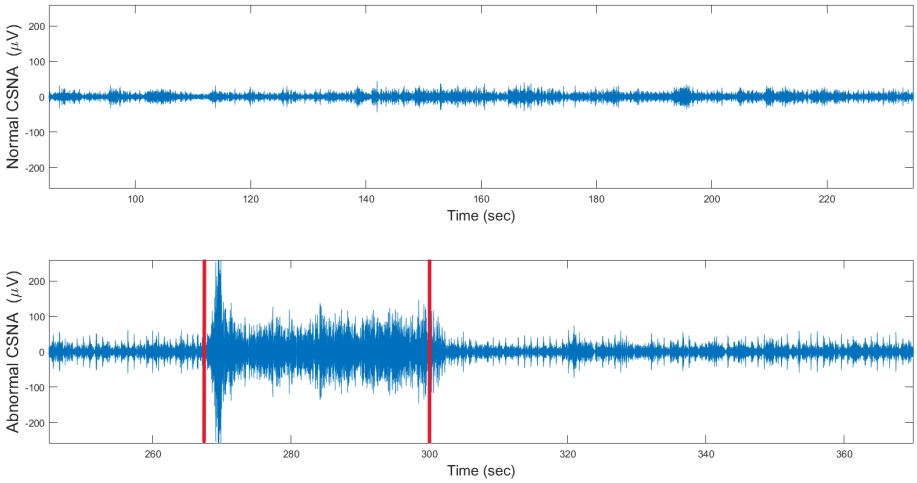

Figure 2.5: A single lead normal and abnormal CSNA signals of a healthy control and myocardial infarction patient in the PTBD database, respectively. The cardiologists annotated the onset and end times of myocardial infarction, which are illustrated with red lines at the 267th second and 300th second, respectively. The abnormal CSNA increases shortly after the onset of myocardial infarction and decreases after the termination of myocardial infarction.

Moreover, the findings of the study indicated that the increase in the amplitude of the abnormal CSNA signals during myocardial infarction was accompanied by simultaneous elevation or depression in the ST segment, and polarity or amplitude changes in the QRS complex, and the T wave of ECG signals, as illustrated in Figure 2.6 . Therefore, the results suggested that there is a correlation between the increase in the amplitude of CSNA signals and the anomalies in ECG signals during myocardial infarction. Thus, the investigations conducted on the STAFF III and PTBD databases showed that CSNA can be utilized as a new biomarker in the diagnosis and classification of myocardial ischemia and myocardial infarction, both of which are types of coronary artery disease.

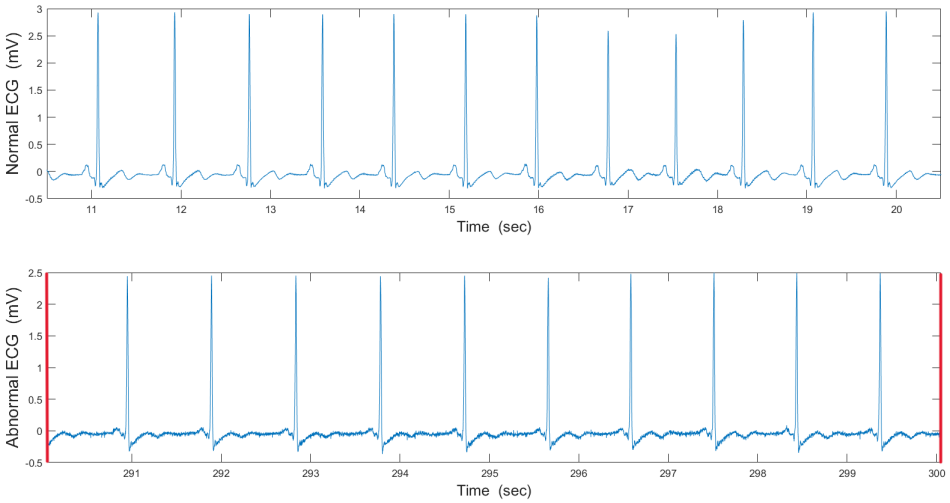

Figure 2.6: A single lead normal and abnormal ECG signals of the same healthy control and myocardial infarction patient in the PTBD database, respectively. There is an elevation in the ST segment and a decrease in the amplitude of the QRS complex, and T wave of the abnormal ECG signal, which are very common symptoms of myocardial infarction. Hence, the anomalies in the ECG signal that occurred during myocardial infarction were accompanied by the simultaneous increase in the amplitude of the CSNA signal.

For the development of the proposed supervised classification technique, we utilized the 12-lead normal CSNA and ECG data of the healthy controls, and the 12-lead abnormal CSNA and ECG data of the myocardial infarction patients. Moreover, we used only the 12-lead normal CSNA and ECG data of the healthy controls for the development of the proposed unsupervised clustering technique. The main motivation for developing the unsupervised clustering technique with the Neyman-Pearson criterion that can work using only the normal data was to construct a method that can successfully diagnose myocardial infarction even in cases where the abnormal data are missing.

Table 2.14 presents the confusion matrix of the hybrid Gaussian mixture model-based clustering technique on the test set of the PTBD database, which reveals its strong ability to discriminate between patients with and without myocardial infarction (i.e., coronary artery disease). Out of a total of 132 coronary artery disease (abnormal) recordings of myocardial infarction patients in the test set, the proposed technique correctly classified 125 recordings, while misclassifying only 7 recordings as non-coronary artery disease (normal). Furthermore, out of a total of 132 non-coronary artery disease (normal) recordings of the healthy controls in the test set, the proposed technique accurately classified 124 recordings, while misclassifying only 8 recordings as coronary artery disease (abnormal).

TABLE 2.14: The CONFUSION MATRIX of the HYBRID GAUSSIAN MIXTURE MODEL based CLUSTERING TECHNIQUE on the TEST SET of the PTBD DATABASE for CORONARY ARTERY DISEASE DIAGNOSIS

TECHNIQUE	**CONFUSION MATRIX**			
			True Label	
			CAD	**NON-CAD**
GMM_{HYB}	**Predicted Label**	**CAD**	True Positive (TP) = **125**	False Positive (FP)= **8**
		NON-CAD	False Negative (FN) = **7**	True Negative (TN) = **124**

CAD: Coronary Artery Disease, NON-CAD: Not Coronary Artery Disease.

Table 2.15 presents the confusion matrix of the hybrid artificial neural network based classification technique on the test set of the PTBD database, which reveals its strong ability to effectively discriminate between patients with and without coronary artery disease. Out of a total of 132 coronary artery disease (abnormal) recordings of myocardial infarction patients in the test set, the proposed technique correctly classified 130 recordings, while misclassifying only 2 recordings as non-coronary artery disease (normal). Additionally, out of a total of 132 non-coronary artery disease (normal) recordings of the healthy controls in the test set, the proposed technique accurately classified 129 recordings, while misclassifying only 3 recordings as coronary artery disease (abnormal).

TABLE 2.15: The CONFUSION MATRIX of the HYBRID ARTIFICIAL NEURAL NETWORK-based CLASSIFICATION TECHNIQUE on the TEST SET of the PTBD DATABASE for CORONARY ARTERY DISEASE DIAGNOSIS

TECHNIQUE	**CONFUSION MATRIX**			
			True Label	
			CAD	**NON-CAD**
ANN_{HYB}	**Predicted Label**	**CAD**	True Positive (TP) = **130**	False Positive (FP)= **3**
		NON-CAD	False Negative (FN) = **2**	True Negative (TN) = **129**

CAD: Coronary Artery Disease, NON-CAD: Not Coronary Artery Disease.

Table 2.16 demonstrates the statistical performance results of the optimum Gaussian mixture model-based clustering technique and the optimum artificial neural network based classification technique on the test set of the PTBD database. The performance results of the developed techniques that separately utilized either only 12-lead CSNA data or only 12-lead ECG data are indicated by the notations $\mathrm{GMM_{CSNA}}$, $\mathrm{ANN_{CSNA}}$ or $\mathrm{GMM_{ECG}}$, $\mathrm{ANN_{ECG}}$, respectively. Similarly, the performance results of the hybrid techniques that jointly and simultaneously utilized the 12-lead CSNA and ECG data are represented by the notations $\mathrm{GMM_{HYB}}$ and $\mathrm{ANN_{HYB}}$.

TABLE 2.16: The STATISTICAL PERFORMANCE RESULTS (%) of the OPTIMUM GAUSSIAN MIXTURE MODEL based CLUSTERING TECHNIQUE and OPTIMUM ARTIFICIAL NEURAL NETWORK-based CLASSIFICATION TECHNIQUE on the TEST SET of the PTBD DATABASE for CORONARY ARTERY DISEASE DIAGNOSIS

Performance Measures	**12-Lead CSNA Features**		**12-Lead ECG Features**		**12-Lead CSNA and ECG Features**	
	$\mathbf{GMM_{CSNA}}$	$\mathbf{ANN_{CSNA}}$	$\mathbf{GMM_{ECG}}$	$\mathbf{ANN_{ECG}}$	$\mathbf{GMM_{HYB}}$	$\mathbf{ANN_{HYB}}$
ACC	76.14	81.44	84.85	89.77	**94.32**	**98.11**
TPR	76.52	81.82	85.61	90.15	**94.70**	**98.48**
TNR	75.76	81.06	84.09	89.39	**93.94**	**97.73**
PPV	75.94	81.20	84.33	89.47	**93.98**	**97.74**
NPV	76.34	81.68	85.38	90.08	**94.66**	**98.47**
F1	76.23	81.51	84.96	89.81	**94.34**	**98.11**

The best results are written with bold characters.

The experimental results on the PTBD database revealed that the proposed artificial neural network based classification technique has a relatively higher performance for the diagnosis of myocardial infarction compared to the Gaussian mixture model-based clustering technique for both separate and joint use of the 12-lead CSNA and ECG data.

This can be explained by the fact that the artificial neural network based classification technique utilizes both the normal data of the healthy controls and the abnormal data of myocardial infarction patients to detect the anomalies in CSNA and/or ECG data. On the other hand, the Gaussian mixture model-based clustering technique exclusively utilizes the normal data of the healthy controls to effectively detect the anomalies in CSNA and/or ECG data.

Moreover, the comparison between the performance results of all developed techniques indicated that the hybrid artificial neural network based classification technique (ANN_{HYB}), which jointly and simultaneously used CSNA and ECG data, achieved significantly higher performance compared to the other techniques that separately used either only CSNA data or only ECG data. Therefore, by taking advantage of the diversity in different data types, the proposed hybrid artificial neural network based classification technique (ANN_{HYB}) significantly increased the detection performance of myocardial infarction. Thus, the findings of this study indicated that CSNA can serve as an additional diagnostic feature to ECG for considerably increasing the detection performance of coronary artery disease (i.e., myocardial infarction, myocardial ischemia, silent (asymptomatic) myocardial ischemia) and decreasing the number of false negatives, which can lead to reduced mortality and morbidity rates.

Furthermore, the previous studies reported that the sensitivity (TPR) and specificity (TNR) of the gold standard diagnostic test ECG in the diagnosis of myocardial infarction were approximately 84% and 91%, respectively [174]. In this study, the results obtained on the PTBD database showed that the proposed hybrid artificial neural network based classification technique (ANN_{HYB}), which jointly and simultaneously uses CSNA and ECG data, exhibits superior sensitivity (TPR) and specificity (TNR) compared to the gold standard diagnostic test ECG in the diagnosis of myocardial infarction (Table 2.16). For these reasons, the hybrid artificial neural network based classification technique (ANN_{HYB}) was selected to be used as the classification method in the proposed automated artificial intelligence-based hybrid anomaly detection technique.

Additionally, among the unsupervised machine learning methods developed

using only the normal data of healthy controls, the hybrid Gaussian mixture model-based clustering technique (GMM_{HYB}), which jointly and simultaneously uses CSNA and ECG data, achieved the best performance. Therefore, it was selected to be used as the clustering method in the proposed automated artificial intelligence-based hybrid anomaly detection technique.

Consequently, the results we obtained on the PTBD database using the proposed automated artificial intelligence-based hybrid anomaly detection technique strongly supported our previous results on the STAFF III database. In addition, the consistently high performance results of the automated artificial intelligence-based hybrid anomaly detection technique on two different databases that contain different and diverse patients with coronary artery disease indicate that the technique is quite robust and generalizable.

Moreover, the performance of the automated artificial intelligence-based hybrid anomaly detection technique on the PTBD database is relatively higher compared to its performance on the STAFF III database. There are several reasons that may have contributed to this outcome. It is important to consider the characteristics of the two databases to justify the differences in the artificial intelligence-based hybrid anomaly detection technique's performance on these two databases. Firstly, the ECG patterns obtained during percutaneous coronary intervention in the STAFF III database may differ from those of patients in the PTBD database who have suffered from myocardial infarction. Specifically, the anomalies in ECG signals of myocardial infarction patients in the PTBD database were generally more pronounced, distinct, and apparent compared to those of myocardial ischemia patients in the STAFF III database [168, 170, 171]. Hence, the data in the STAFF III database are comparatively more difficult to classify than the data in the PTBD database.

Secondly, the two databases have different characteristics in terms of the context in which the data was collected. The inflation (abnormal) recordings in the STAFF III database were acquired at the cardiac catheterization laboratory (operation room), however, this was not the case for the PTBD database. Moreover, the recordings in the STAFF III database were acquired during percutaneous

coronary intervention, which implies that they were collected in real-time during an invasive procedure in a clinical setting under specific conditions. Factors such as interference from other medical equipment in the operating room may have introduced noise and artifacts into the raw recordings in the STAFF III database. Therefore, the quality of the raw recordings in the PTBD database may be better than those in the STAFF III database.

2.2 Discussion

The accurate and timely diagnosis of coronary artery disease is crucial for effective patient treatment and management. The visual and manual interpretation of the 12-lead ECG signals by cardiologists for diagnosing various cardiovascular diseases is a complex and time-consuming task that requires experienced physicians. Moreover, misdiagnoses are very likely to occur during visual inspection by physicians due to the small amplitudes of ECG signals [175, 176]. Therefore, there is a great need for computer-aided machine learning methods that accurately perform automated detection of cardiovascular diseases to reduce the number of misdiagnoses by human experts and decrease the workload of physicians in daily clinical practice.

In patients with coronary artery disease, significant anomalies in the ST segment, QRS complex, and T wave of ECG signals occur during myocardial ischemia and myocardial infarction [177]. However, a considerable number of coronary artery disease patients worldwide suffer from silent (asymptomatic) myocardial ischemia, in which there are no anomalies in patients' ECG signals. Hence, ECG alone is limited in its ability to diagnose asymptomatic coronary artery disease patients with silent (asymptomatic) myocardial ischemia. Thus, an ECG signal without anomalies does not exclude the possibility of coronary artery disease. This limitation makes silent (asymptomatic) myocardial ischemia more dangerous and fatal, as asymptomatic coronary artery disease patients with silent (asymptomatic) myocardial ischemia who do not experience any symptoms are prone to misinterpretation by cardiologists, leading to false negative results.

The significance of this innovative study lies in its proposal of the first automated artificial intelligence technique that consists of various signal processing, feature extraction, supervised, and unsupervised machine learning methods that jointly and simultaneously analyze 12-lead CSNA and ECG data to perform fast, early, and accurate diagnosis of coronary artery disease (i.e., silent (asymptomatic) myocardial ischemia, myocardial ischemia, and myocardial infarction).

The proposed automated artificial intelligence-based hybrid anomaly detection technique was implemented on two different publicly available databases to ensure data heterogeneity, and diversify the results and findings of the study. By using the automated artificial intelligence-based hybrid anomaly detection technique, we demonstrated for the first time that there are anomalies in CSNA signals during coronary artery disease, which further supports the well-established fact that there is a direct and strong relationship between the sympathetic nervous system and cardiovascular diseases [14, 15]. Therefore, this study's findings support those of previous studies, which have shown that the sympathetic nervous system plays an important role in regulating the cardiovascular system [14, 15].

As discussed earlier, recent studies in the literature have shown a significant association between CSNA and cardiac arrhythmias [15, 16, 17, 18, 19]. However, our study is the first to demonstrate a significant association between CSNA and coronary artery disease using the proposed automated artificial intelligence-based hybrid anomaly detection technique, which fills the research gap in the literature [1]. This association offers new perspectives on the connection between electrical and physiological alterations in the cardiac system during coronary artery disease, which in turn enhances comprehension of the underlying pathological processes.

Moreover, the findings indicated that there is a correlation between the increase in CSNA and the anomalies in ECG signals during coronary artery disease. For these reasons, the findings of recent studies [15, 16, 17, 18, 19] and our study [1] collectively suggested that CSNA can be a new biomarker for the diagnosis and classification of both cardiac arrhythmia and coronary artery disease, respectively.

The performance results of the automated artificial intelligence-based hybrid

anomaly detection technique on the STAFF III and PTBD databases suggested that the technique achieves highly accurate and reliable diagnosis of coronary artery disease by simultaneously and robustly detecting anomalies in the 12-lead CSNA and ECG data. Additionally, it has been shown that the automated artificial intelligence-based hybrid anomaly detection technique achieves superior performance compared to the gold standard diagnostic test ECG in the diagnosis of coronary artery disease. This achievement signifies the potential of the automated artificial intelligence-based hybrid anomaly detection technique to provide an efficient and reliable alternative to the current diagnostic method for diagnosing coronary artery disease.

Moreover, the automated artificial intelligence-based hybrid anomaly detection technique outperformed other artificial intelligence techniques developed in this study, which separately used either only CSNA data or only ECG data. Therefore, by leveraging the strengths of different data types, the artificial intelligence-based hybrid anomaly detection technique considerably improved the detection performance of coronary artery disease. Hence, the study's findings indicate that CSNA can serve as an additional diagnostic feature to ECG for considerably improving the performance of coronary artery disease diagnosis and decreasing the number of false negatives, potentially leading to reduced mortality and morbidity rates.

The performance comparison between the proposed automated artificial intelligence-based hybrid anomaly detection technique and previously proposed machine learning approaches that used only ECG data to diagnose or classify coronary artery disease is summarized in Table 3.16 , which presents all statistical performance evaluation metrics to comprehensively evaluate the effectiveness of the artificial intelligence-based hybrid anomaly detection technique.

The performance of the proposed automated artificial intelligence-based hybrid anomaly detection technique is superior to that of most previously proposed machine learning approaches that exclusively used ECG data to diagnose or classify coronary artery disease. Specifically, the binary classification performance results of the automated artificial intelligence-based hybrid anomaly detection technique on the PTBD database demonstrated higher sensitivity (TPR), higher

specificity (TNR), higher accuracy (ACC), comparable precision (PPV), and higher negative predictive value (NPV) compared to most of the existing studies in the literature that utilized machine learning methods and only ECG data to diagnose or classify coronary artery disease (Table 3.16).

TABLE 2.17: The PERFORMANCE COMPARISON between the PROPOSED AUTOMATED ARTIFICIAL INTELLIGENCE-BASED HYBRID ANOMALY DETECTION TECHNIQUE and RECENT MACHINE LEARNING STUDIES that used ONLY ECG DATA for CORONARY ARTERY DISEASE DIAGNOSIS or CLASSIFICATION

STUDY	**TECHNIQUE**	**DATABASE**	***TPR*** (%)	***TNR*** (%)	***PPV*** (%)	**F1** (%)	***ACC*** (%)	***NPV*** (%)
Magrans et al.[72]	Support Vector Machine	STAFF III Database	83.3	91.7	90.9	-	-	85.7
Proposed Method	**Artificial Intelligence-based Hybrid Anomaly Detection Technique**	**STAFF III Database**	**96.21**	**93.18**	**93.38**	**94.78**	**94.70**	**96.09**
Sadhukhan et al.[73]	Logistic Regression	PTBD Database	96.5	92.7	-	-	95.6	-
Tripathy et al.[74]	Least-Squares-Support Vector Machine	PTBD Database	99.8	99.6	-	-	99.7	-
Dohare et al.[54]	Support Vector Machine	PTBD Database	96.6	96.6	-	-	96.6	-
Ahmad et al.[75]	Support Vector Machine	PTBD Database	94	-	98	-	98.4	-
Acharya et al.[76]	K-Nearest Neighbor	PTBD Database	99.4	96.2	-	-	98.8	-
Sharma et al.[49]	K-Nearest Neighbor	PTBD Database	98.3	99.4	99.4	-	99	-
Jothiramalingam et al.[77]	K-Nearest Neighbor	PTBD Database	77.4	81.8	-	-	82.8	-
Sraitih et al.[78]	Random Forest	PTBD Database	73	-	74	-	75	-
Agrawal et al.[79]	Decision Tree	PTBD Database	-	96.5	-	-	98.3	-
Liu et al.[80]	Random Tree	PTBD Database	94.2	74	-	-	89.5	-
Chang et al.[81]	Gaussian Mixture Model	PTBD Database	85.7	79.8	-	-	82.5	-
Proposed Method	**Artificial Intelligence-based Hybrid Anomaly Detection Technique**	**PTBD Database**	**98.48**	**97.73**	**97.74**	**98.11**	**98.11**	**98.47**
Al-Zaiti et al.[82]	Gradient Boosting Machine	Self-Collected ECG Data	77	76	43	-	-	94
Daraei et al.[83]	J48 Decision Tree (C4.5)	Self-Collected ECG Data	86.6	-	-	80	82.6	-
Sun et al.[84]	Support Vector Machine, Boosting Tree	Self-Collected ECG Data	91.7	82.7	-	-	89.1	-
Bashir et al.[59]	Naive Bayes, Support Vector Machine, Decision Tree	UCI Machine Learning Repository	93.7	92.8	-	82.1	87.3	-
Ramasamy et al.[41]	K-Nearest Neighbor	MIT-BIH Database	95.4	99.4	-	-	99.4	-
Exarchos et al.[69]	Association Rule Mining	European ST-T Database	87	93	-	-	-	-

Moreover, the performance comparison between the proposed automated artificial intelligence-based hybrid anomaly detection technique and previously proposed deep learning approaches that used only ECG data to diagnose or classify coronary artery disease are summarized in Table 3.17. Most of the existing deep learning methods are based on the development of various convolutional neural network architectures commonly trained using transfer learning or fine-tuning methods and using only ECG data to diagnose or classify various cardiovascular diseases [26, 27, 85, 86, 103, 104, 111, 114].

The performance of the automated artificial intelligence-based hybrid anomaly detection technique is better than that of most previously proposed deep learning approaches that exclusively used ECG data to diagnose or classify coronary artery disease. Specifically, the binary classification performance results of the automated artificial intelligence-based hybrid anomaly detection technique on the PTBD database showed that the technique has higher sensitivity (TPR), higher specificity (TNR), higher F_1-score (F1), higher precision (PPV), higher accuracy (ACC), and higher negative predictive value (NPV) compared to most of the existing studies in the literature that utilized deep learning methods and only ECG data to diagnose or classify coronary artery disease (Table 3.17).

However, a few studies in the literature that used machine or deep learning approaches and only ECG data demonstrated slightly better performance compared to our proposed automated artificial intelligence-based hybrid anomaly detection technique [41, 49, 74, 76, 93]. This is a highly anticipated result, since deep learning methods often work with larger amounts of data, which improves their performance results. Moreover, they can benefit from transfer learning, in which they are pretrained on significantly larger databases and then fine-tuned on the specific database of interest. Additionally, some of these existing studies [41, 93] were developed and evaluated on different databases, which may have contributed to their slightly better performance results. Although these few existing studies [49, 74, 76] achieved slightly better performance, our results are still highly competitive.

Compared to existing related methods, one of the biggest advantages of the

proposed automated artificial intelligence-based hybrid anomaly detection technique is that it can provide accurate and reliable diagnosis of silent (asymptomatic) myocardial ischemia, which was one of the aims and motivations of this study. Therefore, the artificial intelligence-based hybrid anomaly detection technique targets to address the limitations of existing related studies that have used only ECG data to detect coronary artery disease and fill the research gaps in the literature. Thus, the automated artificial intelligence-based hybrid anomaly detection technique can be highly beneficial and useful by providing improved diagnosis, particularly for asymptomatic coronary artery disease patients with silent (asymptomatic) myocardial ischemia, for whom the diagnostic information provided by ECG alone is not sufficient to reliably diagnose the disease.

Another advantage of the proposed artificial intelligence-based hybrid anomaly detection technique, over some of the existing machine and deep learning methods, is that it can automatically process all 12-leads for enhanced coronary artery disease diagnosis, instead of only one-lead. This is particularly important as each lead provides diagnostic information about the heart from a different angle, and multiple leads are required for the accurate and reliable diagnosis of coronary artery disease [27, 28, 31, 33, 62, 93, 113, 175]. Therefore, the automated artificial intelligence-based hybrid anomaly detection technique benefits from the diversity in diagnostic information provided by all 12-leads and can accurately detect coronary artery disease cases that cannot be diagnosed using only one-lead. This advantage may have substantially contributed to the relatively higher performance of the automated artificial intelligence-based hybrid anomaly detection technique on the STAFF III and PTBD databases.

Conversely, either one-lead or a limited number of leads was used to diagnose or classify coronary artery disease in some of the existing methods in Tables 3.16 and 3.17 [40, 41, 49, 69, 73, 75, 93, 101, 103, 105, 109, 112, 113, 177]. However, certain types of coronary artery disease are lead-specific and can only be detected through particular leads. Consequently, they might be missed by methods that monitor only one-lead or a very few number of leads. This limitation may result in poor generalization and these existing methods may not provide a reliable diagnosis for coronary artery disease that are localized in various heart locations

[49, 54, 76, 81, 82, 84, 178, 179].

Another advantage of the automated artificial intelligence-based hybrid anomaly detection technique is its very short implementation time, which is highly desirable for real-time detection of coronary artery disease. This may support fast decision-making by physicians in clinical settings, which could have significant implications in emergency situations where rapid diagnosis is crucial for timely patient treatment.

TABLE 2.18: The PERFORMANCE COMPARISON between the PROPOSED AUTOMATED ARTIFICIAL INTELLIGENCE-BASED HYBRID ANOMALY DETECTION TECHNIQUE and RECENT DEEP LEARNING STUDIES that used ONLY ECG DATA for CORONARY ARTERY DISEASE DIAGNOSIS or CLASSIFICATION

STUDY	**TECHNIQUE**	**DATABASE**	***TPR*** (%)	***TNR*** (%)	***PPV*** (%)	**F1** (%)	***ACC*** (%)	***NPV*** (%)
Brisk et al.[102]	Convolutional Neural Network	STAFF III Database	84.2	94.7	-	81.4	80.3	-
Proposed Method	**Artificial Intelligence-based Hybrid Anomaly Detection Technique**	**STAFF III Database**	**96.21**	**93.18**	**93.38**	**94.78**	**94.70**	**96.09**
Reasat et al.[103]	Convolutional Neural Network	PTBD Database	85.3	84.1	-	-	84.5	-
Makimoto et al.[104]	Convolutional Neural Network	PTBD Database	65	86	82	72	75	71
Hammad et al.[105]	Convolutional Neural Network	PTBD Database	81.1	-	88.5	83	89.7	-
Darmawahyuni et al.[106]	Recurrent Neural Network	PTBD Database	98.4	97.9	95.6	96.3	-	-
Feng et al.[180]	Convolutional Neural Network, Recurrent Neural Network	PTBD Database	98.2	86.5	-	96.8	95.4	-
Rath et al.[108]	Self-Organizing Map-Autoencoder	PTBD Database	-	-	-	97.1	98.4	-
Proposed Method	**Artificial Intelligence-based Hybrid Anomaly Detection Technique**	**PTBD Database**	**98.48**	**97.73**	**97.74**	**98.11**	**98.11**	**98.47**
Prabhakararao et al.[88]	Recurrent Neural Network	PhysioNet Database	97.6	99.4	-	-	97.7	-
Hernandez et al.[109]	Recurrent Neural Network	PhysioNet Database	94.7	-	-	-	97.4	-
Miao et al.[110]	Deep Neural Network	UCI Machine Learning Repository	93.5	72.8	79.1	85.7	83.6	-
Bigler et al.[111]	Convolutional Neural Network	Self-Collected ECG Data	83	98	-	89.9	91.5	-
Altan et al.[33]	Deep Belief Network	Long-Term ST Database	96	98.8	-	-	98	-
Xiao et al.[112]	Convolutional Neural Network	Long-Term ST Database	82.6	80.3	-	87.3	-	-
Butun et al.[93]	1D-CADCapsNet	St. Petersburg ICT Database	97.9	98.7	93.3	-	98.6	-
Acharya et al.[113]	Convolutional Neural Network	St. Petersburg ICT Database	91.1	95.8	80.8	-	95.1	-
Dutta et al.[114]	Convolutional Neural Network	NHANES Database	77	-	-	-	79.5	-
Sharma et al.[40]	Long Short-Term Memory	MIT-BIH Database	65.1	86.8	-	76.5	78.4	-

Furthermore, the advantage of the automated artificial intelligence-based hybrid anomaly detection technique over the microneurography technique, which is the conventional method for invasively recording and monitoring sympathetic nervous system activities, is that it uses wideband recordings non-invasively acquired from patients to record CSNA. Thus, it significantly reduces the risks associated with invasive procedures and the limitations associated with the requirement of highly specialized skills and expertise from trained clinicians, while also improving patient comfort.

Moreover, in clinical practice, two different physicians can often make inconsistently different diagnoses for the same patient successively [181]. An important advantage of the automated artificial intelligence-based hybrid anomaly detection technique is its ability to provide the patient with consistently accurate diagnoses successively.

Additionally, two publicly available databases were used for the development and evaluation of the automated artificial intelligence-based hybrid anomaly detection technique. The results obtained on both databases using the automated artificial intelligence-based hybrid anomaly detection technique strongly support each other. The consistently high performance results of the artificial intelligence-based hybrid anomaly detection technique on two different databases that contain different and diverse patients with coronary artery disease indicate that the technique is quite robust and generalizable.

The common drawback of most of the previously proposed artificial intelligence studies that investigated the diagnosis or classification of coronary artery diseases is that they only utilized ECG data [24, 25, 28, 31, 33, 36, 41, 42, 44, 45, 46, 49, 52, 53, 54, 55, 56, 57, 59, 60, 61, 63, 67, 68, 69, 72, 73, 74, 75, 76, 77, 78, 79, 80, 81, 82, 83, 84, 88, 93, 99, 100, 101, 102, 103, 104, 105, 106, 108, 109, 110, 111, 112, 113, 114, 172, 175, 177, 178, 179, 180, 181, 182, 183, 184, 185, 186, 187, 188, 189]. To the best of our knowledge, this is the first study that proposes a hybrid artificial intelligence technique that jointly and simultaneously analyzes 12-lead CSNA and ECG data to provide fast, early, and accurate diagnosis of a heart disease. Since, there are no other studies in the literature that proposed a hybrid artificial

intelligence technique that jointly uses CSNA and ECG data or separately uses only CSNA data to diagnose or classify cardiovascular diseases, it is not possible to compare the performance results of the proposed artificial intelligence-based hybrid anomaly detection technique with those of other studies.

Chapter 3

Artificial Intelligence based Hybrid Clinical Decision Support Technique for COVID-19 Diagnosis via RT-PCR Curves, Computed Tomography Images, and Laboratory Data

In this single-center retrospective study, the Ankara University Faculty of Medicine COVID-19 (AUFM-CoV) database was constructed by physicians from the Departments of Chest Diseases, Radiology, Infectious Diseases, and Medical Microbiology at the Ankara University Faculty of Medicine Hospital. All data were obtained from patients who applied to the Ankara University Faculty of Medicine Hospital between May and December 2020. The study was approved by the Turkish Ministry of Health and the Ethics Committee of the Ankara University Faculty of Medicine Hospital (I8-501-20), and it was performed in accordance with the ethical standards outlined in the Helsinki Declaration and its subsequent

amendments. The requirement to obtain patients' written informed consent was waived as per legislation governing the retrospective analysis of anonymized data, in accordance with the Council for International Organizations of Medical Sciences guidelines. The study was also registered in the U.S. National Library of Medicine database ClinicalTrials.gov [Identifier (NCT) Number: NCT04479319].

According to the data inclusion and exclusion criteria jointly determined by physicians at the Ankara University Faculty of Medicine Hospital, only clinically suspected patients who were older than 18 years and had undergone all RT-PCR, thorax computed tomography, and laboratory examinations, as well as multiple RT-PCR tests within seven days before and after the thorax computed tomography examination date, were enrolled in the study. Patients who did not have results for each of the RT-PCR, thorax computed tomography, and laboratory examinations or who had undergone any of these examinations in another hospital were excluded from the study.

Since COVID-19 is a relatively new disease, the numbers and sizes of publicly available COVID-19 databases were limited and small, respectively [190, 191]. This limitation posed an obstacle to the development and benchmarking of artificial intelligence techniques for detecting COVID-19. Moreover, collecting and labeling different types of medical data takes a significant amount of time and results in a heavy workload. As a result, almost all of these databases only contained chest X-ray or thorax computed tomography images, and the numbers of images in different classes were imbalanced. Therefore, among the publicly available COVID-19 databases, the AUFM-CoV database contains the widest variety of data, including RT-PCR curves and test results, thorax computed tomography images and reports, and laboratory data for each patient. Thus, it provides an excellent testbed for the development and evaluation of supervised and unsupervised artificial intelligence techniques.

Under the routine clinical approach at the Ankara University Faculty of Medicine Hospital, thorax computed tomography was conducted when patients suspected of having COVID-19 exhibited moderate or severe respiratory symptoms and/or hypoxemia. All thorax computed tomography images were acquired

in axial, coronal, and sagittal planes without the use of intravenous contrast material at the end of inspiration during a single breath-hold period in a supine position. Radiological examinations were carried out using two different models of computed tomography scanners from two different brands. These scanners were the four-detector sequential computed tomography devices (Toshiba Medical Systems, Japan and Siemens Healthcare, Germany) with a tube voltage of 120 kV and tube current modulation ranging from 100 mAs to 350 mAs.

In total, the AUFM-CoV database includes thorax computed tomography images of 646 COVID-19 patients and 1936 Control Group patients who were admitted to the Ankara University Faculty of Medicine Hospital. Specifically, the Control Group includes thorax computed tomography images of the healthy lungs and lung diseases containing ground-glass opacities (GGO), such as other viral and bacterial pneumonias (VBP), and parenchymal lung diseases (PLD). These are the most frequently confused diseases in the differential diagnosis with COVID-19 pneumonia (CVP). Thorax computed tomography images of all Control Group patients were collected via the hospital information management system (HIMS) from radiological data acquired before December 2019 to ensure that they do not contain pathological features of COVID-19 pneumonia (CVP). Thorax computed tomography images in the AUFM-CoV database contained slice numbers ranging from 100 to 400 and slice thicknesses ranging between 0.1 mm and 2 mm.

All thorax computed tomography images were annotated and labeled by an expert radiologist with over 10 years of experience, who was blinded to the RT-PCR findings. These images were initially divided into four groups, which are typical, atypical, indeterminate, and negative according to the Radiological Society of North America (RSNA) recommendations (Figure 3.1) [121]. Atypical or indeterminate thorax computed tomography images were re-evaluated by a pulmonologist. They were then labeled as either compatible or incompatible with COVID-19 pneumonia (CVP) by taking into account the clinical data (e.g., fever, cough) of the respective patients.

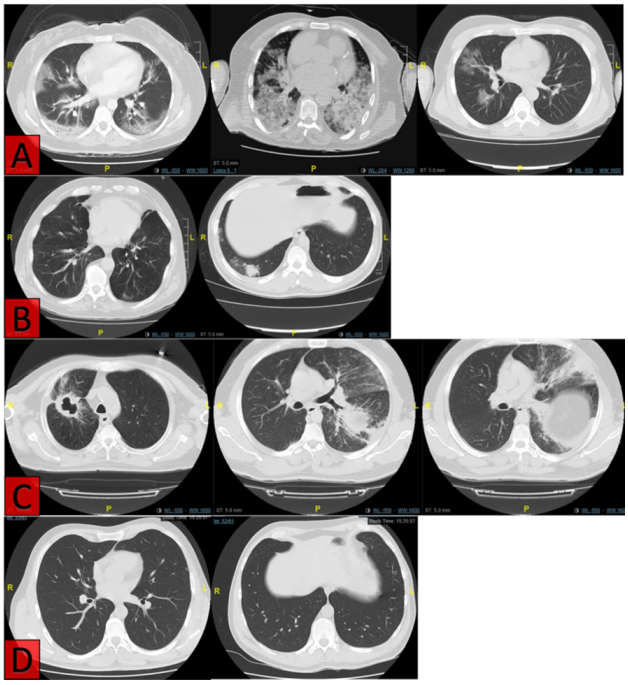

Figure 3.1: Anonymized typical, atypical, indeterminate, and negative thorax computed tomography slices in terms of COVID-19 pneumonia (CVP), according to the Radiological Society of North America (RSNA) classification.
A: Typical thorax computed tomography slices in terms of COVID-19 pneumonia (CVP) containing bilateral patchy ground-glass opacities (GGO) and consolidation.
B: Indeterminate thorax computed tomography slices in terms of COVID-19 pneumonia (CVP) containing ground-glass opacities (GGO) and consolidation that do not fit the typical COVID-19 pneumonia (CVP) distribution.
C: Atypical thorax computed tomography slices in terms of COVID-19 pneumonia (CVP) containing opacities associated with cavitation, consolidation, and atelectasis, respectively.
D: Negative thorax computed tomography slices with no findings suggestive of COVID-19 pneumonia (CVP).

Moreover, nasopharyngeal swab specimens were collected by trained medical staff using viral lysis buffer (vNAT, Bioeksen, Turkey) as transportation medium. All samples were transported to the Central Molecular Microbiology Laboratory

at the Ankara University Faculty of Medicine Hospital within four hours while being stored at +4°C. For RT-PCR analysis, various versions of three different brand kits (BioSpeedy [Bioeksen, Turkey], Coronex [Gensutek, Turkey], Diagnovital [RTA, Turkey]) were used. Viral RNA extraction was performed using a four-channel RT-PCR device named Rotor-Gene Q 5Plex HRM (Qiagen, Malaysia).

TABLE 3.1: TWO CHANNELS of the RT-PCR DEVICE that PROVIDED NECESSARY DIAGNOSTIC INFORMATION for COVID-19 DIAGNOSIS

Yellow Channel	**Green Channel**	**SARS-CoV-2**
+	+	+
+	-	-
-	+	+
-	-	Invalid Result

(+): Positive for COVID-19, (-): Negative for COVID-19.
Yellow Channel: Internal control, Green Channel: Target.

In suspected patients who initially test negative on RT-PCR, the mean time for the test to become positive was reported as 5.1 ± 1.5 days in various publications [192, 193]. In our study, by considering the incubation period of COVID-19, patients who underwent multiple RT-PCR tests within a 15-day period, covering the 7 days before and after the thorax computed tomography examination date (which was considered as the reference date), were included in the AUFM-CoV database.

All RT-PCR curves were evaluated via hospital information management system (HIMS) and labeled as either positive or negative for SARS-CoV-2 by an expert microbiologist with over 10 years of experience, who was blinded to the

thorax computed tomography and laboratory findings. Consequently, the AUFM-CoV database included the positive and negative RT-PCR curves of 593 and 838 patients, respectively.

Furthermore, laboratory data (lymphocyte counts and neutrophil-lymphocyte ratios), which were acquired on the same day as each patient's thorax computed tomography examination date, were obtained from complete blood count examinations registered in hospital information management system (HIMS). Previous studies have reported that patients with viral infections have significantly lower lymphocyte counts ($<1500\ mm^3$) and higher neutrophil-lymphocyte ratios (>3.2) [194].

Based on these criteria, in our study, laboratory data were labeled as compatible or incompatible with viral infection through the evaluation of each patient's complete blood counts, as well as symptoms, fever findings, and contact histories by an expert clinician who was blinded to thorax computed tomography and RT-PCR findings. Laboratory data were analyzed using the Sysmex XN-10 automated hematology analyzer (Sysmex Corporation).

By using the labels of thorax computed tomography images, RT-PCR curves, and laboratory data, the criteria for patient labeling presented in Table 3.2 were jointly established by the microbiologist, radiologist, and clinician at the Ankara University Faculty of Medicine Hospital. These criteria aim to specify the multi-class classification classes of the artificial intelligence-based hybrid clinical decision support technique that correspond to patients' final diagnosis.

TABLE 3.2: PATIENT LABELING CRITERIA for ARTIFICIAL INTELLIGENCE based HYBRID CLINICAL DECISION SUPPORT TECHNIQUE

Classes	**Thorax CT**$_L$	**RT-PCR**$_L$	**LAB**$_L$
COVID-19 Pneumonia (CVP)	+	+	+
	+	+	-
	+	-	+
Non-Pneumonia COVID-19 (NPC)	-	+	+
	-	+	-
Non-COVID-19 Pneumonia (NCVP)	+	-	-
Not COVID-19 (NC)	-	-	+
	-	-	-

Thorax CT$_L$: Label of thorax computed tomography image,

RT-PCR$_L$: Label of RT-PCR curve, **LAB**$_L$: Label of laboratory data.

Thorax computed tomography images were labeled as compatible (+) or incompatible (-) with COVID-19 pneumonia (CVP).

RT-PCR curves were labeled as positive (+) or negative (-) for SARS-CoV-2.

Laboratory data were labeled as compatible (+) or incompatible (-) with viral infection.

3.0.1 Convolutional Neural Network-based Deep Learning Method for Thorax Computed Tomography Images

The proposed artificial intelligence-based hybrid clinical decision support technique comprises a preprocessing method and a convolutional neural network-based supervised learning method, which we developed for thorax computed tomography images in the AUFM-CoV database. The preprocessing method consists of Hounsfield unit (HU) conversion, voxel resampling, pixel truncation, and pixel normalization (Figure 3.2).

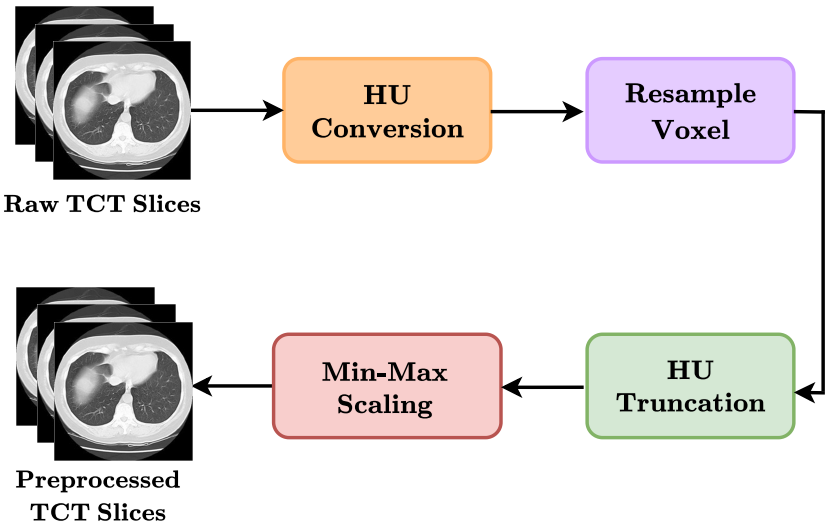

Figure 3.2: The proposed preprocessing method developed for thorax computed tomography (TCT) images in the AUFM-CoV database. It consists of Hounsfield unit (HU) conversion, voxel resampling, pixel truncation, and pixel normalization.

Depending on the computed tomography device and the radiologist's decision, the number of scans, image resolution, and pixel spacing in the computed tomography images varied among different patients. Together these factors allowed us to generate a heterogeneous database that accounts for differences in computed tomography images among different patients within the medical community. This broad heterogeneity within the image collection aimed to resolve potential bias in image analysis towards specific image qualities or types of computed tomography imaging devices.

All thorax computed tomography images were batch anonymized by removing confidential data using Sante DICOM Editor (Santesoft, Greece) and RadiAnt DICOM Viewer (Medixant, Poland) to protect patients' privacy, in accordance with the Personal Data Protection Law.

The pixel values of all thorax computed tomography slices were then converted to Hounsfield units (Figure 3.3(a)). The voxels of all thorax computed tomography slices were resampled to unit-spacing along three axes (z, y, x) with [1.0, 1.0, 1.0] mm intervals to ensure that each voxel has a consistent distance and to compensate for voxel dimension variations among different patients (Figure 3.3(b)).

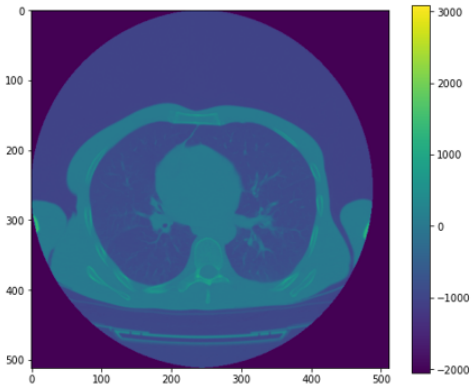

(a) Hounsfield unit conversion of pixels of a thorax computed tomography slice. Pixels outside the lung region were set to zero Hounsfield unit. Physical distance of the original image was [1.5, 0.76, 0.76] mm and its dimensions were 208∗512∗512 (slice number∗image width∗image height).

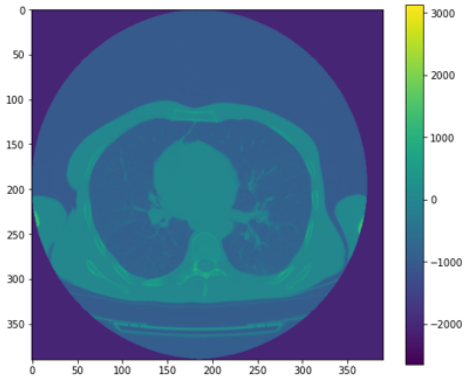

(b) Resampling voxels of the thorax computed tomography slice to unit-spacing. Physical distance of the resampled image is [1.0, 1.0, 1.0] mm, and its dimensions are 312∗390∗390 (slice number∗image width∗image height).

Figure 3.3: The implementation of the developed preprocessing method on the thorax computed tomography images in the AUFM-CoV database.

The pixel values of the resampled computed tomography images (3D) were optimized to achieve an appropriate range of Hounsfield units. In our database, the least dense object, such as air, is assigned a value of -1000 Hounsfield units. The lung, being an organ filled with air, typically exhibits Hounsfield unit values ranging from -700 to -500. Other organs that may influence our analysis include water (0 Hounsfield units), fat (-90 to -120 Hounsfield units), soft tissue (100 to 300 Hounsfield units), and bone (300 to 1900 Hounsfield units).

Consequently, we filtered thorax computed tomography slices (2D) to remove extrapulmonary tissues that could potentially negatively impact our analysis. Hence, pixels from all resampled thorax computed tomography slices were truncated to the [-1000, 400] Hounsfield unit range to focus solely on the lung region (Figure 3.4(a)). Using the min-max normalization method, pixels from all truncated thorax computed tomography slices were normalized to the [0.0, 1.0] Hounsfield unit range to prevent the vanishing and exploding gradient problem during the training of the deep learning model (Figure 3.4(b)).

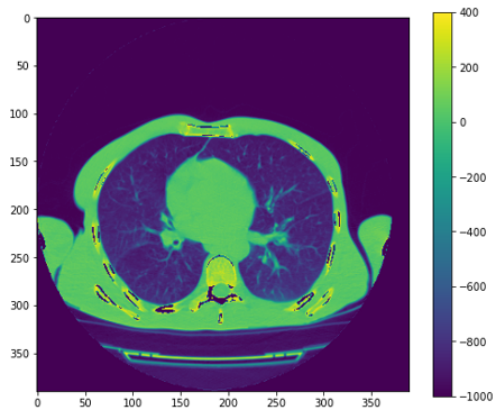

(a) The truncation of the resampled thorax computed tomography slice pixels to the [-1000, 400] Hounsfield unit range to focus only on the lung region.

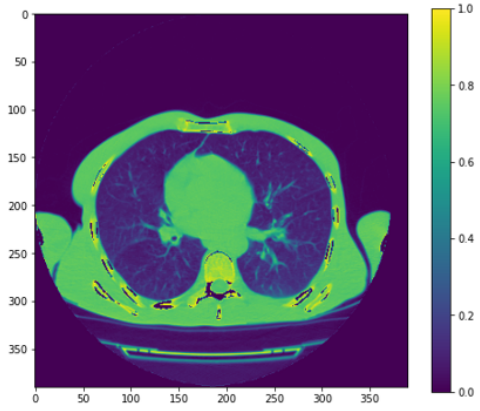

(b) Normalization of the truncated thorax computed tomography slice pixels to the [0.0, 1.0] Hounsfield unit range using the min-max normalization method.

Figure 3.4: The implementation of the developed preprocessing method on the thorax computed tomography images in the AUFM-CoV database.

Lastly, pixels from all normalized thorax computed tomography slices were dimension-wise resized to a uniform $128 * 128$ pixels to compensate for pixel size variations among different patients. Using the preprocessed thorax computed tomography slices, a novel supervised learning method based on BCDU-Net and 3D-convolutional neural networks was developed to perform multi-class classification and differential diagnosis of COVID-19 pneumonia (CVP) for robust detection of COVID-19 (Figure 3.5).

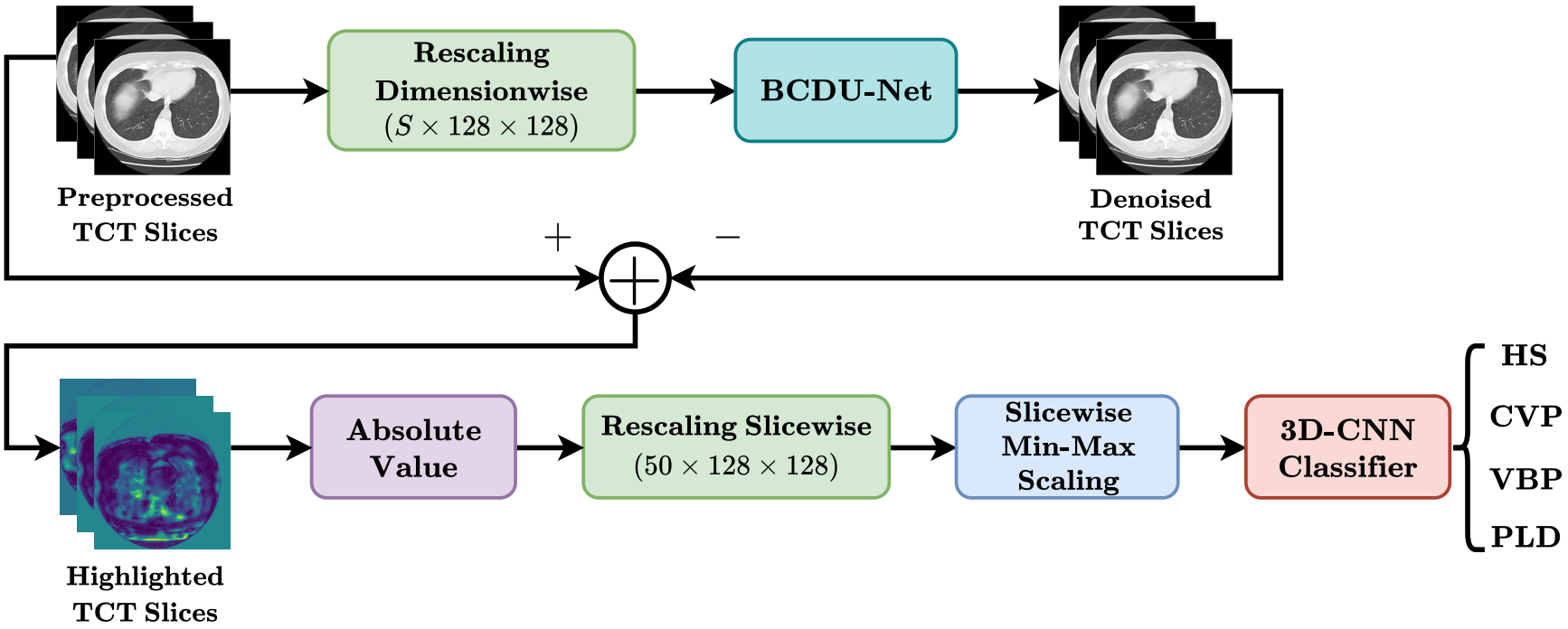

Figure 3.5: The proposed novel supervised learning method based on BCDU-Net and 3D-convolutional neural network (CNN) classifier. It was developed to perform multi-class classification for COVID-19 diagnosis and to differentiate between COVID-19 pneumonia (CVP), other viral and bacterial pneumonias (VBP), parenchymal lung diseases (PLD), and healthy subjects (HS) using thorax computed tomography (TCT) slices in the AUFM-CoV database.

We conducted various experiments to test whether the use of BCDU-Net increases the performance of our technique and whether it is necessary for preprocessing. Hence, we developed and implemented the 3D-convolutional neural network classifier both with and without the use of BCDU-Net. The experimental results demonstrated that the implementation of BCDU-Net increased the performance of our technique, thus proving the necessity and usefulness of applying BCDU-Net to enhance the technique's robustness.

All preprocessed and dimension-wise resized thorax computed tomography slices were given as input to BCDU-Net, which is a 2D-convolutional neural network model designed based on U-Net [195]. We developed BCDU-Net as the backbone of our model for several purposes. The first reason was to remove extrapulmonary organs and eliminate infected pathological regions from the preprocessed thorax computed tomography slices (Figure 3.6). The second purpose was to eliminate noise for accurately identifying lung infections and lesions. The third purpose was to achieve a high-performing model that remains unbiased, even when sample sizes are small and heterogeneous. Consequently, the output of BCDU-Net consists of de-noised thorax computed tomography images.

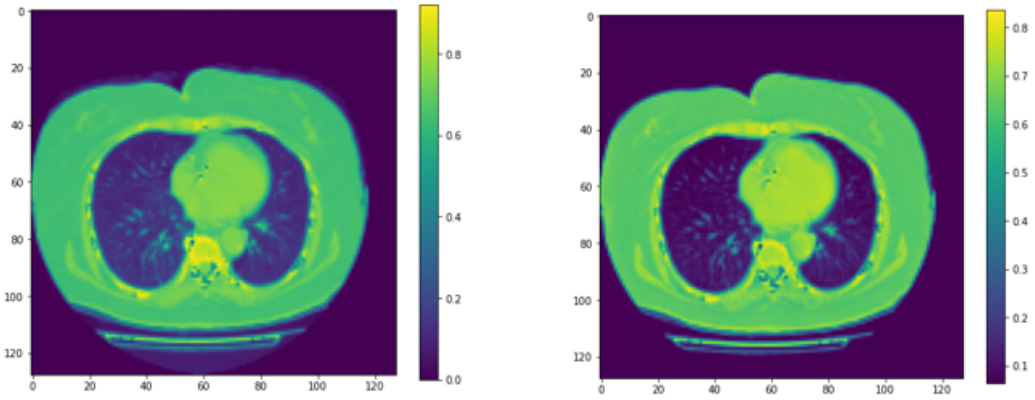

(a) BCDU-Net input, which represents preprocessed and dimension-wise rescaled thorax computed tomography slice.

(b) BCDU-Net output, which represents de-noised thorax computed tomography slice.

Figure 3.6: The implementation of the developed BCDU-Net on the preprocessed thorax computed tomography images in the AUFM-CoV database.

By computing the difference between the input and output of BCDU-Net, we obtained highlighted thorax computed tomography slices in which infected pathological regions in the lungs were emphasized (Figure 3.7(a)). The absolute values of these highlighted thorax computed tomography slices were computed to facilitate the detection and multi-class classification of COVID-19 pneumonia (CVP) (Figure 3.7(b)).

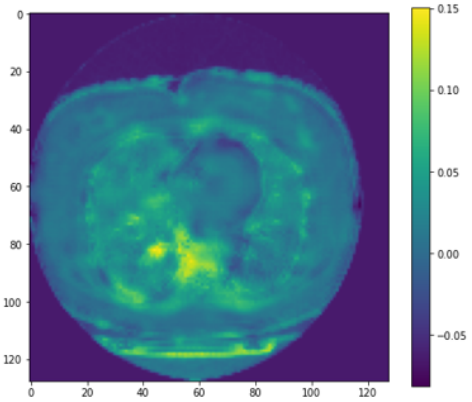

(a) Highlighted thorax computed tomography slice obtained by computing the difference between the BCDU-Net input and output to emphasize infected pathological regions in the lungs.

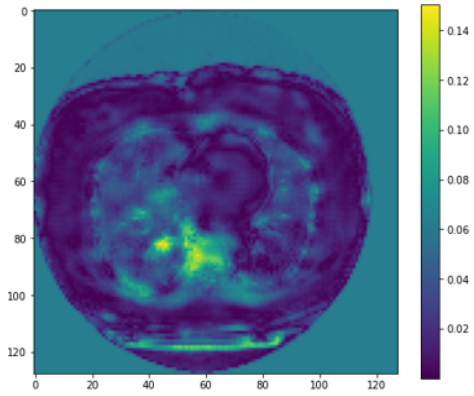

(b) The absolute value of the highlighted thorax computed tomography slice that facilitates the detection and classification of COVID-19 pneumonia (CVP) by further emphasizing infected pathological regions in the lungs.

Figure 3.7: Sharpening and enhancing thorax computed tomography images in the AUFM-CoV database for detection of lung infections and lesions.

The computed tomography slices along the z-axis were concatenated to generate the 3D-computed tomography image, which served as the input for the 3D-convolutional neural network classifier. The convolutional layers in the 3D-convolutional neural network classifier can only process a fixed number of thorax computed tomography slices. Therefore, the voxels of all absolute value slices were resized slice-wise to have dimensions of 50∗128∗128 (Figure 3.5). Here, '50'

on the z axis indicates that all the patients' computed tomography slices were resized to 50 slices. This ensured that the thorax computed tomography images of all patients had equal sizes and compensated for variations in the number of slices between different patients.

By using the min-max normalization method, the pixels of all thorax computed tomography slices were normalized to the [0.0, 1.0] Hounsfield unit range to prevent vanishing and exploding gradient problem. These thorax computed tomography images in the AUFM-CoV database were then split into non-intersecting training, validation, and test sets to perform multi-class classification (Table 3.3).

Data augmentation methods, such as Gaussian noise, random rotation, and random flipping, were employed during training to regularize the model and increase its diagnostic performance. Consequently, the training, validation, and test sets contained thorax computed tomography slices from each of the four classes, which are COVID-19 pneumonia (CVP), other viral and bacterial pneumonias (VBP), parenchymal lung diseases (PLD), and healthy subjects (HS). The numbers of thorax computed tomography slices belonging to each of the four classes in the training and validation sets were independently selected to be equal. The absence of class imbalance between different classes in the training and validation sets prevented bias and over-fitting during training and ensured that the developed model generalizes well to previously unseen data.

TABLE 3.3: PATIENT DISTRIBUTIONS in the TRAINING, VALIDATION, and TEST SETS for MULTI-CLASS CLASSIFICATION using BCDU-NET and 3D-CONVOLUTIONAL NEURAL NETWORK CLASSIFIER

Classes	Training Set	Validation Set	Test Set	Total
COVID-19 Pneumonia (CVP)	370	30	246	646
Other Viral and Bacterial Pneumonias (VBP)	370	30	84	484
Parenchymal Lung Diseases (PLD)	370	30	116	516
Healthy Subjects (HS)	370	30	536	936
Total	1480	120	982	2582

The thorax computed tomography slices in the training set were given as input to the 3D-convolutional neural network classifier. This architecture consists of 3D-convolutional layer, 3D-batch normalization layer, 3D-max pooling layer, 3D-global average pooling layer, linear layer, dropout layer, and softmax layer, as illustrated in Figure 3.8 . Instead of employing transfer learning or fine-tuning during training, the 3D-convolutional neural network classifier was end-to-end trained from scratch. In the training phase, it learned to distinguish between COVID-19 pneumonia (CVP), other viral and bacterial pneumonias (VBP), parenchymal lung diseases (PLD), and healthy subjects (HS). Hence, it learned to classify thorax computed tomography images of each patient into one of the four classes.

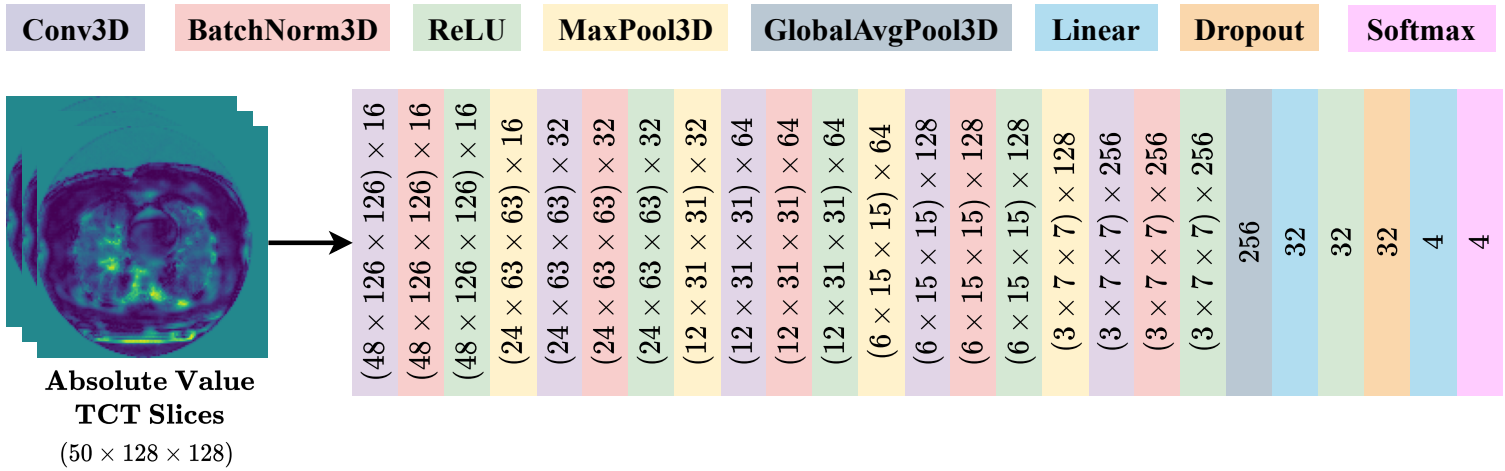

Figure 3.8: The proposed 3D-convolutional neural network classifier that performs multi-class classification for COVID-19 diagnosis using thorax computed tomography images in the AUFM-CoV database. The numbers outside the parentheses in the 3D-convolutional neural network classifier represent the number of channels. The classifier successfully differentiates COVID-19 pneumonia (CVP) from other viral and bacterial pneumonias (VBP), parenchymal lung diseases (PLD), and healthy subjects (HS), where the first three have very similar radiological findings.

The equations for the 3D-convolutional layer can be mathematically formulated as follows:

$$\mathbf{Y}_{c,i,j,k} = \sigma\left(\sum_{m=1}^{M}\sum_{p=1}^{P}\sum_{q=1}^{Q}\sum_{r=1}^{R}\mathbf{W}_{c,m,p,q,r}\cdot\mathbf{X}_{m,i+p,j+q,k+r} + \mathbf{b}_c\right) \tag{3.1}$$

where

- $\mathbf{Y}_{c,i,j,k}$: Output feature map at channel c and spatial position (i, j, k).
- $\mathbf{X}_{m,i,j,k}$: Input feature map at channel m and spatial position (i, j, k).
- $\mathbf{W}_{c,m,p,q,r}$: Convolutional filter weights for channel c, with filter size (P, Q, R).
- $\mathbf{b}_c$: Bias term for channel c.
- σ: Rectified linear unit (ReLU) activation function.

The 3D-batch normalization regularization method was employed to prevent over-fitting and reduce training time. The equations for the 3D-batch normalization layer can be mathematically formulated as follows:

$$\mathbf{Y}_{c,i,j,k} = \frac{\mathbf{X}_{c,i,j,k} - \mu_c}{\sqrt{\sigma_c^2 + \epsilon}} \cdot \gamma_c + \beta_c \tag{3.2}$$

where

- $\mathbf{Y}_{c,i,j,k}$: Output after batch normalization.
- $\mathbf{X}_{c,i,j,k}$: Input feature map.
- μ_c: Mean of the feature map c over the mini-batch.
- σ_c: Standard deviation of the feature map c over the mini-batch.
- ϵ: A small constant to avoid division by zero.
- γ_c: Scaling parameter.
- β_c: Shifting parameter.

The feature maps extracted from the convolutional layers were passed through the rectified linear unit (ReLU) activation function. The equation of the rectified linear unit (ReLU) activation function, which was applied element-wise to the feature maps extracted from the convolutional layers, can be written as follows:

$$\mathbf{Y}_{c,i,j,k} = \max(0, \mathbf{X}_{c,i,j,k}) \tag{3.3}$$

where

- $\mathbf{Y}_{c,i,j,k}$: Output feature map at channel c and spatial position (i, j, k).
- $\mathbf{X}_{c,i,j,k}$: Input feature map at channel c and spatial position (i, j, k).

The 3D-max-pooling layer was added to reduce the output dimensions of the convolutional layers and decrease the computational load. The equations for the 3D-max pooling layer can be mathematically formulated as follows:

$$\mathbf{Y}_{c,i,j,k} = \max_{p,q,r} (\mathbf{X}_{c,i+p,j+q,k+r}) \tag{3.4}$$

where

- $\mathbf{Y}_{c,i,j,k}$: Output feature map at channel c and spatial position (i, j, k).

The 3D-global average pooling layer was added to reduce the output dimensions of the convolutional layers and decrease the computational load. The equations for the 3D-global average pooling layer can be mathematically formulated as follows:

$$\mathbf{Y}_c = \frac{1}{N} \sum_{i=1}^{H} \sum_{j=1}^{W} \sum_{k=1}^{D} \mathbf{X}_{c,i,j,k} \tag{3.5}$$

where

- $\mathbf{Y}_c$: Output for channel c.
- N: Total number of spatial positions in the feature map ($H \times W \times D$).
- H: Height of the feature map.
- W: Width of the feature map.
- D: Depth of the feature map.

A fully connected layer with a softmax activation function was added to perform multi-class classification. The equations of the fully connected (linear) layer can be mathematically formulated as follows:

$$\mathbf{Y}_c = \sum_{i=1}^{N} w_i \, x_i + b \tag{3.6}$$

where

- $\mathbf{Y}_c$: Output for class c.
- w_i : Weight for input x_i.
- x_i : Input value.
- b: Bias term.

The dropout regularization method was then applied to prevent over-fitting during training. The equations of the softmax layer can be mathematically formulated as follows:

$$P(y = c \,|\, \mathbf{X}) = \frac{e^{\mathbf{Y}_c}}{\sum_{c'} e^{\mathbf{Y}_{c'}}} \tag{3.7}$$

where

- $P(y = c \,|\, \mathbf{X})$: Probability of the input $\mathbf{X}$ belonging to class c.
- $\mathbf{Y}_c$: Output for class c.
- $\sum_{c'} e^{\mathbf{Y}_{c'}}$: Sum of exponential values of all class outputs.

The (hyper)parameters of the 3D-convolutional neural network classifier were optimized using the validation set (Table 3.4). The output of the best performing 3D-convolutional neural network classifier is a numerical value that indicates a given patient's probability of belonging to one of the four classes, which are COVID-19 pneumonia (CVP), other viral and bacterial pneumonias (VBP), parenchymal lung diseases (PLD), or healthy subjects (HS).

TABLE 3.4: The (HYPER)PARAMETERS of the 3D-CONVOLUTIONAL NEURAL NETWORK CLASSIFIER

Dropout Ratio	0.25
Number of Epochs	200
Optimization Method	Adam
Learning Rate	5×10^{-4}
Batch Size	16
Loss Function	Categorical Cross Entropy

The proposed BCDU-Net and 3D-convolutional neural network classifier were trained, optimized, and tested using a workstation with dual GPUs (Table 3.5).

TABLE 3.5: The PROPERTIES of the WORKSTATION

Operating System	Ubuntu 20.04.3 LTS
CPU	Intel Xeon W2245 (16 Cores)
GPU	NVIDIA Quadro RTX 6000 x 2
Memory	128 GB
Platform	Tensorflow 2.6.0 (PYTHON 3.8)
Training Time	32 hours

3.0.2 Long Short-Term Memory based Deep Learning Method for RT-PCR Curves

The proposed artificial intelligence-based hybrid clinical decision support technique contains a preprocessing method, 1D-convolutional filter, and long short-term memory-based supervised learning method, which we developed for analyzing RT-PCR curves in the AUFM-CoV database. The raw data of all RT-PCR

curves consisted of fluorescence values measured over 35, 40, or 45 PCR cycles, which varied depending on the RT-PCR kit used. Initially, these data were recorded in .REX (rotor gene experiment) format using the RT-PCR device. Subsequently, they were converted to .CSV (comma separated values) format, which is suitable for use in PYTHON, using Rotor-Gene Q Series software (Qiagen, Malaysia). Various preprocessing methods were developed to determine the method that yields the best performance, which include median filtering, min-max scaling, and start padding (Figure 3.9).

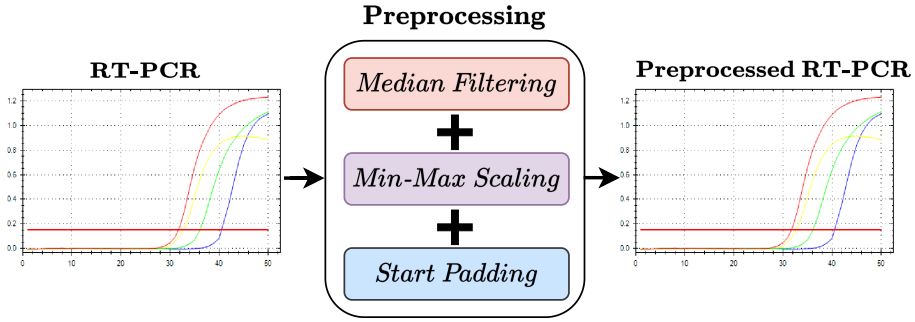

Figure 3.9: The preprocessing method developed for the RT-PCR curves in the AUFM-CoV database. It consists of median filtering, min-max scaling, and start padding.

We implemented median filtering on the raw data of all RT-PCR curves to effectively remove noise from the data, while preserving edge information. We then normalized all median-filtered RT-PCR data to the [0.0, 1.0] range using the min-max scaling method to prevent the vanishing and exploding gradient problem during the training of the long short-term memory classifier.

By using the start-padding method, we equalized the lengths of RT-PCR curves for all patients and subjects to ensure that all RT-PCR curves had a maximum of 45 PCR cycles and to compensate for variations in the lengths of RT-PCR curves among different patients (Figure 3.10).

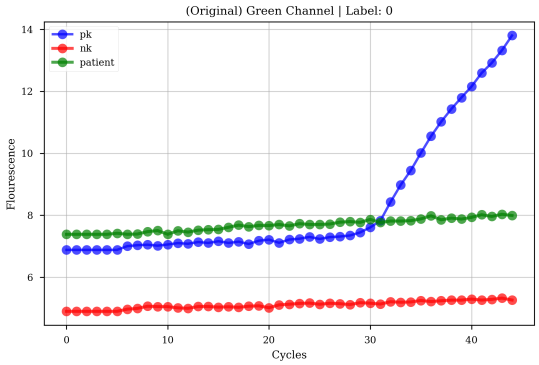

(a) The original RT-PCR curve (green) of a subject labeled as negative for SARS-CoV-2 by the microbiologist.

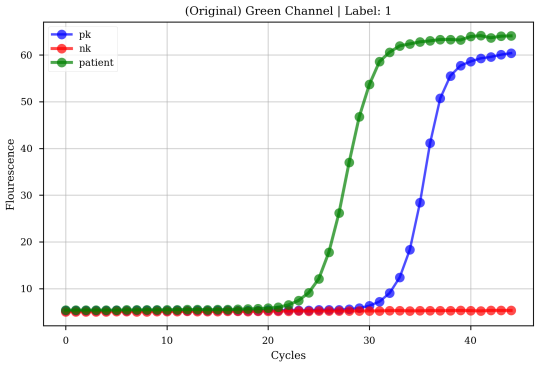

(b) The original RT-PCR curve (green) of a COVID-19 patient labeled as positive for SARS-CoV-2 by the microbiologist.

Figure 3.10: The implementation of the developed preprocessing method on RT-PCR curves in the AUFM-CoV database. RT-PCR curves were obtained using the green (target) channel of the Rotor-Gene Q 5Plex HRM device. They were preprocessed and visually displayed using PYTHON. The **y**-axis represents fluorescence intensity, and the **x**-axis represents the number of PCR cycles. The "pk" curve (blue) and the "nk" curve (pink) represent the positive and negative control lines, respectively, indicating that the RT-PCR device was fully calibrated and functioning correctly.

Preprocessed RT-PCR data in the AUFM-CoV database were divided into non-intersecting training, validation, and test sets to perform binary classification (Table 3.6). The absence of class imbalance between the two classes in the training and validation sets prevented bias and over-fitting during training, and ensured that the developed classifier generalizes well on previously unseen data.

TABLE 3.6: PATIENT and DATA DISTRIBUTIONS in the TRAINING, VALIDATION, and TEST SETS for BINARY CLASSIFICATION using 1D-CONVOLUTIONAL FILTER and LONG SHORT TERM MEMORY CLASSIFIER

Classes	Training (p)	Training (n)	Validation (p)	Validation (n)	Test (p)	Test (n)	Total (p)	Total (n)
Positive	278	300	97	100	291	320	593	720
Negative	283	300	99	100	668	792	838	1192
Total	561	600	196	200	959	1112	1431	1912

p: number of patients, **n**: number of data.

We developed various 1D-convolutional filters with different (hyper)parameters to extract feature maps from preprocessed RT-PCR data (Figure 3.11).

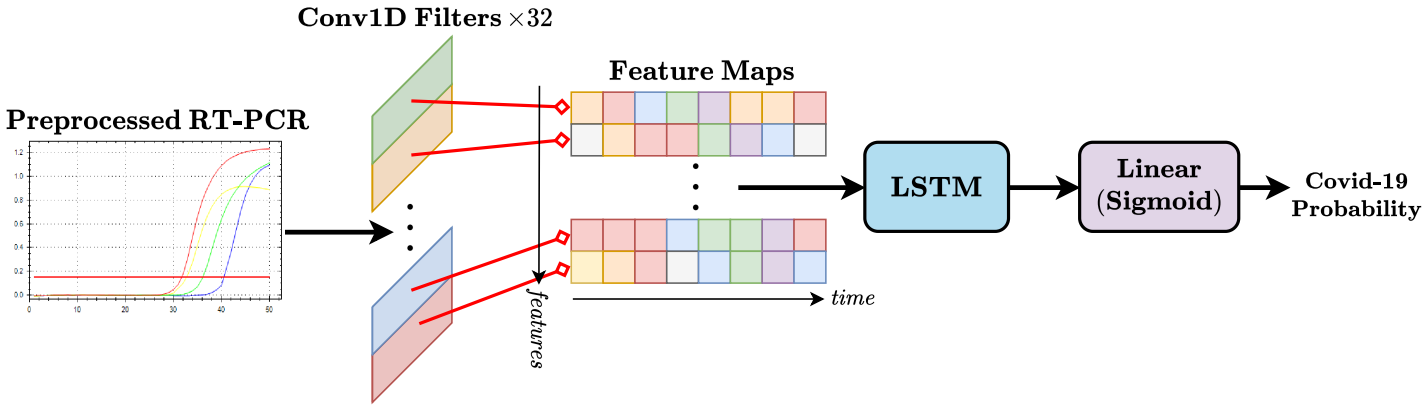

Figure 3.11: The proposed 1D-convolutional filter and long short-term memory (LSTM) classifier were developed to perform binary classification for COVID-19 diagnosis using preprocessed RT-PCR data in the AUFM-CoV database.

By evaluating the performance of the developed 1D-convolutional filters on the validation set, we determined the best performing model with the ideal (hyper)parameters (Table 3.7).

TABLE 3.7: (HYPER)PARAMETERS of the 1D-CONVOLUTIONAL FILTER

Number of Convolutional Filters	32
Learning Rate	10^{-3}
Kernel Size	5

RT-PCR curves demonstrate the characteristics of time series data. Therefore, we utilized long short-term memory networks due to their ability to learn variable-length sequential time series data with long-term dependencies and to overcome the vanishing and exploding gradient problem. Feature maps obtained using the best performing 1D-convolutional filter were given as input to the long short-term memory classifiers to perform the reliable detection of COVID-19. We developed various long short-term memory classifiers with different (hyper)parameters using the training set.

The following equations elucidate the forward pass of the long short-term memory network, providing insight into how this network manages information flow and state updates.

- **Input Gate**:

$$i_t = \sigma(W_i \, [h_{t-1}, \, x_t] + b_i) \tag{3.8}$$

  It regulates the flow of information from the current input (x_t) and the previous hidden state (h_{t-1}) by applying the sigmoid activation function (σ). It determines how much of the candidate cell state is added to form the updated cell state.

- **Forget Gate**:

$$f_t = \sigma(W_f \, [h_{t-1}, \, x_t] + b_f) \tag{3.9}$$

It controls the flow of information through the cell state, allowing the network to decide what information to preserve and what information to discard from the previous cell state.

- **Output Gate**:

$$o_t = \sigma(W_o \, [h_{t-1}, \, x_t] + b_o) \tag{3.10}$$

It regulates the information flow from the cell state to the hidden state. Hence, it determines the final output of the long short-term memory cell. The sigmoid activation function (σ) determines how much of the cell state should contribute to the output.

- **Candidate Cell State**:

$$\tilde{C}_t = \tanh(W_c \, [h_{t-1}, \, x_t] + b_c) \tag{3.11}$$

It represents new information that can be added to the cell state based on the current input and the previous hidden state by applying the hyperbolic tangent activation function.

- **Cell State**:

$$C_t = f_t \odot C_{t-1} + i_t \odot \tilde{C}_t \tag{3.12}$$

It is updated by combining the previous cell state with the new candidate cell state after applying the forget gate and input gate.

- **Hidden State**:

$$h_t = o_t \odot \tanh(C_t) \tag{3.13}$$

It represents the output of the long short-term memory network and it is computed by applying the output gate (o_t) to the cell state (C_t) after employing the hyperbolic tangent activation. This gate-controlled combination ensures that the hidden state retains relevant information from the cell state, while suppressing irrelevant information.

The explanations of the notations in the above equations are summarized as follows:

- σ: Sigmoid activation function.
- tanh: Hyperbolic tangent activation function.
- W_f, W_i, W_o, W_c: Weights for the respective gates and cell state.
- b_f, b_i, b_o, b_c: Biases for the respective gates and cell state.
- $\odot$: Element-wise multiplication.
- $[h_{t-1}, x_t]$: Concatenation of the previous hidden state (h_{t-1}) and the current input (x_t).

Moreover, we evaluated the performances of the developed long short-term memory classifiers on the validation set to determine the classifier with the ideal (hyper)parameters that provide the best performance (Table 3.8).

TABLE 3.8: (HYPER)PARAMETERS of the LONG SHORT-TERM MEMORY CLASSIFIER

Hidden State Dimension	16
Number of Epochs	100
Dropout Ratio	0.25
Optimization Method	Adam
Batch Size	32
Loss Function	Binary Cross Entropy

Dropout was applied to the hidden state (output) of the best-performing long short-term memory (LSTM) classifier for regularization. The hidden state (output) of the long short-term memory (LSTM) classifier was then given as input to a linear (sigmoid) layer to robustly estimate a patient's probability of having COVID-19 (Figure 3.12). The proposed 1D-convolutional filter and long short-term memory (LSTM) classifier were trained, optimized, and tested using our workstation (Table 3.5).

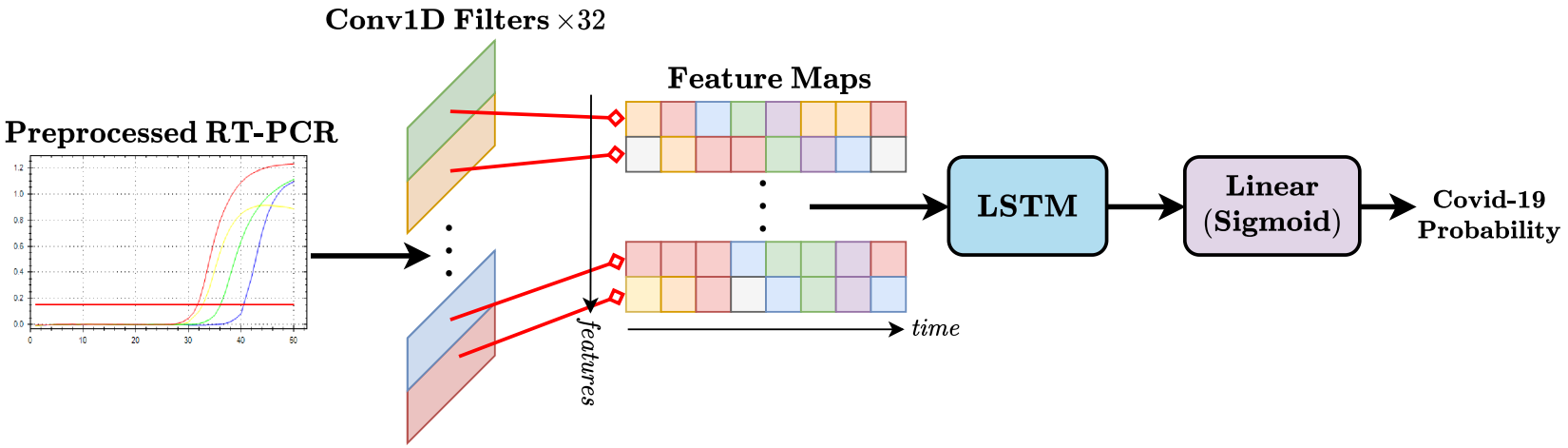

Figure 3.12: The proposed 1D-convolutional filter and long short-term memory (LSTM) classifier were developed to perform binary classification for COVID-19 diagnosis using preprocessed RT-PCR data in the AUFM-CoV database.

3.0.3 Artificial Intelligence based Hybrid Clinical Decision Support Technique

The proposed automated artificial intelligence-based hybrid clinical decision support technique is an ensemble learning approach that utilizes multiple different learning algorithms to achieve better performance than what could be obtained from a single artificial intelligence model alone. It comprises two preprocessing methods, convolutional neural network-based deep learning method and long short-term memory-based deep learning method, along with an artificial neural network (ANN)-based machine learning method developed to provide rapid and robust detection of COVID-19 (Figure 3.13). By jointly analyzing RT-PCR curves, thorax computed tomography images, and laboratory data of each patient, it benefits from the diversity in different data types that are critical for the reliable detection of COVID-19 and leverages their strengths.

Convolutional neural network and long short-term memory-based deep learning methods were independently trained and optimized using thorax computed tomography images and RT-PCR curves in the training and validation sets, respectively. The feature maps generated by the latent space (global average pooling layer) of the 3D-convolutional neural network classifier and the hidden state of the long short-term memory classifier were sequentially concatenated with laboratory data. All concatenated data were then split into non-intersecting training, validation, and test sets to perform multi-class classification for COVID-19 diagnosis (Table 3.9).

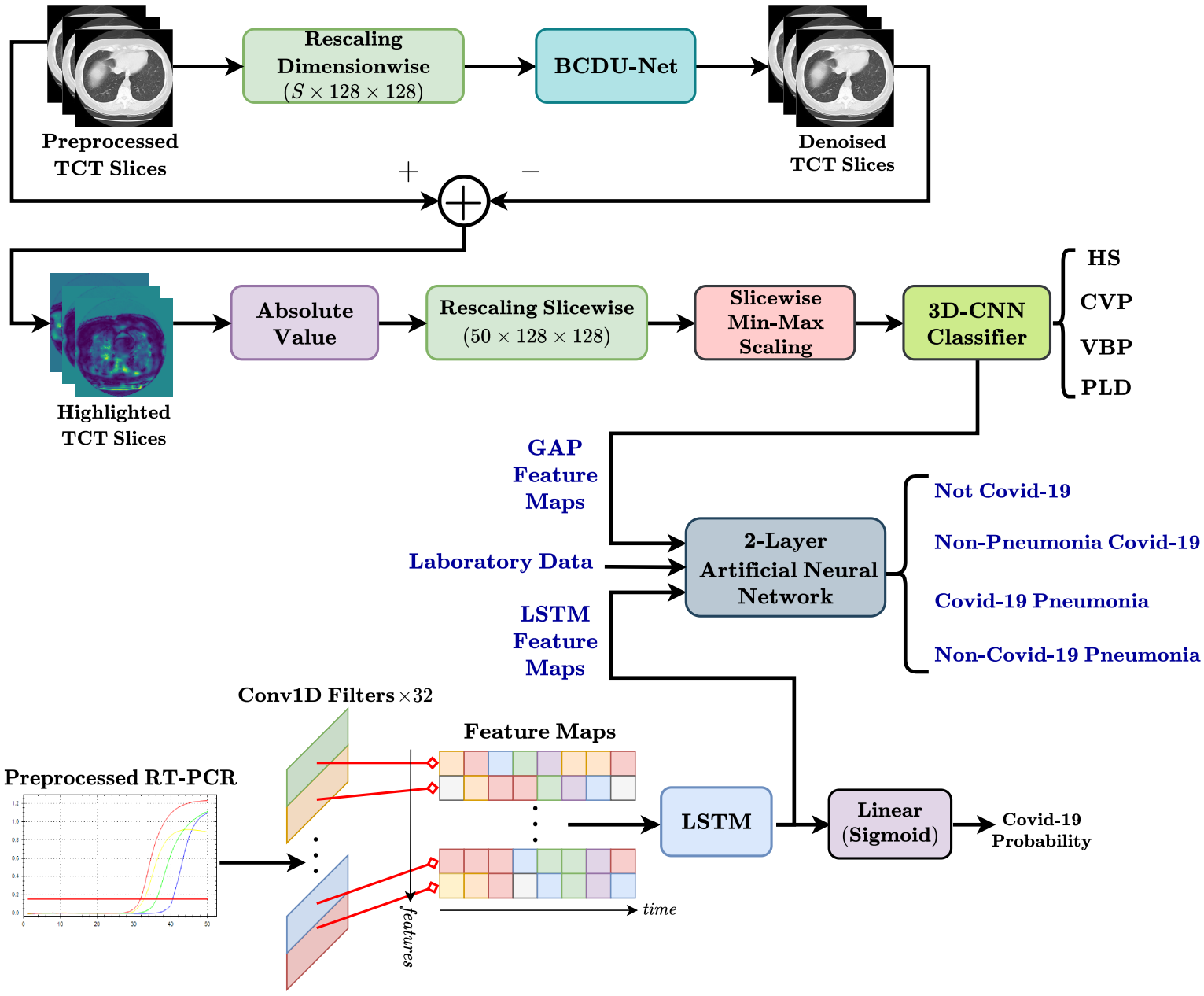

Figure 3.13: The proposed automated artificial intelligence-based hybrid clinical decision support technique that jointly analyzes RT-PCR curves, thorax computed tomography images, and laboratory data in the AUFM-CoV database to perform multi-class classification. The four classes are COVID-19 pneumonia (CVP), non-pneumonia COVID-19 (NPC), non-COVID-19 pneumonia (NCVP), and not COVID-19 (NC).

TABLE 3.9: PATIENT DISTRIBUTIONS in the TRAINING, VALIDATION, and TEST SETS for MULTI-CLASS CLASSIFICATION using ARTIFICIAL INTELLIGENCE-based HYBRID CLINICAL DECISION SUPPORT TECHNIQUE

Classes	**Training Set**	**Validation Set**	**Test Set**	**Total**
COVID-19 Pneumonia (CVP)	149	37	187	373
Non-Pneumonia COVID-19 (NPC)	148	37	185	370
Non-COVID-19 Pneumonia (NCVP)	66	17	83	166
Not COVID-19 (NC)	269	67	336	672
Total	632	158	791	1581

We labeled all concatenated data in the training, validation, and test sets according to the patient labeling criteria presented in Table 3.2. These criteria indicate the multi-class classification classes for the artificial intelligence-based hybrid clinical decision support technique corresponding to the patients' final diagnosis. We developed various two-layered artificial neural network classifiers with different (hyper)parameters and trained them using the training set.

To address class imbalance, we implemented a class-wise weighting technique, which is inversely proportional to the number of data, during training. In other words, we assigned different weights to different classes in the training set. The weight assigned to each class was inversely related to the class's size. Minority classes received higher weights, while majority classes received lower weights. These weights determined how much the network focused on learning each class during training and the importance the network assigned to each class. This helps the network learn more effectively and make accurate predictions for the underrepresented (minority) classes during training, thereby improving its class-wise performance.

The performances of the developed artificial neural network classifiers were evaluated on the validation set to determine the best-performing network with ideal (hyper)parameters (Table 3.10). The softmax activation function was utilized on the output layer of the network to perform multi-class classification. The output of the artificial neural network classifier demonstrates a patient's probability of belonging to one of the four classes, which are COVID-19 pneumonia (CVP), non-pneumonia COVID-19 (NPC), non-COVID-19 pneumonia (NCVP), and not COVID-19 (NC) (Figure 3.13).

TABLE 3.10: The (HYPER)PARAMETERS of the ARTIFICIAL NEURAL NETWORK CLASSIFIER

Number of Hidden Layers	1
Number of Hidden Neurons	32
Number of Output Neurons	4
Number of Epochs	100
Dropout Ratio	0.25
Optimization Method	Adam
Learning Rate	10^{-3}
Loss Function	Categorical Cross Entropy

3.1 Statistical Analysis

Cohen's Kappa coefficient was employed to measure the agreement between the developed artificial intelligence models and physicians. **p** values less than 0.05 were considered significant. The statistical analyses were carried out using IBM SPSS statistics software v26 (IBM Statistics, U.S.), except for confidence intervals (CI), for which MedCalc v19 (MedCalc Software, Belgium) was utilized.

The statistical performance measures, such as sensitivity (TPR), specificity (TNR), positive predicted value (PPV), and F_1-score (F_1), were calculated to evaluate the performance of the developed models, as shown in Equations 3.14, 3.15, 3.16, 3.17 . Here, TP represents true positive, TN represents

true negative, FP represents false positive, and FN represents false negative.

$$\mathrm{TPR} = \frac{\mathrm{TP}}{\mathrm{TP} + \mathrm{FN}} \tag{3.14}$$

$$\mathrm{TNR} = \frac{\mathrm{TN}}{\mathrm{TN} + \mathrm{FP}} \tag{3.15}$$

$$\mathrm{PPV} = \frac{\mathrm{TP}}{\mathrm{TP} + \mathrm{FP}} \tag{3.16}$$

$$\mathrm{F}_1 = 2 * \frac{\mathrm{PPV} * \mathrm{TPR}}{\mathrm{PPV} + \mathrm{TPR}} \tag{3.17}$$

3.2 Results

3.2.1 Performance Results of the BCDU-Net and 3D-Convolutional Neural Network Classifier

The multi-class classification performance results of the proposed BCDU-Net and 3D-convolutional neural network classifier were evaluated on the test set. The confusion matrices in Figure 3.14 demonstrate the proposed classifier's strong ability to differentiate COVID-19 pneumonia (CVP) from other viral and bacterial pneumonias (VBP) and parenchymal lung diseases (PLD).

Out of a total of 246 COVID-19 pneumonia (CVP) cases in the test set, the proposed classifier correctly classified 226 cases, while misclassifying only 18 cases as healthy subjects (HS), and 2 cases as parenchymal lung diseases (PLD). Out of a total of 84 viral and bacterial pneumonias (VBP) cases in the test set, it correctly classified 69 cases, while misclassifying only 15 cases as parenchymal lung diseases (PLD). Moreover, out of a total of 116 parenchymal lung diseases (PLD) cases in the test set, it correctly classified 94 cases, while misclassifying only 1 case as healthy subjects (HS), 2 cases as COVID-19 pneumonia (CVP), and 19 cases as other viral and bacterial pneumonias (VBP). Finally, out of a total of 536 healthy subjects (HS) cases in the test set, it correctly classified 478

cases, while misclassifying 53 cases as COVID-19 pneumonia (CVP) and 5 cases as other viral and bacterial pneumonias (VBP).

Cohen's Kappa was calculated as 0.814 ± 0.016 ($\mathbf{p} < 0.001$), indicating strong agreement between the proposed BCDU-Net and 3D-convolutional neural network classifier, and the expert radiologist.

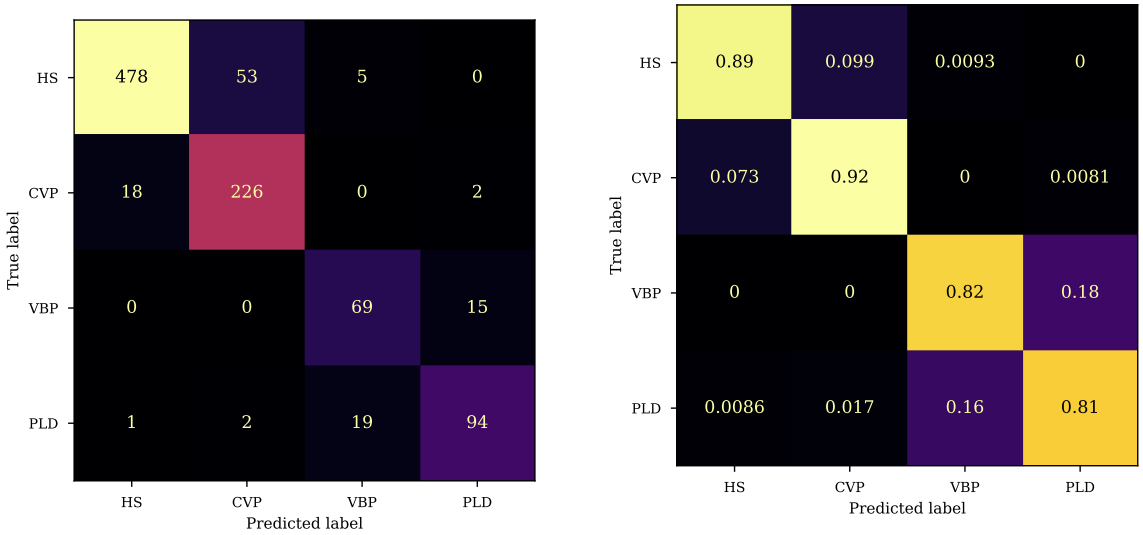

(a) Confusion matrix.

(b) Normalized confusion matrix with respect to the true labels.

Figure 3.14: Multi-class classification performance results of the BCDU-Net and 3D-convolutional neural network classifier on the test set, where the four classes are COVID-19 pneumonia (CVP), other viral and bacterial pneumonias (VBP), parenchymal lung diseases (PLD), and healthy subjects (HS).

Table 3.11 illustrates the multi-class classification statistical performance results of the proposed BCDU-Net and 3D-convolutional neural network classifier on the test set. Previous studies have reported that the specificity of the thorax computed tomography for COVID-19 diagnosis ranged from 25% to 53% [121, 196, 197, 198]. In this study, the results obtained on the AUFM-CoV database showed that the developed BCDU-Net and 3D-convolutional neural network classifier outperformed thorax computed tomography in terms of the specificity of COVID-19 diagnosis (Table 3.11).

Furthermore, it has been shown that the proposed classifier very successfully differentiates COVID-19 pneumonia (CVP) from other viral and bacterial pneumonias (VBP), as well as parenchymal lung diseases (PLD). This differential diagnosis presents a significant challenge due to the high similarity in ground-glass opacities (GGO) and consolidation patterns observed in radiological images of COVID-19 pneumonia (CVP), other viral and bacterial pneumonias (VBP), and parenchymal lung diseases (PLD). Therefore, the proposed classifier has great potential for successful use in the differential diagnosis of pulmonary diseases containing ground-glass opacities (GGO).

TABLE 3.11: MULTI-CLASS CLASSIFICATION STATISTICAL PERFORMANCE RESULTS of the BCDU-NET and 3D-CONVOLUTIONAL NEURAL NETWORK CLASSIFIER on the TEST SET

Classes	**TPR (%)**	**TNR (%)**	**PPV (%)**	**F_1 (%)**	**NP**
COVID-19 Pneumonia (CVP)	91.9	92.5	80.4	86	246
Other Viral and Bacterial Pneumonias (VBP)	82.1	97.3	74.2	78	84
Parenchymal Lung Diseases (PLD)	81	98	84.7	83	116
Healthy Subjects (HS)	89.2	95.7	96.2	93	536

NP: Number of patients in the test set.

The binary classification performance results of the developed BCDU-Net and 3D-convolutional neural network classifier were evaluated on the test set. The confusion matrices in Figure 3.15 demonstrate the strong ability of the proposed classifier to distinguish between patients with COVID-19 and those without COVID-19. Out of a total of 246 COVID-19 cases in the test set, the proposed classifier correctly classified 225 cases, while misclassifying only 21 cases as not COVID-19 (NC). Furthermore, out of a total of 736 not COVID-19 (NC) cases in the test set, it correctly classified 698 cases, while misclassifying only 38 cases as COVID-19.

Cohen's Kappa was calculated as 0.844 ± 0.020 ($\mathbf{p} < 0.001$), indicating strong agreement between the BCDU-Net and 3D-convolutional neural network classifier, and the expert radiologist.

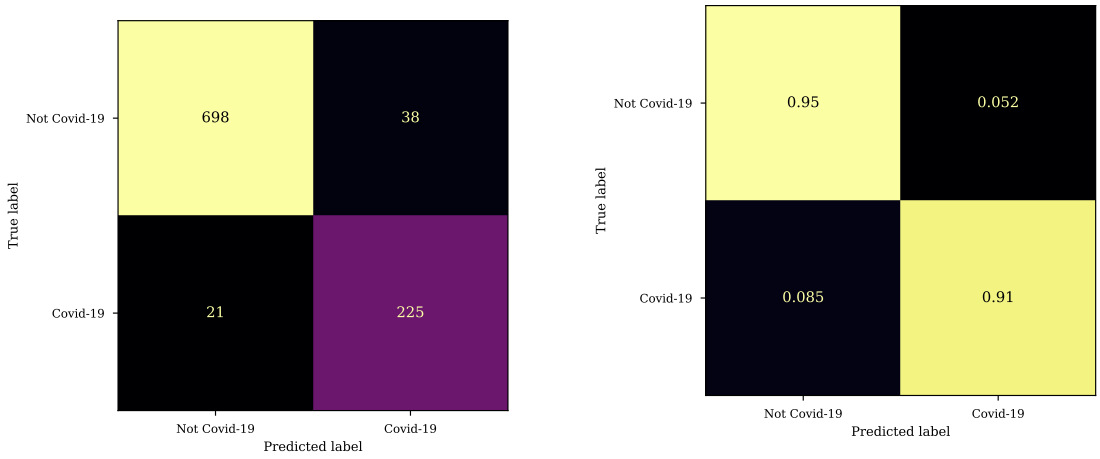

(a) Confusion matrix.

(b) Normalized confusion matrix with respect to the true labels.

Figure 3.15: The binary classification performance results of the BCDU-Net and 3D-convolutional neural network classifier on the test set, where the two classes are COVID-19 and not COVID-19.

Table 3.12 shows the binary classification statistical performance results of the proposed BCDU-Net and 3D-convolutional neural network classifier on the test

set. Previous studies have reported that the sensitivity of thorax computed tomography in COVID-19 diagnosis ranged from 60% to 94% [121, 196, 197, 198]. In this study, the results obtained on the AUFM-CoV database showed that the developed BCDU-Net and 3D-convolutional neural network classifier have comparable sensitivity to thorax computed tomography in COVID-19 diagnosis (Table 3.12). Furthermore, it is shown that the proposed classifier provides a highly reliable diagnosis of COVID-19 and very successfully differentiates between COVID-19 and not COVID-19 (NC) classes.

TABLE 3.12: BINARY CLASSIFICATION STATISTICAL PERFORMANCE RESULTS of the BCDU-NET and 3D-CONVOLUTIONAL NEURAL NETWORK CLASSIFIER on the TEST SET

Classes	**TPR (%)**	**TNR (%)**	**PPV (%)**	**F_1 (%)**	**NP**
Not COVID-19	94.8	91.5	97.1	95.9	736
COVID-19	91.5	94.8	85.6	88.4	246

NP: Number of patients in the test set.

3.2.2 Performance Results of the 1D-Convolutional Filter and Long Short-Term Memory Classifier

The binary classification performance results of the developed 1D-convolutional filter and long short-term memory classifier were evaluated on the test set. The confusion matrices in Figure 3.16 demonstrate the proposed classifier's strong ability to discriminate between Positive and Negative cases for SARS-CoV-2. Out of a total of 320 Positive cases in the test set, the proposed classifier correctly classified 309 cases, while misclassifying only 11 cases as Negative. Moreover, out of a total of 792 Negative cases in the test set, it correctly classified 786 cases, while misclassifying only 6 cases as Positive.

Cohen's Kappa was calculated as 0.963 ± 0.009 ($\mathbf{p} < 0.001$), indicating almost perfect agreement between the proposed 1D-convolutional filter and long short-term memory classifier, and the expert microbiologist.

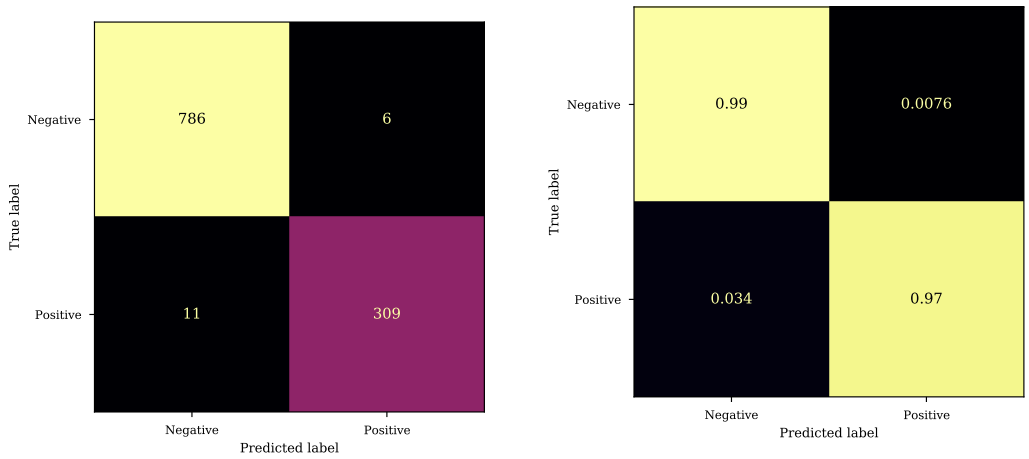

(a) Confusion matrix.

(b) Normalized confusion matrix with respect to the true labels.

Figure 3.16: The binary classification performance results of the 1D-convolutional filter and long short-term memory classifier on the test set, where the two classes are Positive and Negative for SARS-CoV-2.

Table 3.13 shows the binary classification statistical performance results of the proposed 1D-convolutional filter and long short-term memory classifier on the test set. Previous studies have reported that the RT-PCR test has a low sensitivity ranging from 59% to 70% for COVID-19 diagnosis [116, 117, 192, 199]. In this study, the results obtained on the AUFM-CoV database showed that the developed 1D-convolutional filter and long short-term memory classifier outperformed the gold standard RT-PCR test in terms of the sensitivity of COVID-19 diagnosis (Table 3.13). Furthermore, it is shown that the developed classifier provides a highly reliable diagnosis of COVID-19 and very successfully distinguishes between Positive and Negative cases for SARS-CoV-2.

TABLE 3.13: BINARY CLASSIFICATION STATISTICAL PERFORMANCE RESULTS of the 1D-CONVOLUTIONAL FILTER and LONG SHORT-TERM MEMORY CLASSIFIER on the TEST SET

Classes	TPR (%)	TNR (%)	PPV (%)	F_1 (%)	NP
Negative	99.2	96.5	98.6	98.9	792
Positive	96.6	99.2	98.1	97.3	320

NP: Number of patients in the test set.

3.2.3 Performance Results of the Artificial Intelligence based Hybrid Clinical Decision Support Technique

The multi-class classification performance results of the proposed artificial intelligence-based hybrid clinical decision support technique were evaluated on the test set. The confusion matrices in Figure 3.17 demonstrate the strong ability of the proposed technique to distinguish COVID-19 pneumonia (CVP) from non-COVID-19 pneumonia (NCVP), non-pneumonia COVID-19 (NPC), and not COVID-19 (NC).

Out of a total of 336 not COVID-19 (NC) cases in the test set, the artificial intelligence-based hybrid clinical decision support technique correctly classified 308 cases, while misclassifying only 2 cases as non-pneumonia COVID-19 (NPC), 7 cases as COVID-19 pneumonia (CVP), and 19 cases as non-COVID-19 pneumonia (NCVP). Out of a total of 185 non-pneumonia COVID-19 (NPC) cases in the test set, it correctly classified 168 cases, while misclassifying only 6 cases as not COVID-19 (NC), 10 cases as COVID-19 pneumonia (CVP), and 1 case as non-COVID-19 pneumonia (NCVP). Moreover, out of a total of 187 COVID-19 pneumonia (CVP) cases in the test set, it correctly classified 124 cases, while misclassifying only 15 cases as not COVID-19 (NC), 28 cases as non-pneumonia COVID-19 (NPC), and 20 cases as non-COVID-19 pneumonia (NCVP). Lastly, out of a total of 83 non-COVID-19 pneumonia (NCVP) cases in the test set, it correctly classified 54 cases, while misclassifying 15 cases as not COVID-19 (NC),

14 cases as COVID-19 pneumonia (CVP), and only 0 cases as non-pneumonia COVID-19 (NPC).

Cohen's Kappa was calculated as 0.752 ± 0.022 ($\mathbf{p} < 0.001$), indicating substantial agreement between the proposed artificial intelligence-based hybrid clinical decision support technique and the expert physicians.

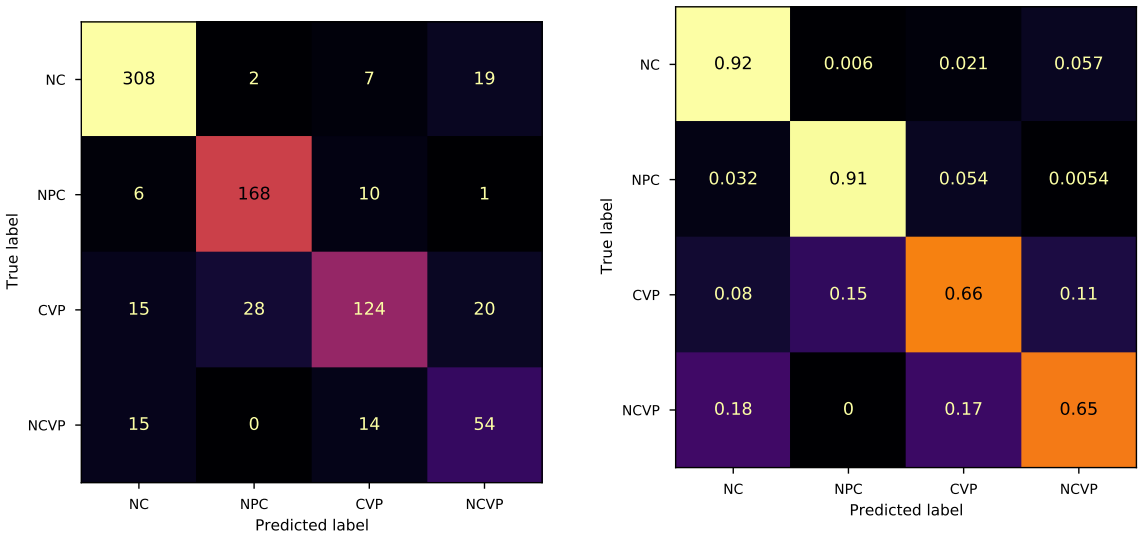

(a) Confusion matrix.

(b) Normalized confusion matrix with respect to the true labels.

Figure 3.17: The multi-class classification performance results of the artificial intelligence-based hybrid clinical decision support technique on the test set, where the four classes are COVID-19 pneumonia (CVP), non-pneumonia COVID-19 (NPC), non-COVID-19 pneumonia (NCVP), and not COVID-19 (NC).

Table 3.14 illustrates the multi-class classification statistical performance results of the proposed automated artificial intelligence-based hybrid clinical decision support technique on the test set. The four classes were determined according to the patient labeling criteria in Table 3.2 .

The results obtained on the AUFM-CoV database showed that the developed artificial intelligence-based hybrid clinical decision support technique provides highly reliable diagnosis of COVID-19 by jointly using RT-PCR data, thorax computed tomography images, and laboratory data.

Furthermore, it is shown that the hybrid clinical decision support technique exhibits higher specificity compared to thorax computed tomography in COVID-19 diagnosis (Table 3.14). Therefore, it holds great potential for successful use in the differential diagnosis of COVID-19 pneumonia (CVP) and other pneumonias.

TABLE 3.14: MULTI-CLASS CLASSIFICATION STATISTICAL PERFORMANCE RESULTS of the ARTIFICIAL INTELLIGENCE-BASED HYBRID CLINICAL DECISION SUPPORT TECHNIQUE on the TEST SET

Classes	**TPR (%)**	**TNR (%)**	**PPV (%)**	**F_1 (%)**	**NP**
Not COVID-19 (NC)	91.7	92.1	89.5	91	336
COVID-19 Pneumonia (CVP)	66.3	94.9	80	73	187
Non-Pneumonia COVID-19 (NPC)	90.8	95	84.8	88	185
Non-COVID-19 Pneumonia (NCVP)	65.1	94.3	57.4	61	83

NP: Number of patients in the test set.

Moreover, the artificial intelligence-based hybrid clinical decision support technique has demonstrated high performance in the differential diagnosis of COVID-19 pneumonia (CVP), non-COVID-19 pneumonia (NCP), and not COVID-19 (NC). This is achieved through the joint analysis of RT-PCR data, thorax computed tomography images, and laboratory data, benefiting from the diversity among various medical data types and leveraging their strengths.

However, its performance in diagnosing non-COVID-19 pneumonia (NCP) is relatively low due to the limited number of patients in the training, validation, and test sets who belong to the non-COVID-19 pneumonia (NCP) class. Therefore, the performance of the hybrid clinical decision support technique in diagnosing non-COVID-19 pneumonia (NCP) can be improved by increasing the number of patients in the non-COVID-19 pneumonia (NCP) class. Similarly, overall performance of the hybrid clinical decision support technique can be further improved by increasing the number of patients in all four classes.

The binary classification performance results of the proposed artificial intelligence-based hybrid clinical decision support technique were evaluated on the test set. The confusion matrices in Figure 3.18 demonstrate the strong ability of the hybrid clinical decision support technique to distinguish between patients with COVID-19 and without COVID-19.

Out of a total of 372 COVID-19 cases in the test set, the proposed hybrid clinical decision support technique correctly classified 335 cases, while misclassifying only 37 cases as not COVID-19 (NC). Furthermore, out of a total of 419 not COVID-19 (NC) cases in the test set, it correctly classified 389 cases, while misclassifying only 30 cases as COVID-19.

Cohen's Kappa was calculated as 0.850 ± 0.021 ($\mathbf{p} < 0.001$), indicating strong agreement between the proposed artificial intelligence-based hybrid clinical decision support technique and the expert physicians.

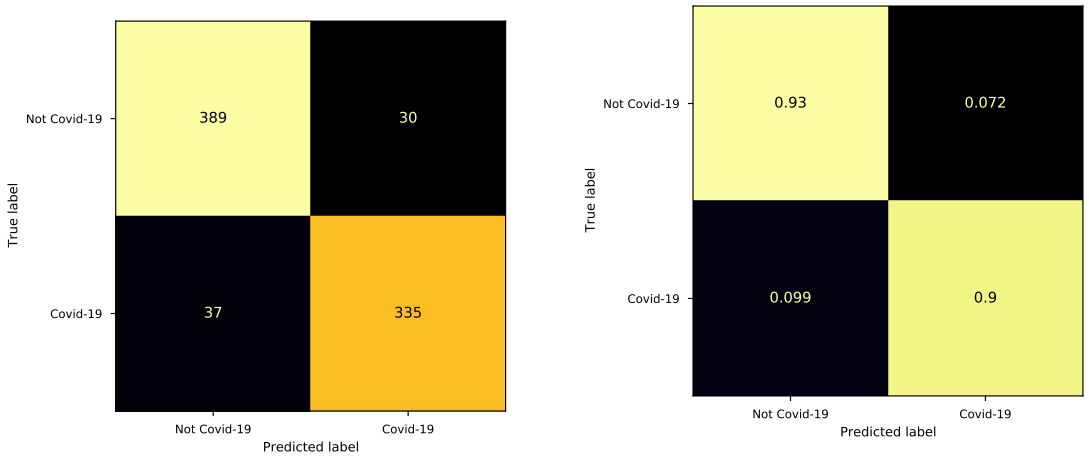

(a) Confusion matrix.

(b) Normalized confusion matrix with respect to the true labels.

Figure 3.18: The binary classification performance results of the artificial intelligence-based hybrid clinical decision support technique on the test set, where the two classes are COVID-19 and Not COVID-19.

Table 3.15 presents the binary classification statistical performance results of the proposed artificial intelligence-based hybrid clinical decision support technique on the test set. The results obtained on the AUFM-CoV database indicated that the developed hybrid clinical decision support technique outperformed the gold standard RT-PCR test in terms of the sensitivity of COVID-19 diagnosis (Table 3.15). Moreover, the proposed hybrid clinical decision support technique has demonstrated remarkable success in distinguishing between patients with COVID-19 and those without COVID-19.

Additionally, previous studies have reported that the sensitivity and specificity of laboratory data in diagnosing COVID-19 were approximately 62% and 76%, respectively [194, 200, 201]. In this study, the results obtained on the AUFM-CoV database showed that the proposed artificial intelligence-based hybrid clinical decision support technique exhibits superior sensitivity and specificity compared to laboratory data in COVID-19 diagnosis (Table 3.15).

TABLE 3.15: BINARY CLASSIFICATION STATISTICAL PERFORMANCE RESULTS of the HYBRID CLINICAL DECISION SUPPORT TECHNIQUE on the TEST SET

Classes	TPR (%)	TNR (%)	PPV (%)	F_1 (%)	NP
Not COVID-19	92.8	90	91.3	92.1	419
COVID-19	90	92.8	91.8	90.9	372

NP: Number of patients in the test set.

3.3 Discussion

To the best of our knowledge, the AUFM-CoV database constructed in this study has the widest variety of medical data compared to any publicly available COVID-19 databases [118, 119, 120, 122, 202]. Moreover, it is the most comprehensive database containing thorax computed tomography images of a wide variety of lung diseases containing ground-glass opacities (GGO), which are very difficult to distinguish from COVID-19 pneumonia (CVP). By intentionally including RT-PCR tests with gray zones and thorax computed tomography images with disease-indeterminate groups in the AUFM-CoV database, we aimed to develop an automated artificial intelligence-based hybrid clinical decision support technique that can perform robust and reliable detection of COVID-19.

The drawback of existing artificial intelligence studies investigating COVID-19 diagnosis or classification is that they rely solely on RT-PCR test positivity to diagnose patients with COVID-19 [203, 204, 205, 206, 207, 208, 209, 210, 211, 212]. However, these studies did not address the issue of false-negative RT-PCR tests, which present the main challenge faced by clinicians. If patients are labeled only based on their RT-PCR test results, it will not be possible to improve the performance of COVID-19 diagnosis due to the high false-negative rate associated with the RT-PCR test.

In contrast to previous studies, in our study, patients were labeled through the

joint evaluation of their RT-PCR curves, thorax computed tomography images, and laboratory data, in accordance with the patient labeling criteria presented in Table 3.2 . These criteria combine the interpretations of microbiologists, radiologists, pulmonologists, and clinicians.

Moreover, suspicious RT-PCR test results falling within the gray zone are susceptible to misinterpretation by microbiologists. In such cases, the radiological, laboratory, and clinical data of the respective patients become essential for accurately diagnosing COVID-19 [124, 166, 167, 193, 213, 214, 215, 216, 217, 218]. However, in the midst of a pandemic or when dealing with an increased daily workload, it is not feasible to expect a microbiologist to review all these diverse types of medical data.

In our study, suspicious RT-PCR curves in the gray zone were re-evaluated and labeled as either positive or negative for SARS-CoV-2 by all of the physicians, who also independently evaluated patients' radiological images, laboratory data, and clinical data. Eventually, the final labels were determined through consensus among the microbiologists, radiologists, pulmonologists, and clinicians.

As a result, suspicious RT-PCR curves in the gray zone were correctly classified as either positive or negative, eliminating the need for unnecessary re-testing. This ensured the efficient utilization of resources and prevented the accidental discharge of patients with false-negative results.

To the best of our knowledge, only two studies in the literature have utilized artificial intelligence techniques on RT-PCR data to detect COVID-19 [199, 208]. One study investigated anomaly detection on RT-PCR data using a machine learning method to determine positive, negative, and abnormal classes [208]. The abnormal class was used to identify suspicious cases in the gray zone. However, unlike our study, it did not provide any decision support to the physicians. Another study aimed to reduce the diagnosis time of COVID-19 by analyzing RT-PCR time series data using a deep learning method [199].

Unlike the two previous studies [199, 208], in our study, we utilized several RT-PCR data of each patient, all obtained within ± 7 days from the respective patient's thorax computed tomography date, when developing the automated artificial intelligence-based hybrid clinical decision support technique.

Table 3.16 illustrates the performance comparison between our 1D-convolutional filter and long short-term memory classifier, as well as the two previous artificial intelligence studies that utilized RT-PCR data for COVID-19 diagnosis by performing binary classification. The binary classification performance results of our 1D-convolutional filter and long short-term memory classifier showed that it has comparable sensitivity, higher specificity, higher precision, and higher F_1-score when compared to the previous studies in the literature.

TABLE 3.16: PERFORMANCE COMPARISON of the PROPOSED 1D-CONVOLUTIONAL FILTER and LONG SHORT-TERM MEMORY CLASSIFIER with PREVIOUS ARTIFICIAL INTELLIGENCE STUDIES investigating COVID-19 DIAGNOSIS by performing BINARY CLASSIFICATION using RT-PCR DATA

STUDY	**METHOD**	**TPR (%)**	**TNR (%)**	**PPV (%)**	**F_1 (%)**
[208]	Random Forest	99.3	-	91.5	95.3
[199]	Long Short-Term Memory Network	93.3	75.7	29.9	-
Proposed Study	**1D-Convolutional Filter + Long Short-Term Memory Network**	**96.6**	**99.2**	**98.1**	**97.3**

Furthermore, most of the existing artificial intelligence techniques developed for COVID-19 diagnosis or classification are based on various convolutional neural network architectures, usually trained using transfer learning or fine-tuning methods [196, 197, 198, 207, 209, 210, 212, 215, 216, 217, 219, 220]. In contrast to these existing techniques, in our study, we trained the 3D-convolutional neural network classifier end-to-end from scratch, which is a more challenging and time-consuming approach compared to using transfer learning or fine-tuning methods.

Furthermore, most of the existing artificial intelligence techniques developed for the diagnosis or classification of COVID-19 utilized only digital radiological images [118, 124, 143, 145, 147, 148, 149, 152, 153, 158, 160, 164, 196, 197, 198, 203, 204, 205, 207, 209, 210, 211, 216, 217, 219, 220, 221, 222, 223, 224]. However, current guidelines from the American College of Radiology indicate that radiological images are necessary, but not sufficient for the reliable diagnosis of COVID-19 [121]. In contrast to these existing techniques, our study utilized thorax computed tomography images, RT-PCR curves, and laboratory data of the patients to develop a reliable and robust automated artificial intelligence-based hybrid clinical decision support technique.

Additionally, most of the previous artificial intelligence studies have performed binary classification to distinguish between COVID-19 pneumonia (CVP) and healthy lungs [118, 124, 143, 145, 147, 148, 152, 153, 160, 164, 196, 197, 198, 203, 204, 205, 207, 209, 211, 216, 217, 219, 220, 221, 222, 223]. A few studies have investigated the differential diagnosis of COVID-19 pneumonia (CVP), other pneumonias, and/or healthy lungs by performing multi-class classification [50, 115, 149, 158, 210].

In contrast to these previous studies, our BDCU-Net and 3D-convolutional neural network classifier learned to accurately distinguish COVID-19 pneumonia (CVP) from other viral and bacterial pneumonias (VBP), parenchymal lung diseases (PLD), and healthy subjects (HS) by performing four-class classification, which is a very difficult task compared to binary classification.

Additionally, the performance of our BCDU-Net and 3D-convolutional neural network classifier was evaluated using the AUFM-CoV database, which comprises a wide variety of lung diseases with ground-glass opacities (GGO) that are particularly challenging to distinguish from COVID-19 pneumonia (CVP).

Table 3.17 presents the performance comparison between our BCDU-Net and 3D-convolutional neural network classifier, and recent artificial intelligence studies that employed radiological images for COVID-19 diagnosis by performing multi-class classification. The multi-class classification performance results of our BCDU-Net and 3D-convolutional neural network classifier indicated that it has higher sensitivity, comparable specificity, comparable precision, and comparable F_1-score compared to existing methods in the literature that performed four-class classification.

Moreover, our classifier exhibits relatively higher sensitivity, lower specificity, lower precision, and lower F_1-score compared to existing methods that conducted three-class classification. This is a highly anticipated result, since three-class classification is an easier task compared to four-class classification, which was performed by our classifier.

To the best of our knowledge, this is the first study that proposed an automated artificial intelligence-based hybrid clinical decision support technique, which consists of both deep learning and machine learning methods that jointly analyze RT-PCR data, thorax computed tomography images, and laboratory data to perform fast and robust detection of COVID-19. The binary and multi-class classification performance results of the proposed technique on the AUFM-CoV database showed that it provides highly accurate and reliable diagnosis of COVID-19.

Since there are no other studies in the literature that proposed a hybrid artificial intelligence technique that jointly utilizes RT-PCR curves, thorax computed tomography images, and laboratory data to diagnose or classify COVID-19, it is not possible to compare the performance results of our artificial intelligence-based hybrid clinical decision support technique with those of other previous studies.

TABLE 3.17: PERFORMANCE COMPARISON of the PROPOSED BCDU-NET and 3D-CONVOLUTIONAL NEURAL NETWORK CLASSIFIER with RECENT ARTIFICIAL INTELLIGENCE STUDIES investigating COVID-19 DIAGNOSIS by performing MULTI-CLASS CLASSIFICATION using RADIOLOGICAL IMAGES

STUDY	**METHOD**	**# of CLASSES**	**TPR (%)**	**TNR (%)**	**PPV (%)**	**F1 (%)**
[207]	Convolutional Neural Network	3	98.2	-	98.2	98.2
[198]	Visual Geometry Group16 (VGG16)	3	65	90	79	71
	Residual Network (ResNet50)		55	92.3	81	66
[219]	DarkCovidNet	3	85.3	92.1	89.9	87.3
[211]	Capsule Network (CapsNet)	3	84.2	91.7	84.6	84.2
[212]	EfficientNet	3	96.6	-	97.5	97.1
[220]	Stacked Convolutional Neural Network	3	97.6	98.5	97.4	97.5
[225]	DenseNet169 + XGBoost	3	88.5	100	94.1	92.4
[197]	InceptionV2	3	76	-	69	72
[226]	COV19-CNNet	3	94.3	96.9	-	94.2
[215]	Visual Geometry Group16 (VGG16)	3	76	-	79	78
[216]	ULNet	3	89.7	-	87.9	88.3
[223]	LW-CBRGPNet	3	98.7	98.6	97.3	-
[227]	COVID-Transformer	3	89	-	93	91
[217]	NASNet Large	4	90	92	87	-
[209]	Deep Convolutional Neural Network	4	85.6	92.3	80.9	80.8
[210]	Coronet	4	89.9	96.4	90	89.8
[203]	XGBoost (XGB-L)	4	74.5	95.3	83.8	-
Proposed Study	**BCDU-Net + 3D-Convolutional Neural Network**	**4**	**91.9**	**92.5**	**80.4**	**86**

Chapter 4

Conclusions and Future Works

Firstly, we have proposed a novel automated hybrid artificial intelligence technique that simultaneously and robustly detects anomalies in the 12-lead CSNA and ECG data for fast, early, and accurate diagnosis of coronary artery diseases. We evaluated the performance and generalizability of the proposed automated artificial intelligence-based hybrid anomaly detection technique using the fully-labeled STAFF III and PTBD databases. The experimental results have demonstrated that the automated artificial intelligence-based hybrid anomaly detection technique yields highly promising results for the reliable and robust detection of coronary artery diseases using the 12-lead ECG and CSNA data.

Secondly, we constructed a new fully-labeled COVID-19 database that contains RT-PCR curves, thorax computed tomography images, and laboratory data of patients with COVID-19 pneumonia (CVP), other viral and bacterial pneumonias (VBP), parenchymal lung diseases (PLD), and healthy subjects (HS). Among the publicly available COVID-19 databases [190, 191], our database contains the widest variety of medical data, which are critical for the reliable diagnosis of COVID-19.

We proposed a new automated, artificial intelligence-based hybrid clinical decision support technique that provides highly reliable diagnosis of COVID-19 by

jointly analyzing RT-PCR curves, thorax computed tomography images, and laboratory data. Hence, this approach benefits from the diversity in different data types and leverages their strengths. The proposed artificial intelligence-based hybrid clinical decision support technique is an ensemble learning approach consisting of preprocessing methods, long short-term memory network-based deep learning method, convolutional neural network-based deep learning method, as well as artificial neural network-based machine learning method that performs fast and accurate detection of COVID-19. It has been proven to be highly successful in performing differential diagnosis of COVID-19 pneumonia (CVP) and other pneumonias.

In the future, the automated artificial intelligence-based hybrid anomaly detection technique and artificial intelligence-based hybrid clinical decision support technique can be integrated into hospitals' software systems and clinically validated through multi-center prospective studies to demonstrate their high performance, generalizability, and robustness on a larger and more diverse patient population. This process will also help determine the amount of time they can save physicians in daily clinical practice.

After ensuring the reliability of the artificial intelligence-based hybrid anomaly detection technique for widespread clinical applicability, it can be seamlessly integrated into wearable devices, such as wireless patches and smartwatches, for continuous, simultaneous, and long-term monitoring of CSNA and ECG in real-time. This integration may provide early warnings to patients for improved diagnosis and treatment of coronary artery diseases, highlighting the potential benefits of this study in real-world medical scenarios.

Consequently, the automated artificial intelligence-based hybrid anomaly detection technique and artificial intelligence-based hybrid clinical decision support technique may serve as efficient decision-support systems to increase the success rate and reduce the workload of physicians in fast and accurate diagnosis of coronary artery diseases and COVID-19, respectively. This can help reduce the risk of misdiagnosis by human experts or the gold standard diagnostic tests, and it can assist physicians in making well-informed diagnostic decisions efficiently.

The contribution of the automated artificial intelligence-based hybrid anomaly detection technique to the reliable diagnosis of coronary artery diseases can be significantly greater than that of conventional ECG devices, and the utilization of CSNA in the diagnosis of cardiovascular diseases can gain a new perspective.

In addition, the promising areas for future research and development concerning the joint detection of COVID-19 and COVID-19-related heart diseases using various artificial intelligence techniques can be summarized as follows:

- **Multimodal Data Fusion:** Development of comprehensive diagnostic and predictive artificial intelligence models capable of analyzing and fusing data from various modalities and sources, including medical images, electronic health records, and wearable devices, to enable robust detection of COVID-19 and its associated heart diseases.
- **Explainable Artificial Intelligence:** Improvement of the transparency and interpretability of artificial intelligence models to gain trust and acceptance from healthcare professionals and facilitate their integration into clinical practice. Development of artificial intelligence models to offer clear explanations for their predictions and recommendations, particularly in complex medical decision-making scenarios associated with COVID-19-related heart diseases that could have significant clinical consequences.
- **Few-Shot Learning:** Exploration of transfer learning techniques, such as pre-trained models and few-shot learning, to develop diagnostic artificial intelligence models with high performance that can quickly adapt to emerging variants of the virus or new heart diseases associated with COVID-19. These techniques will be highly valuable and beneficial, especially in situations where the availability of labeled data is limited, as it can significantly reduce the amount of data needed for model training, making it more applicable to real-world scenarios where collecting large databases may be challenging.

- **Clinical Decision Support Systems:** Development of artificial intelligence-powered clinical decision support systems that can further assist physicians in real-time by offering treatment recommendations and risk assessments for COVID-19 patients with associated heart diseases.

- **Long-Term Health Monitoring and Predictive Modeling:** Conducting longitudinal studies to understand the long-term health consequences of COVID-19 on the cardiovascular system by tracking patients over extended periods. Developing artificial intelligence models that can predict and anticipate the evolution and progression of heart diseases in COVID-19 survivors over time.

- **Ethical Considerations and Data Privacy:** Investigation of the ethical implications of artificial intelligence-driven healthcare solutions, with a focus on issues such as data privacy, patient consent, and bias mitigation. Development of guidelines and regulations to ensure the responsible utilization of artificial intelligence in clinical settings.

- **Validation and Clinical Trials:** Conducting validation studies and clinical trials to assess the real-world impact of artificial intelligence-based diagnostic tools for COVID-19 and related heart diseases. Working with regulatory authorities to ensure that these diagnostic tools meet the necessary safety and efficacy standards for clinical use.

- **Personalized Medicine:** Artificial intelligence can play a pivotal role in customizing treatment plans for patients with COVID-19-related heart diseases. Future research can focus on developing artificial intelligence-driven methods for optimizing and personalizing treatment based on patient-specific characteristics.

- **Large-Scale Data Collaboration:** Encouraging collaborative efforts among healthcare institutions, researchers, and scientists is essential for collecting large and diverse databases for the development and validation of artificial intelligence models. Initiatives focused on data sharing can accelerate advancements in the detection of COVID-19 and its associated heart diseases.

The aforementioned future research directions represent a roadmap for advancing artificial intelligence-driven solutions in the diagnosis of COVID-19-associated heart diseases. Incorporating these future works into research agendas will contribute to improving both the diagnosis and treatment of COVID-19-related heart diseases. It is our hope that this thesis will serve as a foundation for future research endeavors in this critical and rapidly evolving field.

Bibliography

[1] M. B. Terzi and O. Arikan, "Machine learning based hybrid anomaly detection technique for automatic diagnosis of cardiovascular diseases using cardiac sympathetic nerve activity and electrocardiogram," *Biomedical Engineering / Biomedizinische Technik*, 2023.

[2] C. W. Tsao and et al., "Heart disease and stroke statistics—2022 update: a report from the american heart association," *Circulation*, vol. 145, no. 8, pp. e153–e639, 2022.

[3] M. B. Terzı and O. Arikan, "Detection of acute myocardial ischemia based on support vector machines," in *2018 26th Signal Processing and Communications Applications Conference (SIU)*, pp. 1–4, 2018.

[4] M. B. Terzi and et al., "Early diagnosis of acute coronary syndromes with automatic st/t classifier," in *2014 18th National Biomedical Engineering Meeting*, pp. 1–4, 2014.

[5] M. B. Terzı and O. Arikan, "Detection of acute coronary syndrome based on support vector machines and ecg," in *2019 27th Signal Processing and Communications Applications Conference (SIU)*, pp. 1–4, 2019.

[6] M. B. Terzi and O. Arikan, "Coronary artery disease detection by using support vector machines and gaussian mixture model," in *2019 Medical Technologies Congress (TIPTEKNO)*, pp. 1–4, 2019.

[7] M. B. Terzi and et al., "Detection of myocardial ischaemia based on artificial neural networks and skin sympathetic nerve activity," *EasyChair*, no. 2165, 2019.

[8] M. B. Terzı and O. Arikan, "Detection of myocardial ischaemia by using ecg, artificial neural network and gaussian mixture model," in *2020 28th Signal Processing and Communications Applications Conference (SIU)*, pp. 1–4, 2020.

[9] M. Terzi and et al., "Detection of acute myocardial ischemia based on artificial neural networks and skin sympathetic nerve activity," in *International Conference and Exhibition on Digital Transformation and Smart Systems (DTSS), Ankara*, pp. 1–4, 2019.

[10] M. B. TERZİ and O. ARIKAN, "Detection of myocardial infarction using autonomic nervous system, gaussian mixture model and artificial neural network," in *2020 Medical Technologies Congress (TIPTEKNO)*, pp. 1–4, 2020.

[11] M. B. Terzi and O. Arıkan, "Detection of myocardial ischaemia by using sympathetic nerve activity, artificial neural network and gaussian mixture model.," *Anatomy: International Journal of Experimental & Clinical Anatomy*, vol. 14, p. S151, 2020.

[12] M. B. Terzi, *Early Diagnosis of Acute Coronary Syndromes Automatically by using Features of ECG Recordings*. PhD thesis, Bilkent Universitesi (Turkey), 2014.

[13] M. J. Zellweger and et al., "Threshold, incidence, and predictors of prognostically high-risk silent ischemia in asymptomatic patients without prior diagnosis of coronary artery disease," *Journal of nuclear cardiology*, vol. 16, pp. 193–200, 2009.

[14] E. C. Hart and et al., "Guidelines in cardiovascular research: Recording sympathetic nerve activity in conscious humans and other mammals: guidelines and the road to standardization," *American Journal of Physiology-Heart and Circulatory Physiology*, vol. 312, no. 5, p. H1031, 2017.

[15] S. C. Malpas, "Sympathetic nervous system overactivity and its role in the development of cardiovascular disease," *Physiological Reviews*, vol. 90, no. 2, pp. 513–557, 2010. PMID: 20393193.

[16] A. Doytchinova and et al., "Simultaneous noninvasive recording of skin sympathetic nerve activity and electrocardiogram," *Heart Rhythm*, vol. 14, no. 1, pp. 25–33, 2017.

[17] T. Kusayama and et al., "Skin sympathetic nerve activity and the temporal clustering of cardiac arrhythmias," *JCI insight*, vol. 4, no. 4, 2019.

[18] P. Zhang and et al., "Characterization of skin sympathetic nerve activity in patients with cardiomyopathy and ventricular arrhythmia," *Heart Rhythm*, vol. 16, no. 11, pp. 1669 – 1675, 2019.

[19] M. B. Terzi and O. Arikan, "Anomaly detection technique based on sympathetic nerve activity for detection of cardiac arrhythmia," in *2020 28th Signal Processing and Communications Applications Conference (SIU)*, pp. 1–4, 2020.

[20] C. Mateo and J. A. Talavera, "Analysis of atrial and ventricular premature contractions using the short time fourier transform with the window size fixed in the frequency domain," *Biomedical Signal Processing and Control*, vol. 69, p. 102835, 2021.

[21] M. Mironovova and J. Bíla, "Fast fourier transform for feature extraction and neural network for classification of electrocardiogram signals," in *2015 Fourth International Conference on Future Generation Communication Technology (FGCT)*, pp. 1–6, 2015.

[22] D. Giri and et al., "Automated diagnosis of coronary artery disease affected patients using lda, pca, ica and discrete wavelet transform," *Knowledge-Based Systems*, vol. 37, pp. 274–282, 2013.

[23] A. Ghaffari and et al., "High resolution ambulatory holter ecg events detection-delineation via modified multi-lead wavelet-based features analysis: Detection and quantification of heart rate turbulence," *Expert Systems with Applications*, vol. 38, no. 5, pp. 5299–5310, 2011.

[24] H. Yanık and et al., "Electrocardiography (ecg) analysis and a new feature extraction method using wavelet transform with scalogram analysis,"

Biomedical Engineering / Biomedizinische Technik, vol. 65, no. 5, pp. 543–556, 2020.

[25] S. Sahoo and et al., "Multiresolution wavelet transform based feature extraction and ecg classification to detect cardiac abnormalities," *Measurement*, vol. 108, pp. 55–66, 2017.

[26] A. S. Eltrass and et al., "A new automated cnn deep learning approach for identification of ecg congestive heart failure and arrhythmia using constant-q non-stationary gabor transform," *Biomedical Signal Processing and Control*, vol. 65, p. 102326, 2021.

[27] V. Jahmunah and et al., "Automated detection of coronary artery disease, myocardial infarction and congestive heart failure using gaborcnn model with ecg signals," *Computers in Biology and Medicine*, vol. 134, p. 104457, 2021.

[28] U. R. Acharya and et al., "Automated characterization and classification of coronary artery disease and myocardial infarction by decomposition of ecg signals: A comparative study," *Information Sciences*, vol. 377, pp. 17–29, 2017.

[29] R. J. Martis and et al., "Characterization of ecg beats from cardiac arrhythmia using discrete cosine transform in pca framework," *Knowledge-Based Systems*, vol. 45, pp. 76–82, 2013.

[30] S. Raj and K. C. Ray, "Ecg signal analysis using dct-based dost and pso optimized svm," *IEEE Transactions on Instrumentation and Measurement*, vol. 66, no. 3, pp. 470–478, 2017.

[31] U. R. Acharya and et al., "Automated characterization of coronary artery disease, myocardial infarction, and congestive heart failure using contourlet and shearlet transforms of electrocardiogram signal," *Knowledge-Based Systems*, vol. 132, pp. 156–166, 2017.

[32] P. Amorim and et al., "Shearlet and contourlet transforms for analysis of electrocardiogram signals," *Computer Methods and Programs in Biomedicine*, vol. 161, pp. 125–132, 2018.

[33] G. Altan, "Diagnosis of coronary artery disease using deep belief networks," *European journal of engineering and natural sciences*, vol. 2, no. 1, pp. 29–36, 2017.

[34] G. Altan and et al., "A new approach to early diagnosis of congestive heart failure disease by using hilbert–huang transform," *Computer Methods and Programs in Biomedicine*, vol. 137, pp. 23–34, 2016.

[35] C. K. Jha and M. H. Kolekar, "Electrocardiogram data compression using dct based discrete orthogonal stockwell transform," *Biomedical Signal Processing and Control*, vol. 46, pp. 174–181, 2018.

[36] K.-M. Chang, "Ensemble empirical mode decomposition for high frequency ecg noise reduction," *Biomedical Engineering / Biomedizinische Technik*, vol. 55, no. 4, pp. 193–201, 2010.

[37] A. Mert, "Ecg feature extraction based on the bandwidth properties of variational mode decomposition," *Physiological Measurement*, vol. 37, p. 530, mar 2016.

[38] F. Akdeniz and et al., "Using wigner-ville distribution in ecg arrhythmia detection for telemedicine applications," in *2016 39th International Conference on Telecommunications and Signal Processing (TSP)*, pp. 409–412, 2016.

[39] P. K. Chaudhary and et al., "Fourier-bessel representation for signal processing: A review," *Digital Signal Processing*, p. 103938, 2023.

[40] A. Sharma and et al., "Automated pre-screening of arrhythmia using hybrid combination of fourier–bessel expansion and lstm," *Computers in Biology and Medicine*, vol. 120, p. 103753, 2020.

[41] K. Ramasamy and et al., "Detection of cardiac arrhythmias from ecg signals using fbse and jaya optimized ensemble random subspace k-nearest neighbor algorithm," *Biomedical Signal Processing and Control*, vol. 76, p. 103654, 2022.

[42] W. Yang and et al., "Automatic recognition of arrhythmia based on principal component analysis network and linear support vector machine," *Computers in Biology and Medicine*, vol. 101, pp. 22–32, 2018.

[43] R. J. Martis and et al., "Automated detection of atrial fibrillation using bayesian paradigm," *Knowledge-Based Systems*, vol. 54, pp. 269–275, 2013.

[44] F. Castells and et al., "The role of independent component analysis in the signal processing of ecg recordings," *Biomedical Engineering / Biomedizinische Technik*, vol. 52, no. 1, pp. 18–24, 2007.

[45] M. Jayasanthi and et al., "Independent component analysis with learning algorithm for electrocardiogram feature extraction and classification," *Signal, Image and Video Processing*, vol. 15, no. 2, pp. 391–399, 2021.

[46] M. Green and et al., "Comparison between neural networks and multiple logistic regression to predict acute coronary syndrome in the emergency room," *Artificial Intelligence in Medicine*, vol. 38, no. 3, pp. 305–318, 2006.

[47] M. A. Escalona-Morán and et al., "Electrocardiogram classification using reservoir computing with logistic regression," *IEEE Journal of Biomedical and Health Informatics*, vol. 19, no. 3, pp. 892–898, 2015.

[48] M. B. TERZİ and O. ARIKAN, "Detection of cardiac arrhythmia using autonomic nervous system, gaussian mixture model and artificial neural network," in *2020 Medical Technologies Congress (TIPTEKNO)*, pp. 1–4, 2020.

[49] L. Sharma and R. Sunkaria, "Myocardial infarction detection and localization using optimal features based lead specific approach," *IRBM*, vol. 41, no. 1, pp. 58–70, 2020.

[50] E. B. Verdi, M. Gok, D. D. Mülazimoglu, M. B. Terzi, and et al., "Deep learning-based hybrid clinical decision support system algorithm for covid-19 diagnosis via pcr graphics and thorax ct images, preliminary data," *European Respiratory Journal*, vol. 60, no. suppl 66, 2022.

[51] A. K. Sangaiah and et al., "An intelligent learning approach for improving ecg signal classification and arrhythmia analysis," *Artificial Intelligence in Medicine*, vol. 103, p. 101788, 2020.

[52] R. J. Martis and et al., "A two-stage mechanism for registration and classification of ecg using gaussian mixture model," *Pattern Recognition*, vol. 42, no. 11, pp. 2979–2988, 2009.

[53] A. M. Alqudah and et al., "Developing of robust and high accurate ecg beat classification by combining gaussian mixtures and wavelets features," *Australasian physical & engineering sciences in medicine*, vol. 42, no. 1, pp. 149–157, 2019.

[54] A. K. Dohare and et al., "Detection of myocardial infarction in 12 lead ecg using support vector machine," *Applied Soft Computing*, vol. 64, pp. 138–147, 2018.

[55] P. Singh and G. Pradhan, "Noise robust automatic heartbeat classification system using support vector machine and conditional spectral moment," *Physical and Engineering Sciences in Medicine*, vol. 43, no. 4, pp. 1387–1398, 2020.

[56] H. Li and et al., "Classification of electrocardiogram signals with waveform morphological analysis and support vector machines," *Medical & Biological Engineering & Computing*, vol. 60, no. 1, pp. 109–119, 2022.

[57] K. N. Rajesh and R. Dhuli, "Classification of ecg heartbeats using nonlinear decomposition methods and support vector machine," *Computers in Biology and Medicine*, vol. 87, pp. 271–284, 2017.

[58] G. B. Berikol and et al., "Diagnosis of acute coronary syndrome with a support vector machine," *Journal of medical systems*, vol. 40, no. 4, pp. 1–8, 2016.

[59] S. Bashir and et al., "A multicriteria weighted vote-based classifier ensemble for heart disease prediction," *Computational Intelligence*, vol. 32, no. 4, pp. 615–645, 2016.

[60] P. Yang and et al., "Ensemble of kernel extreme learning machine based random forest classifiers for automatic heartbeat classification," *Biomedical Signal Processing and Control*, vol. 63, p. 102138, 2021.

[61] V. Kalidas and L. S. Tamil, "Detection of atrial fibrillation using discrete-state markov models and random forests," *Computers in Biology and Medicine*, vol. 113, p. 103386, 2019.

[62] M. M. Ghiasi and et al., "Decision tree-based diagnosis of coronary artery disease: Cart model," *Computer Methods and Programs in Biomedicine*, vol. 192, p. 105400, 2020.

[63] L. Kumari and et al., "Classification of ecg beats using optimized decision tree and adaptive boosted optimized decision tree," *Signal, Image and Video Processing*, vol. 16, no. 3, pp. 695–703, 2022.

[64] M. Lee and et al., "Heartbeat classification using local transform pattern feature and hybrid neural fuzzy-logic system based on self-organizing map," *Biomedical Signal Processing and Control*, vol. 57, p. 101690, 2020.

[65] G. D. L. Fuente-Cortes and et al., "A fully integrated fuzzy logic algorithm for ischemic heartbeat classification," pp. 873–876, 2018.

[66] A. Gacek, "Preprocessing and analysis of ecg signals – a self-organizing maps approach," *Expert Systems with Applications*, vol. 38, no. 7, pp. 9008–9013, 2011.

[67] M. Javadi and et al., "Classification of ecg arrhythmia by a modular neural network based on mixture of experts and negatively correlated learning," *Biomedical Signal Processing and Control*, vol. 8, no. 3, pp. 289–296, 2013.

[68] R. Ebrahimpour and et al., "Electrocardiogram beat classification via coupled boosting by filtering and preloaded mixture of experts," *Neural Computing and Applications*, vol. 23, pp. 1169–1178, 2013.

[69] T. Exarchos and et al., "An association rule mining-based methodology for automated detection of ischemic ecg beats," *IEEE Transactions on Biomedical Engineering*, vol. 53, no. 8, pp. 1531–1540, 2006.

[70] X. Gu and et al., "A real-time fpga-based accelerator for ecg analysis and diagnosis using association-rule mining," *ACM Trans. Embed. Comput. Syst.*, vol. 15, feb 2016.

[71] Y.-C. Yeh and et al., "Cardiac arrhythmia diagnosis method using linear discriminant analysis on ecg signals," *Measurement*, vol. 42, no. 5, pp. 778–789, 2009.

[72] R. Magrans and et al., "Myocardial ischemia event detection based on support vector machine model using qrs and st segment features," in *2016 Computing in Cardiology Conference (CinC)*, pp. 405–408, 2016.

[73] D. Sadhukhan and et al., "Automated identification of myocardial infarction using harmonic phase distribution pattern of ecg data," *IEEE Transactions on Instrumentation and Measurement*, vol. 67, no. 10, pp. 2303–2313, 2018.

[74] R. K. Tripathy and et al., "A novel approach for detection of myocardial infarction from ecg signals of multiple electrodes," *IEEE Sensors Journal*, vol. 19, no. 12, pp. 4509–4517, 2019.

[75] Z. Ahmad and et al., "Ecg heartbeat classification using multimodal fusion," *IEEE Access*, vol. 9, pp. 100615–100626, 2021.

[76] U. R. Acharya and et al., "Automated detection and localization of myocardial infarction using electrocardiogram: a comparative study of different leads," *Knowledge-Based Systems*, vol. 99, pp. 146–156, 2016.

[77] R. Jothiramalingam and et al., "Diagnosis of coronary artery occlusion by fitting polynomial curve with the ecg signal based on optimization techniques," *Network Modeling Analysis in Health Informatics and Bioinformatics*, vol. 11, no. 1, p. 16, 2022.

[78] M. Sraitih and et al., "A robustness evaluation of machine learning algorithms for ecg myocardial infarction detection," *Journal of Clinical Medicine*, vol. 11, no. 17, p. 4935, 2022.

[79] R. K. Agrawal and et al., "A machine learning approach for classifying healthy and infarcted patients using heart rate variabilities derived vector magnitude," *Healthcare Analytics*, vol. 2, p. 100121, 2022.

[80] B. Liu and et al., "A novel electrocardiogram parameterization algorithm and its application in myocardial infarction detection," *Computers in Biology and Medicine*, vol. 61, pp. 178–184, 2015.

[81] P. C. Chang and et al., "Myocardial infarction classification with multi-lead ecg using hidden markov models and gaussian mixture models," *Applied Soft Computing*, vol. 12, no. 10, 2012.

[82] S. Al-Zaiti and et al., "Machine learning-based prediction of acute coronary syndrome using only the pre-hospital 12-lead electrocardiogram," *Nature communications*, vol. 11, no. 1, pp. 1–10, 2020.

[83] A. Daraei and H. Hamidi, "An efficient predictive model for myocardial infarction using cost-sensitive j48 model," *Iranian journal of public health*, vol. 46, no. 5, p. 682, 2017.

[84] Q. Sun and et al., "Early detection of myocardial ischemia in 12-lead ecg using deterministic learning and ensemble learning," *Computer Methods and Programs in Biomedicine*, vol. 226, p. 107124, 2022.

[85] X. Liu and et al., "Deep learning in ecg diagnosis: A review," *Knowledge-Based Systems*, vol. 227, p. 107187, 2021.

[86] M. M. Al Rahhal and et al., "Convolutional neural networks for electrocardiogram classification," *Journal of Medical and Biological Engineering*, vol. 38, pp. 1014–1025, 2018.

[87] M. B. Terzi, "Anomaly detection with deep long short term memory networks," in *2021 6th International Conference on Computer Science and Engineering (UBMK)*, pp. 129–132, 2021.

[88] E. Prabhakararao and S. Dandapat, "Myocardial infarction severity stages classification from ecg signals using attentional recurrent neural network," *IEEE Sensors Journal*, vol. 20, no. 15, pp. 8711–8720, 2020.

[89] X. Xu and et al., "Interpretation of electrocardiogram (ecg) rhythm by combined cnn and bilstm," *IEEE Access*, vol. 8, pp. 125380–125388, 2020.

[90] L. Guo and et al., "Inter-patient ecg classification with convolutional and recurrent neural networks," *Biocybernetics and Biomedical Engineering*, vol. 39, no. 3, pp. 868–879, 2019.

[91] L. Meng and et al., "Enhancing dynamic ecg heartbeat classification with lightweight transformer model," *Artificial Intelligence in Medicine*, vol. 124, p. 102236, 2022.

[92] C. Che and et al., "Constrained transformer network for ecg signal processing and arrhythmia classification," *BMC Medical Informatics and Decision Making*, vol. 21, no. 1, pp. 1–13, 2021.

[93] E. Butun and et al., "1d-cadcapsnet: One dimensional deep capsule networks for coronary artery disease detection using ecg signals," *Physica Medica*, vol. 70, pp. 39–48, 2020.

[94] Y. Jiao and et al., "Capsule network assisted electrocardiogram classification model for smart healthcare," *Biocybernetics and Biomedical Engineering*, vol. 42, no. 2, pp. 543–555, 2022.

[95] A. Y. Hannun and et al., "Cardiologist-level arrhythmia detection and classification in ambulatory electrocardiograms using a deep neural network," *Nature medicine*, vol. 25, no. 1, pp. 65–69, 2019.

[96] S. W. Smith and et al., "A deep neural network learning algorithm outperforms a conventional algorithm for emergency department electrocardiogram interpretation," *Journal of Electrocardiology*, vol. 52, pp. 88–95, 2019.

[97] G. Sayantan and et al., "Classification of ecg beats using deep belief network and active learning," *Medical and Biological Engineering and Computing*, vol. 56, no. 10, pp. 1887–1898, 2018.

[98] B. Taji and et al., "False alarm reduction in atrial fibrillation detection using deep belief networks," *IEEE Transactions on Instrumentation and Measurement*, vol. 67, no. 5, pp. 1124–1131, 2018.

[99] P. Liu and et al., "Arrhythmia classification of lstm autoencoder based on time series anomaly detection," *Biomedical Signal Processing and Control*, vol. 71, p. 103228, 2022.

[100] F. Samann and T. Schanze, "Multiple ecg segments denoising autoencoder model," *Biomedical Engineering / Biomedizinische Technik*, 2023.

[101] Y. Yan and et al., "A restricted boltzmann machine based two-lead electrocardiography classification," pp. 1–9, 2015.

[102] R. Brisk and et al., "The effect of confounding data features on a deep learning algorithm to predict complete coronary occlusion in a retrospective observational setting," *European Heart Journal - Digital Health*, vol. 2, pp. 127–134, 02 2021.

[103] T. Reasat and C. Shahnaz, "Detection of inferior myocardial infarction using shallow convolutional neural networks," pp. 718–721, 2017.

[104] H. Makimoto and et al., "Performance of a convolutional neural network derived from an ecg database in recognizing myocardial infarction," *Scientific reports*, vol. 10, no. 1, p. 8445, 2020.

[105] M. Hammad and et al., "Myocardial infarction detection based on deep neural network on imbalanced data," *Multimedia Systems*, pp. 1–13, 2021.

[106] A. Darmawahyuni and et al., "Deep learning with a recurrent network structure in the sequence modeling of imbalanced data for ecg-rhythm classifier," *Algorithms*, vol. 12, no. 6, 2019.

[107] K. Feng and et al., "Myocardial infarction classification based on convolutional neural network and recurrent neural network," *Applied Sciences*, vol. 9, no. 9, 2019.

[108] A. Rath and et al., "Improved heart disease detection from ecg signal using deep learning based ensemble model," *Sustainable Computing: Informatics and Systems*, vol. 35, p. 100732, 2022.

[109] A. A. Hernandez and et al., "Continuous monitoring of acute myocardial infarction with a 3-lead ecg system," *Biomedical Signal Processing and Control*, vol. 79, p. 104041, 2023.

[110] K. H. Miao and J. H. Miao, "Coronary heart disease diagnosis using deep neural networks," *International Journal of Advanced Computer Science and Applications*, vol. 9, no. 10, 2018.

[111] M. R. Bigler and et al., "Detection of myocardial ischemia by intracoronary ecg using convolutional neural networks," *PLOS ONE*, vol. 16, pp. 1–17, 06 2021.

[112] R. Xiao and et al., "Monitoring significant st changes through deep learning," *Journal of Electrocardiology*, vol. 51, no. 6, Supplement, pp. S78–S82, 2018.

[113] U. R. Acharya and et al., "Automated detection of coronary artery disease using different durations of ecg segments with convolutional neural network," *Knowledge-Based Systems*, vol. 132, pp. 62–71, 2017.

[114] A. Dutta and et al., "An efficient convolutional neural network for coronary heart disease prediction," *Expert Systems with Applications*, vol. 159, p. 113408, 2020.

[115] E. B. Verdi, M. B. Terzi, and et al., "Artificial intelligence-based hybrid system for covid-19 diagnosis using rt-pcr, thorax ct and laboratory data," *The Lancet*, 2023.

[116] M. T. Hernández-Huerta and et al., "Should rt-pcr be considered a gold standard in the diagnosis of covid-19?," *Journal of medical virology*, vol. 93, no. 1, p. 137, 2021.

[117] V. Pecoraro and et al., "Estimate false-negative rt-pcr rates for sars-cov-2. a systematic review and meta-analysis," *European Journal of Clinical Investigation*, vol. 52, no. 2, p. e13706, 2022.

[118] H. Hossein and et al., "Value of chest computed tomography scan in diagnosis of covid-19; a systematic review and meta-analysis," *Clinical and translational imaging*, vol. 8, pp. 469–481, 2020.

[119] Y. Peng and et al., "Using artificial intelligence technology to fight covid-19: a review," *Artificial intelligence review*, pp. 1–37, 2022.

[120] L. Wang and et al., "Artificial intelligence for covid-19: A systematic review," *Frontiers in Medicine*, vol. 8, 2021.

[121] S. Simpson and et al., "Radiological society of north america expert consensus statement on reporting chest ct findings related to covid-19. endorsed by the society of thoracic radiology, the american college of radiology, and rsna," *Journal of thoracic imaging*, 2020.

[122] Z. A. A. Alyasseri and et al., "Review on covid-19 diagnosis models based on machine learning and deep learning approaches," *Expert Systems*, vol. 39, no. 3, p. e12759, 2022.

[123] H.-J. Kim and et al., "An easy-to-use machine learning model to predict the prognosis of patients with covid-19: Retrospective cohort study," *Journal of Medical Internet Research*, vol. 22, p. e24225, Nov 2020.

[124] Z. Jiao and et al., "Prognostication of patients with covid-19 using artificial intelligence based on chest x-rays and clinical data: a retrospective study," *The Lancet Digital Health*, vol. 3, no. 5, pp. e286–e294, 2021.

[125] A. Soltan and et al., "Rapid triage for covid-19 using routine clinical data for patients attending hospital: development and prospective validation of an artificial intelligence screening test," *The Lancet Digital Health*, vol. 3, no. 2, pp. e78–e87, 2021.

[126] M. Wang and et al., "Deep learning-based triage and analysis of lesion burden for covid-19: a retrospective study with external validation," *The Lancet Digital Health*, vol. 2, no. 10, pp. e506–e515, 2020.

[127] C. K. Kim and et al., "An automated covid-19 triage pipeline using artificial intelligence based on chest radiographs and clinical data," *NPJ Digital Medicine*, vol. 5, no. 1, pp. 1–9, 2022.

[128] Q. Xu and et al., "Ai-based analysis of ct images for rapid triage of covid-19 patients," *NPJ digital medicine*, vol. 4, no. 1, pp. 1–11, 2021.

[129] M. Zandehshahvar and et al., "Toward understanding covid-19 pneumonia: A deep-learning-based approach for severity analysis and monitoring the disease," *Scientific Reports*, vol. 11, no. 1, pp. 1–10, 2021.

[130] A. Wong and et al., "Towards computer-aided severity assessment via deep neural networks for geographic and opacity extent scoring of sars-cov-2 chest x-rays," *Scientific reports*, vol. 11, no. 1, pp. 1–8, 2021.

[131] A. Tariq and et al., "Patient-specific covid-19 resource utilization prediction using fusion ai model," *NPJ digital medicine*, vol. 4, no. 1, pp. 1–9, 2021.

[132] O. Noy and et al., "A machine learning model for predicting deterioration of covid-19 inpatients," *Scientific Reports*, vol. 12, no. 1, pp. 1–9, 2022.

[133] P. Schwab and et al., "Real-time prediction of covid-19 related mortality using electronic health records," *Nature communications*, vol. 12, no. 1, pp. 1–16, 2021.

[134] S. Subudhi and et al., "Comparing machine learning algorithms for predicting icu admission and mortality in covid-19," *NPJ digital medicine*, vol. 4, no. 1, pp. 1–7, 2021.

[135] Y. Gao and et al., "Machine learning based early warning system enables accurate mortality risk prediction for covid-19," *Nature communications*, vol. 11, no. 1, pp. 1–10, 2020.

[136] G. Lichtner and et al., "Predicting lethal courses in critically ill covid-19 patients using a machine learning model trained on patients with non-covid-19 viral pneumonia," *Scientific Reports*, vol. 11, no. 1, pp. 1–10, 2021.

[137] F. Khozeimeh and et al., "Combining a convolutional neural network with autoencoders to predict the survival chance of covid-19 patients," *Scientific Reports*, vol. 11, no. 1, pp. 1–18, 2021.

[138] I. Braithwaite and et al., "Automated and partly automated contact tracing: a systematic review to inform the control of covid-19," *The Lancet Digital Health*, vol. 2, no. 11, pp. e607–e621, 2020.

[139] E. Ong and et al., "Covid-19 coronavirus vaccine design using reverse vaccinology and machine learning," *Frontiers in immunology*, vol. 11, p. 1581, 2020.

[140] Y. Zhou and et al., "Artificial intelligence in covid-19 drug repurposing," *The Lancet Digital Health*, vol. 2, no. 12, pp. e667–e676, 2020.

[141] C. Anastassopoulou and et al., "Data-based analysis, modelling and forecasting of the covid-19 outbreak," *PLOS ONE*, vol. 15, pp. 1–21, 03 2020.

[142] I. D. Apostolopoulos and et al., "Extracting possibly representative covid-19 biomarkers from x-ray images with deep learning approach and image data related to pulmonary diseases," *Journal of Medical and Biological Engineering*, vol. 40, pp. 462–469, 2020.

[143] A. Haghanifar and et al., "Covid-cxnet: Detecting covid-19 in frontal chest x-ray images using deep learning," *Multimedia Tools and Applications*, vol. 81, no. 21, pp. 30615–30645, 2022.

[144] F. Ucar and D. Korkmaz, "Covidiagnosis-net: Deep bayes-squeezenet based diagnosis of the coronavirus disease 2019 (covid-19) from x-ray images," *Medical Hypotheses*, vol. 140, p. 109761, 2020.

[145] A. Sharma and P. K. Mishra, "Covid-manet: Multi-task attention network for explainable diagnosis and severity assessment of covid-19 from cxr images," *Pattern Recognition*, vol. 131, p. 108826, 2022.

[146] P. Kedia and et al., "Covnet-19: A deep learning model for the detection and analysis of covid-19 patients," *Applied Soft Computing*, vol. 104, p. 107184, 2021.

[147] A. M. Ismael and A. Şengür, "Deep learning approaches for covid-19 detection based on chest x-ray images," *Expert Systems with Applications*, vol. 164, p. 114054, 2021.

[148] R. Jain and et al., "Deep learning based detection and analysis of covid-19 on chest x-ray images," *Applied Intelligence*, vol. 51, pp. 1690–1700, 2021.

[149] A. S. Elkorany and Z. F. Elsharkawy, "Covidetection-net: A tailored covid-19 detection from chest radiography images using deep learning," *Optik*, vol. 231, p. 166405, 2021.

[150] H. Ko and et al., "Covid-19 pneumonia diagnosis using a simple 2d deep learning framework with a single chest ct image: Model development and validation," *Journal of Medical Internet Research*, vol. 22, p. e19569, Jun 2020.

[151] V. S. Rohila and et al., "Deep learning assisted covid-19 detection using full ct-scans," *Internet of Things*, vol. 14, p. 100377, 2021.

[152] C. Ouchicha and et al., "Cvdnet: A novel deep learning architecture for detection of coronavirus (covid-19) from chest x-ray images," *Chaos, Solitons & Fractals*, vol. 140, p. 110245, 2020.

[153] L. Wang and et al., "Covid-net: A tailored deep convolutional neural network design for detection of covid-19 cases from chest x-ray images," *Scientific reports*, vol. 10, no. 1, p. 19549, 2020.

[154] Y. Song and et al., "Deep learning enables accurate diagnosis of novel coronavirus (covid-19) with ct images," *IEEE/ACM Transactions on Computational Biology and Bioinformatics*, vol. 18, no. 6, pp. 2775–2780, 2021.

[155] M. Turkoglu, "Covid-19 detection system using chest ct images and multiple kernels-extreme learning machine based on deep neural network," *IRBM*, vol. 42, no. 4, pp. 207–214, 2021.

[156] X. Wu, C. Chen, M. Zhong, J. Wang, and J. Shi, "Covid-al: The diagnosis of covid-19 with deep active learning," *Medical Image Analysis*, vol. 68, p. 101913, 2021.

[157] S. Tiwari and A. Jain, "Convolutional capsule network for covid-19 detection using radiography images," *International Journal of Imaging Systems and Technology*, vol. 31, no. 2, pp. 525–539, 2021.

[158] E. Hussain and et al., "Corodet: A deep learning based classification for covid-19 detection using chest x-ray images," *Chaos, Solitons & Fractals*, vol. 142, p. 110495, 2021.

[159] V. Perumal and et al., "Detection of covid-19 using cxr and ct images using transfer learning and haralick features," *Applied Intelligence*, vol. 51, pp. 341–358, 2021.

[160] T. B. Chandra and et al., "Coronavirus disease (covid-19) detection in chest x-ray images using majority voting based classifier ensemble," *Expert Systems with Applications*, vol. 165, p. 113909, 2021.

[161] M. Pahar and et al., "Covid-19 cough classification using machine learning and global smartphone recordings," *Computers in Biology and Medicine*, vol. 135, p. 104572, 2021.

[162] W. Zheng and et al., "Learning to learn by yourself: Unsupervised meta-learning with self-knowledge distillation for covid-19 diagnosis from pneumonia cases," *International Journal of Intelligent Systems*, vol. 36, no. 8, pp. 4033–4064, 2021.

[163] R. Miao and et al., "Umlf-covid: an unsupervised meta-learning model specifically designed to identify x-ray images of covid-19 patients," *BMC medical imaging*, vol. 21, no. 1, pp. 1–16, 2021.

[164] X. Xu and et al., "A deep learning system to screen novel coronavirus disease 2019 pneumonia," *Engineering*, vol. 6, no. 10, pp. 1122–1129, 2020.

[165] S. Rajaraman and et al., "Analyzing inter-reader variability affecting deep ensemble learning for covid-19 detection in chest radiographs," *PLOS ONE*, vol. 15, pp. 1–32, 11 2020.

[166] F. Cabitza and et al., "Development, evaluation, and validation of machine learning models for covid-19 detection based on routine blood tests," *Clinical Chemistry and Laboratory Medicine (CCLM)*, vol. 59, no. 2, pp. 421–431, 2021.

[167] I. Arpaci and et al., "Predicting the covid-19 infection with fourteen clinical features using machine learning classification algorithms," *Multimedia Tools and Applications*, vol. 80, pp. 11943–11957, 2021.

[168] P. Laguna and L. Sörnmo, "The staff iii ecg database and its significance for methodological development and evaluation," *Journal of Electrocardiology*, vol. 47, no. 4, pp. 408–417, 2014.

[169] A. L. Goldberger and et al., "Physiobank, physiotoolkit, and physionet: components of a new research resource for complex physiologic signals," *Circulation*, vol. 101, no. 23, pp. e215–e220, 2000.

[170] R. Bousseljot and et al., "Nutzung der ekg-signaldatenbank cardiodat der ptb über das internet," 1995.

[171] M. Oeff and et al., "The ptb diagnostic ecg database," *National Metrology Institute of Germany*, 2012.

[172] M. R. Homaeinezhad and et al., "Design of a unified framework for analyzing long-duration ambulatory ecg: Application for extracting qrs geometrical features," *Biomedical Engineering Letters*, vol. 1, no. 2, pp. 116–128, 2011.

[173] J. J. Wang and et al., "Criteria for ecg detection of acute myocardial ischemia: Sensitivity versus specificity," *Journal of Electrocardiology*, vol. 51, no. 6, Supplement, pp. S12–S17, 2018.

[174] J. Rahul and et al., "Short duration vectorcardiogram based inferior myocardial infarction detection: class and subject-oriented approach," *Biomedical Engineering / Biomedizinische Technik*, vol. 66, no. 5, pp. 489–501, 2021.

[175] O. S. Lih and et al., "Comprehensive electrocardiographic diagnosis based on deep learning," *Artificial Intelligence in Medicine*, vol. 103, p. 101789, 2020.

[176] H. M. Rai and K. Chatterjee, "Hybrid cnn-lstm deep learning model and ensemble technique for automatic detection of myocardial infarction using big ecg data," *Applied Intelligence*, vol. 52, no. 5, pp. 5366–5384, 2022.

[177] H. Martin and et al., "Near real-time single-beat myocardial infarction detection from single-lead electrocardiogram using long short-term memory neural network," *Biomedical Signal Processing and Control*, vol. 68, p. 102683, 2021.

[178] A. W. Cairns and et al., "A decision support system and rule-based algorithm to augment the human interpretation of the 12-lead electrocardiogram," *Journal of Electrocardiology*, vol. 50, no. 6, pp. 781 – 786, 2017.

[179] P. C. L. Bentes and J. Nadal, "A telediagnosis assistance system for multiple-lead electrocardiography," *Physical and Engineering Sciences in Medicine*, vol. 44, no. 2, pp. 473–485, 2021.

[180] K. Feng and et al., "Myocardial infarction classification based on convolutional neural network and recurrent neural network," *Applied Sciences*, vol. 9, no. 9, 2019.

[181] W. Ning and et al., "Automatic detection of congestive heart failure based on a hybrid deep learning algorithm in the internet of medical things," *IEEE Internet of Things Journal*, vol. 8, no. 16, pp. 12550–12558, 2021.

[182] O. F. Ertuğrul and et al., "Automatic diagnosis of cardiovascular disorders by sub images of the ecg signal using multi-feature extraction methods and randomized neural network," *Biomedical Signal Processing and Control*, vol. 64, p. 102260, 2021.

[183] I. Shafi and et al., "Reduced features set neural network approach based on high-resolution time-frequency images for cardiac abnormality detection," *Computers in Biology and Medicine*, vol. 145, p. 105425, 2022.

[184] R. Huo and et al., "Ecg segmentation algorithm based on bidirectional hidden semi-markov model," *Computers in Biology and Medicine*, vol. 150, p. 106081, 2022.

[185] M. K. Ojha and et al., "Automatic detection of arrhythmias from an ecg signal using an auto-encoder and svm classifier," *Physical and Engineering Sciences in Medicine*, pp. 1–10, 2022.

[186] L. Meng and et al., "Long-term wearable electrocardiogram signal monitoring and analysis based on convolutional neural network," *IEEE Transactions on Instrumentation and Measurement*, vol. 70, pp. 1–11, 2021.

[187] S. K. Pandey and R. R. Janghel, "Automated detection of arrhythmia from electrocardiogram signal based on new convolutional encoded features with bidirectional long short-term memory network classifier," *Physical and Engineering Sciences in Medicine*, vol. 44, no. 1, pp. 173–182, 2021.

[188] M. Bahaz and R. Benzid, "Efficient algorithm for baseline wander and powerline noise removal from ecg signals based on discrete fourier series," *Australasian physical & engineering sciences in medicine*, vol. 41, no. 1, pp. 143–160, 2018.

[189] S. Dami and M. Yahaghizadeh, "Predicting cardiovascular events with deep learning approach in the context of the internet of things," *Neural Computing and Applications*, vol. 33, pp. 7979–7996, 2021.

[190] C. Jin and et al., "Development and evaluation of an artificial intelligence system for covid-19 diagnosis," *Nature communications*, vol. 11, no. 1, pp. 1–14, 2020.

[191] X. Mei and et al., "Artificial intelligence–enabled rapid diagnosis of patients with covid-19," *Nature medicine*, vol. 26, no. 8, pp. 1224–1228, 2020.

[192] J. B. Lascarrou and et al., "Predictors of negative first sars-cov-2 rt-pcr despite final diagnosis of covid-19 and association with outcome," *Scientific reports*, vol. 11, no. 1, pp. 1–7, 2021.

[193] Y. Boum and et al., "Performance and operational feasibility of antigen and antibody rapid diagnostic tests for covid-19 in symptomatic and asymptomatic patients in cameroon: a clinical, prospective, diagnostic accuracy study," *The Lancet Infectious Diseases*, vol. 21, no. 8, pp. 1089–1096, 2021.

[194] A. A. M. Alkhatip and et al., "The diagnostic and prognostic role of neutrofphil-to-lymphocyte ratio in covid-19: a systematic review and meta-analysis," *Expert Review of Molecular Diagnostics*, vol. 21, no. 5, pp. 505–514, 2021.

[195] O. Ronneberger and et al., "U-net: Convolutional networks for biomedical image segmentation," in *Medical Image Computing and Computer-Assisted Intervention – MICCAI 2015*, (Cham), pp. 234–241, Springer International Publishing, 2015.

[196] T. D. Pham, "A comprehensive study on classification of covid-19 on computed tomography with pretrained convolutional neural networks," *Scientific reports*, vol. 10, no. 1, pp. 1–8, 2020.

[197] D. Dansana and et al., "Early diagnosis of covid-19-affected patients based on x-ray and computed tomography images using deep learning algorithm," *Soft Computing*, pp. 1–9, 2020.

[198] N. K. Mishra and et al., "Automated detection of covid-19 from ct scan using convolutional neural network," *Biocybernetics and Biomedical Engineering*, vol. 41, no. 2, pp. 572–588, 2021.

[199] Y. Lee and et al., "The application of a deep learning system developed to reduce the time for rt-pcr in covid-19 detection," *Scientific Reports*, vol. 12, no. 1, pp. 1–10, 2022.

[200] R. Zahorec and et al., "Rationale use of neutrophil-to-lymphocyte ratio for early diagnosis and stratification of covid-19.," *Bratislava Medical Journal / Bratislavské Lekárske Listy*, vol. 121, no. 7, pp. 466 – 470, 2020.

[201] S. Jimeno and et al., "Prognostic implications of neutrophil-lymphocyte ratio in covid-19," *European Journal of Clinical Investigation*, vol. 51, no. 1, p. e13404, 2021.

[202] W. Ning and et al., "Open resource of clinical data from patients with pneumonia for the prediction of covid-19 outcomes via deep learning," *Nature biomedical engineering*, vol. 4, no. 12, pp. 1197–1207, 2020.

[203] L. Hussain and et al., "Machine-learning classification of texture features of portable chest x-ray accurately classifies covid-19 lung infection," *BioMedical Engineering OnLine*, vol. 19, no. 1, pp. 1–18, 2020.

[204] R. Sadre and et al., "Validating deep learning inference during chest x-ray classification for covid-19 screening," *Scientific reports*, vol. 11, no. 1, pp. 1–10, 2021.

[205] E. H. Lee and et al., "Deep covid detect: an international experience on covid-19 lung detection and prognosis using chest ct," *NPJ digital medicine*, vol. 4, no. 1, pp. 1–11, 2021.

[206] S. Roy and et al., "Deep learning for classification and localization of covid-19 markers in point-of-care lung ultrasound," *IEEE Transactions on Medical Imaging*, vol. 39, no. 8, pp. 2676–2687, 2020.

[207] S. Thakur and et al., "X-ray and ct-scan-based automated detection and classification of covid-19 using convolutional neural networks (cnn)," *Biomedical Signal Processing and Control*, vol. 69, p. 102920, 2021.

[208] R. Villarreal-González and et al., "Anomaly identification during polymerase chain reaction for detecting sars-cov-2 using artificial intelligence trained from simulated data," *Molecules*, vol. 26, no. 1, 2021.

[209] R. C. Joshi and et al., "A deep learning-based covid-19 automatic diagnostic framework using chest x-ray images," *Biocybernetics and Biomedical Engineering*, vol. 41, no. 1, pp. 239–254, 2021.

[210] A. I. Khan and et al., "Coronet: A deep neural network for detection and diagnosis of covid-19 from chest x-ray images," *Computer Methods and Programs in Biomedicine*, vol. 196, p. 105581, 2020.

[211] S. Toraman and et al., "Convolutional capsnet: A novel artificial neural network approach to detect covid-19 disease from x-ray images using capsule networks," *Chaos, Solitons & Fractals*, vol. 140, p. 110122, 2020.

[212] G. Marques and et al., "Automated medical diagnosis of covid-19 through efficientnet convolutional neural network," *Applied Soft Computing*, vol. 96, p. 106691, 2020.

[213] A. S. Yadaw and et al., "Clinical features of covid-19 mortality: development and validation of a clinical prediction model," *The Lancet Digital Health*, vol. 2, no. 10, pp. e516–e525, 2020.

[214] N. Lassau and et al., "Integrating deep learning ct-scan model, biological and clinical variables to predict severity of covid-19 patients," *Nature communications*, vol. 12, no. 1, pp. 1–11, 2021.

[215] B. Nigam and et al., "Covid-19: Automatic detection from x-ray images by utilizing deep learning methods," *Expert Systems with Applications*, vol. 176, p. 114883, 2021.

[216] T. Wu and et al., "Ulnet for the detection of coronavirus (covid-19) from chest x-ray images," *Computers in Biology and Medicine*, vol. 137, p. 104834, 2021.

[217] N. S. Punn and et al., "Automated diagnosis of covid-19 with limited posteroanterior chest x-ray images using fine-tuned deep neural networks," *Applied Intelligence*, vol. 51, no. 5, pp. 2689–2702, 2021.

[218] C. Gangloff and et al., "Machine learning is the key to diagnose covid-19: a proof-of-concept study," *Scientific reports*, vol. 11, no. 1, pp. 1–11, 2021.

[219] T. Ozturk and et al., "Automated detection of covid-19 cases using deep neural networks with x-ray images," *Computers in Biology and Medicine*, vol. 121, p. 103792, 2020.

[220] M. Gour and et al., "Automated covid-19 detection from x-ray and ct images with stacked ensemble convolutional neural network," *Biocybernetics and Biomedical Engineering*, vol. 42, no. 1, pp. 27–41, 2022.

[221] A. Kumar and et al., "Sars-net: Covid-19 detection from chest x-rays by combining graph convolutional network and convolutional neural network," *Pattern Recognition*, vol. 122, p. 108255, 2022.

[222] M. A. Al-Antari and et al., "Fast deep learning computer-aided diagnosis of covid-19 based on digital chest x-ray images," *Applied Intelligence*, vol. 51, no. 5, pp. 2890–2907, 2021.

[223] S. R. Nayak and et al., "An automated lightweight deep neural network for diagnosis of covid-19 from chest x-ray images," *Arabian journal for science and engineering*, pp. 1–18, 2021.

[224] A. A. Ardakani and et al., "A practical artificial intelligence system to diagnose covid-19 using computed tomography: A multinational external validation study," *Pattern Recognition Letters*, vol. 152, pp. 42–49, 2021.

[225] H. Nasiri and et al., "A novel framework based on deep learning and anova feature selection method for diagnosis of covid-19 cases from chest x-ray images," *Computational intelligence and neuroscience*, 2022.

[226] A. Keles and et al., "Cov19-cnnet and cov19-resnet: diagnostic inference engines for early detection of covid-19," *Cognitive Computation*, pp. 1–11, 2021.

[227] D. Shome and et al., "Covid-transformer: Interpretable covid-19 detection using vision transformer for healthcare," *International Journal of Environmental Research and Public Health*, vol. 18, no. 21, 2021.